DIRECT ADAPTIVE CONTROL FOR A TRAJECTORY TRACKING UAV

A Dissertation

Submitted to the Faculty

of

Embry-Riddle Aeronautical University

by

Nirmit Prabhakar

In Partial Fulfillment of the

Requirements for the Degree

of

Doctor of Philosophy in Aerospace Engineering

November 2018

Embry-Riddle Aeronautical University

Daytona Beach, Florida

Direct Adaptive Control of a Trajectory Tracking UAV

By

Nirmit Prabhakar

This Dissertation was prepared under the direction of the candidate's Dissertation Committee Chairs, Dr. Richard Prazenica and Dr. Mark Balas, Department of Aerospace Engineering, and has been approved by the members of the dissertation committee. It was submitted to College of Engineering and was accepted in partial fulfillment of the requirements for the

Degree of

Doctor of Philosophy in Aerospace Engineering

Dr. Richard Prazenica, Ph.D.
Committee Chair

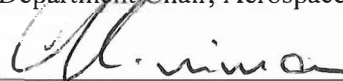Dr. Mark Balas, Ph.D.
Committee Co-Chair
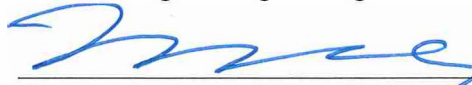
Dr. Hever Moncayo, Ph.D.
Committee Member

Dr. Tasos Lyrintzis, Ph.D.
Department Chair, Aerospace Engineering

Dr. Eric Coyle, Ph.D.
Committee Member

Dr. Maj Mirmirani, Ph.D.
Dean, College of Engineering

Dr. Lon D Moeller, J.D
Senior Vice President for Academic Affairs
and Provost

11-19-18
Date

DEDICATION

I'd like to dedicate this to Mumma and Babu (my grandparents) for showing me and my parents how to persist in the face of hardships, and for their unwavering love and support through every phase of my life. I owe it to them for the person I have become.

ACKNOWLEDGEMENTS

Last, but not least, I would like to appreciate all that Jennifer Roberts has done for me in the past two years. For being a perfect partner and fostering this environment of love which has helped me through the toughest of times.

TABLE OF CONTENTS

LIST OF TABLES

LIST OF FIGURES

Figure   Page

ABSTRACT

Prabhakar, Nirmit PhD, Embry-Riddle Aeronautical University, November, 2018. Direct Adaptive Control for a Trajectory Tracking UAV.

This research focuses on the theoretical development and analysis of a direct adaptive control algorithm to enable a fixed-wing UAV to track reference trajectories while in the presence of persistent external disturbances. A typical application of this work is autonomous flight through urban environments, where reference trajectories would be provided by a path planning algorithm and the vehicle would be subjected to significant wind gust disturbances. Full 6-DOF nonlinear and linear UAV simulation models are developed and used to study the performance of the direct adaptive control system for various scenarios. A stability proof is developed to prove convergence of the direct adaptive control system under certain conditions. Specific adaptive controller implementation details are provided, including the use of a sensor blending algorithm to address the non-minimum phase properties of the UAV models. The robustness of the adaptive system pertaining to the amount of modeling error that can be accommodated by the controller is studied, and the disturbance rejection capabilities and limitations of the controllers are also analyzed. The overall results of this research demonstrate that the direct adaptive control algorithm can enable trajectory tracking in cases where there are both significant uncertainties in the external disturbances and considerable error in the UAV model.

1. Introduction

1.1 Motivation

Unmanned Aerial Vehicles (UAVs) represent the fastest growing section of the aerospace industry. Their agility and adaptability to a plethora of missions make them ideal machines, supporting the growth of this industry. The past decade has seen a rise in the commercial applications of UAVs such as product delivery, agricultural applications, aerial photography and surveillance.

The less stringent regulations for the operation of UAVs, which makes their operating costs significantly cheaper than their manned counterparts, also entail that UAVs go through less testing and validation. Flight and wind tunnel tests are an integral and expensive part of the certification process of commercial or general aviation aircraft. Less safety regulations in unmanned systems eliminates the need for an extensive testing program for these vehicles. These tests are required for an accurate mathematical representation of flight dynamics of an aircraft (Morelli, 2012). The dynamics of unmanned vehicles therefore lack the accuracy typically achieved for commercial aircraft. The reduced fidelity of UAV dynamic models leads to need for more robust controllers to navigate these autonomous systems in fulfilling their missions. The smaller sizes of UAVs is one of their most advantageous features but it also causes them to have limited endurance. To maximize the time of operation, there is a need to develop optimum trajectories and controls for various mission requirements.

Modern linear control algorithms require a well-defined state space structure to effectively develop suitable controllers for a dynamical system. However, unmanned systems lack proper dynamic modeling and are susceptible to modeling errors, which can affect the efficiency of the control system. The robustness of linear control systems is limited in the amount of modeling error that can be accounted for in the system (Stengel & Ryan, 1991). This creates a significant problem for unmanned aircraft where there is a lack of high fidelity models available. This uncertainty may lead to the development of a sub-optimal control system where the aircraft would be unable to reach its peak performance parameters.

The focus of this research is on the development of control systems that can address the issue of low fidelity dynamic modeling while operating in adverse conditions like urban environments. Wind follows the path of least resistance; therefore in urban environments it will move around the edge of the buildings, generating an increase in velocity and density (Ragheb, 2008). This phenomenon causes persistent wind disturbances of high magnitude which make it difficult for an autonomous vehicles to follow its planned mission. The control system development presented in this dissertation concentrates on the ability to track a pre-determined trajectory while rejecting persistent disturbances from external sources.

1.2 Objective

This dissertation provides a novel implementation of a direct adaptive scheme as a sole controller for a fixed wing UAV. There have been previous instances of direct adaptive controller being used as an outer loop controller (Noriega et al., 2017). This research fur-

ther expands on the work done by Balas, Wen, Fuentes, and Frost (Wen & Balas, 1989), (M. J. Balas, 1995), (Fuentes & Balas, 2000), (Fuentes & Balas, 2002), (M. Balas & Fuentes, 2004), (Balas & Frost, 2016), and (Balas et al., 2009) by utilizing a general form of the direct adaptive controller and modifying it to fit the aircraft framework. It also analyzes the robustness of the controller with respect to its ability to accommodate modeling error in the aircraft system. The role of aircraft dynamics in the stability of the controller is studied, and margins of stability are determined while dynamics stability coefficients and their significance in the normal form is investigated.

The main objective of this research is to develop a standalone adaptive controller that can guide an autonomous UAV through a preconceived trajectory while in the presence of persistent disturbances that occur frequently in urban settings. This includes simulating various scenarios with multiple trajectories to follow, ranging from simple longitudinal/lateral maneuvers to complex path following; a wide array of disturbance is also modeled. An analysis of controller performance with respect to error in the disturbance model is also studied. Different modeling error simulations are run and the robustness to these errors is studied.

The contributions of this dissertation can be summarized as follows:

- A Disturbance Accommodating Controller (DAC) is formulated and augmented to include disturbance rejection while following a reference trajectory. This formulation is then implemented on a UAV dynamic model and the results are compared to a standard LQR application with regards to persistent disturbance rejection capabilities.

- Direct adaptive control is implemented as a stand-alone controller for UAV applications. The controller is able to act as a trajectory following, disturbance rejection algorithm in addition to performing its standard stabilizing role. The DAC and direct adaptive control algorithms are compared and the benefits of using adaptive control are listed.

- A proof of boundedness for this particular adaptive control configuration is presented using the Lyapunov theory, which can then be expanded for asymptotic stability using the Lyapunov-Barbalat lemma.

- Sensor blending of non-minimum phase systems is implemented on the UAV model using the Bass-Gura method.

- An analysis of robustness with respect to the aircraft dynamics is carried out. This analysis introduces the idea of stability margins that can be used to develop a robustness study using aerodynamic coefficients. An implementation of this idea is reported where the handling qualities of a poorly handling UAV are augmented to improve the Cooper-Harper Handling rating. Various simulations are performed with the lateral-directional linear model of the UAV that document changes in the roll and yaw damping coefficients and how that affects the tracking capabilities of the various aircraft states.

- The effects of various types of persistent disturbances are studied, which includes an analysis of errors in the modeling of such disturbances. This is further expanded with an analysis of how error propagation takes place between the adaptive regulator and

the disturbance adaptive gain when there is an error in the disturbance model and the

input disturbance.

2. Literature Review

2.1 Adaptive Control

The most common methods for achieving control of autonomous unmanned aerial vehicles uses state or output feedback. State feedback uses a feedback from the directly observed or estimated states and calculates a gain matrix to achieve desirable pre-calculated dynamics. Output feedback follows the same general principle but use the outputs as a feedback instead of the states. High performance systems require precision tuning for their controllers; however the plant parameters may not satisfy the accuracy required to achieve that precision. Adaptive control techniques provide real time online tuning of these gains by approximating nonlinear stochastic control problems to maintain an acceptable level of performance.

An adaptive controller adapts its gains to closely resemble a desirable system or curb any variable uncertainties in the system. Adaptive controllers can be classified into various categories based on their implementation or adaptation law. Direct adaptive control schemes directly estimate the parameters used in the controller, whereas indirect methods estimate parameters that are then used to calculate the controller gains. An example of an adaptive control system can be seen in Fig.2.1. Open loop adaptive control takes advantage of a known relationship between some states and variables e.g. gain scheduling. There are various control schemes that can be used to estimate the adaptive gains. Some of the most frequently used methods are model reference adaptive control, direct adaptive control, neu-
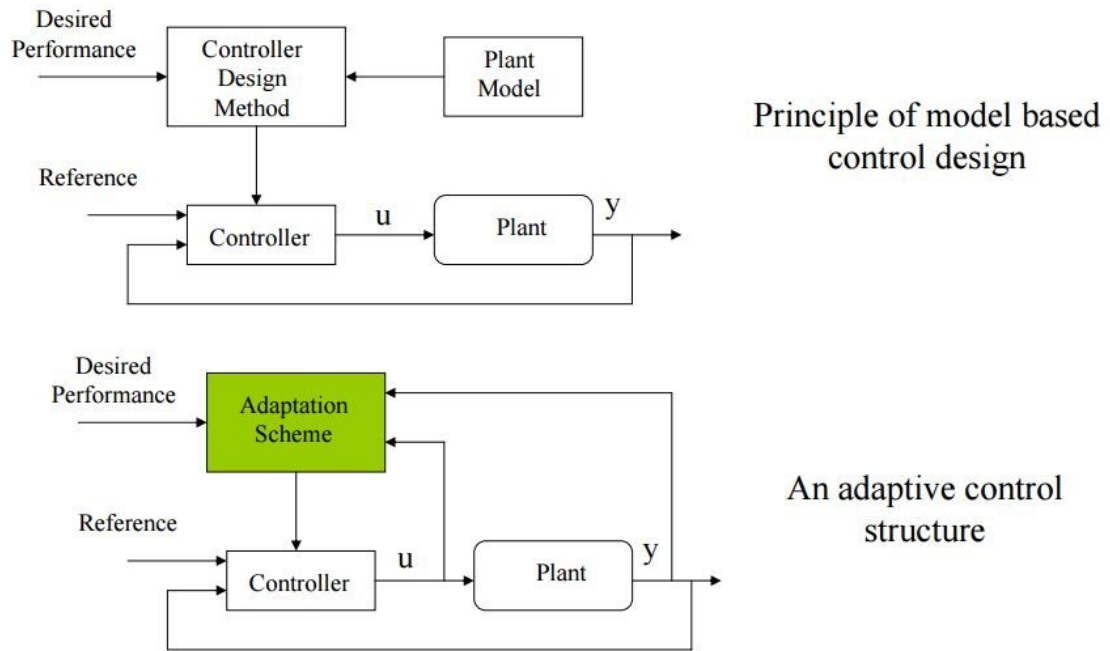
Figure 2.1. Structure of an Adaptive System (Landau, Lonzano, M'Saad, and Karimi, 2004)

ral networks, and model identification adaptive controllers. In this research, direct adaptive control laws are developed and implemented.

Adaptive contollers have been previously applied by researchers for the control of UAVs. For example, an adaptive controller was developed for a small fixed wing Unmanned Air Vehicle by the U.S. Naval Research Lab (Kahn, 2010). The control law used was based on approximate dynamic inversion and utilized a neural network which was trained to cancel errors during the online model inversion. This controller was shown to have benefits over a traditional linear controller in the presence of modeling errors for linear flight regimes and tracking commands. A combined adaptive controller (Fradkov & Andrievsky, 2005) was developed for attitude control of UAVs. This variable controller

structure used forced sliding motion (bang-bang controller), a parallel feedforward compensator and a parameter identification algorithm. The simulation results for this controller verified efficiency in the presence of significant uncertainty in parameters and time dependency of the kinematic relations. (Rysdyk et al., 1999) demonstrated the use of a robust adaptive nonlinear flight controller where the linearized system (XV-15 tilt-rotor) was inverted. Neural networks were developed to compensate for the inversion errors and the Lyapunov method was used to update the controller weights subsequently guaranteeing boundedness. (De Filippis et al., 2014) presented a novel approach of using a graph search system linked to a nonlinear model predictive controller to control the trajectory of a UAV. This system solves an open loop optimal control problem to minimize the tracking error with respect to the reference path.

The advent of large geometrical morphing in aircraft/wing shape has caused a need for more robust controllers that can handle large changes in inertia. Shi et al (Shi & Wan, 2015) analyzed the flight characteristics of a large-scale morphing aircraft to find the special effects morphing has on mass distribution and flight stability, providing a basis for designing a flight control system. Nigam et al. (Nigam et al., 2016) developed an indirect adaptive control technique which used a linear quadratic regulator (LQR) to estimate the gains used by a proportional integral derivative (PID) controller on a geometrical morphing wing. This gain scheduling technique identifies the plant parameters using subspace system identification and then uses LQR to calculate the PID gains for the new morphed configuration. This technique uses in the state space formulation and both the algorithms are compatible with each other, providing a substantial advantage. Gain scheduling was

also implemented by Prabhakar et al. to control a variable sweep-variable span aircraft to achieve transient stability. An adaptive critic neural network based controller, called Single Network Adaptive Critic (Nobleheart, 2008) was developed to control a single engine light airplane (such as a Cessna-182) that could perform rapid changes in wing sweep.

Adaptive controllers have been used extensively for developing controllers for various linear time invariant (LTI) as well as linear parameter varying (LPV) Morphing systems (Baldelli et al., 2008). (Calise et al., 1998) developed a neural network based direct adaptive control to maintain handling qualities in the event of a large scale actuation failure in a fighter aircraft configuration. This mitigated the need for parameter identification for control allocation during the failure. (Rajagopal et al., 2010) developed a modified state observer (MSO) based adaptive controller to compensate for modeling errors that stem from the nonlinear inversion of the dynamical model of a general aviation aircraft. It was shown that the adaptive controller adapted to the changing aircraft behavior and restored acceptable handling qualities. The MSO methodology was used to allow for fast adaptation without inducing any high frequency oscillations, and simulation results of the controller performance while subjected to unanticipated failures were also presented. (Gavilan et al., 2015) developed an adaptive backstepping method for an output-feedback controller to control the longitudinal dynamics of an aircraft. This method does not require a prior knowledge of aircraft aerodynamics other than the well-known physical properties of the aircraft. The controller is shown to be adept at following given references in airspeed and flight-path angle using elevator, thrust, and control parameters. A saturation limit is designed using a Lyapunov function to incorporate engine limitations. (Calise et al., 2000)

used an online neural network to account for errors arising from the approximations result-
ing from an inverted controller design for guided munitions. The paper highlights that this
method eliminates the need for a detailed design process and aerodynamic data, which is
beneficial especially at high angles of attack where the aerodynamics are highly nonlinear.
(Sharma et al., 2006) provided flight test results for the adaptive autopilot system detailed
in the previous paper. The adaptive system works in parallel with a baseline controller,
the outputs from the adaptive system are added to the baseline controls to achieve required
tracking.

(Kol et al., 1997) investigated nonlinear control laws and closed loop stability for aeroe-
lastic systems that include polynomial structural nonlinearities. Both local and globally
asymptotically stable systems were analyzed to develop feedback controllers, and numer-
ical simulations were used to provide empirical validation of some results. (Behal et al.,
2006) developed a similar approach of utilizing adaptive control to drive the pitch angle to
a set value while compensating for uncertainties in the aeroelastic model parameters. This
output feedback law is able to suppress flutter, limit cyclic oscillations, and reduce vibra-
tion levels in sub-critical flight ranges. Simulation results were provided to showcase the
performance of the proposed controller. (Yucelen et al., 2011) developed a derivative free
model reference adaptive controller (MRAC) for uncertain systems. Boundedness of the
error dynamics is proven using the Lyapunov-Karsovskii functions. Various modifications
terms to the controller that improve the robustness and performance are discussed. The
benefits of the controller are shown when applied to systems that undergo sudden change
in dynamics.

Robustness is the ability of a controller to deal with uncertainties in the system. An important property of adaptive controllers is their ability to deal with modeling and external uncertainties. A new model reference adaptive control (MRAC) algorithm was proposed by Kreisselmeier and Anderson (Kreisselmeier & Anderson, 1986), which made the closed loop adaptive control system more robust. They used a relative error signal combined with a dead zone and a projection in the adaptive law to achieve robustness. (Ioannou & Kokotovic, 1984) analyzed five different kinds of instability mechanisms to study the effect of unmodeled high frequency gains on stability and performance of adaptive control schemes. A modified algorithm was devised that was more robust and guaranteed a large area where all the trajectories remain bounded and the errors converge to a smaller residual set. (Patel et al., 2009) presents an L1 adaptive control scheme applied to a multi-input, multi-output (MIMO) open loop unstable, unmanned aircraft. The adaptive controller is able to accommodate actuator failures and pitch break uncertainty. Results are provided to show improved transient command tracking as well as guaranteed time delay margins.(Wise et al., 2006) details the flight testing of a guided weapons system that uses adaptive flight controls. The adaptive system uses a reference model of the baseline control which makes the weapon system follow the reference model closely. The adaptive controller was successfully shown to compensate for large uncertainties (external and internal). (Gregory et al., 2010) presented results of flight tests conducted on a sub-scale turbine powered generic transport model using an L1 adaptive control used to compensate for uncertainties in nonlinear system cross-couplings. (Choe et al., 2011) details the use of an L1 adaptive flight controller to improve the aircraft handling qualities and to help prevent negative interac-

tions between the pilot and the aircraft in the event of small aircraft failures. Preliminary simulation results show that the controller is able to meet the required handling qualities in the presence of faults and failures.

(Liu et al., 2010) addresses the application of model reference adaptive control to aircrafts with structural damages. The paper presents the linearized aircraft models with damage to include details such as coupling between derivatives and partial derivatives of the lateral longitudinal system. Simulation studies are performed to obtain design and performance results for the adaptive flight control system. (Moncayo et al., 2012) developed another adaptive control solution designed to handle malfunction of aircraft sub-systems and environmental upset conditions. This approach used nonlinear dynamic inversion augmented with an artificial immune system mechanism, inspired by the human immune system, which is to directly compensate for failures. (Lavretsky et al., 2010) predicted improved transient characteristics of a predictor-based model reference adaptive control derived using the Lyapunov framework when compared to classical model reference adaptive controllers.

Direct adaptive control (Narendra & Valavani, 1977) holds a distinct advantage over conventional controller designs in that it does not require a precise knowledge of the 'A' matrix of the system. The sensor dynamics ('C') and the actuator dynamics ('B') are usually very well defined for aerospace grade sensors and actuators; hence there is usually a high confidence level associated with these values. The adaptive control scheme uses these B and C matrices to adapt to the control gains required by the system. This controller concept was further developed by (Wen & Balas, 1989), (M. J. Balas, 1995), (Fuentes &

Balas, 2000), (Fuentes & Balas, 2002), (M. Balas & Fuentes, 2004), (Balas & Frost, 2016), and (Balas et al., 2009). Modeling of wind turbines poses a challenge due to their complex machinery and their interaction with unpredictable conditions during operation, which in turn poses difficulties in the development of a control system. Frost et al. extended the direct model reference adaptive approach for implementation in a utility-scale wind turbine for speed regulation (Frost et al., 2009), mitigating the challenges faced by other control schemes due to lack of accurate dynamical modeling.

2.2 Trajectory Tracking and Disturbance Rejection

One of the most important functions of an autonomous UAV is to be able to follow a specified path, pertinent to the mission. Trajectory tracking is often accomplished using a combination of a waypoint path planner and a control system that is used to follow the obtained waypoints. Path planning is an extensively researched topic but is not pertinent to this investigation, which focuses on the control schemes used to track planned trajectories. The waypoints generated by path planners can be converted into 3-D trajectories, and control input required to achieve these maneuvers can be calculated and then be used by the controller to follow the trajectory.

Ren et al. (Ren & Beard, 2004) developed a five layer system architecture which consist of waypoint path planner, dynamic trajectory smoother, trajectory tracker, longitudinal and lateral autopilots and the UAV system in a feedback loop. The waypoint path planner generates straight line segments that are affected by the external environment like obstacles, location and target. The dynamic trajectory smoothing creates a feasible trajectory with a

reference altitude, heading and position. These references are then utilized by the trajectory tracker to command the required position, heading and altitude. The autopilot system then calculates the control deflections required to command the heading and positions given by the trajectory tracker. These are then fed in as actuator inputs into the UAV system. Sensor data then acts as a feedback system for the autopilot systems, completing the loop. Back-stepping techniques were then used to design the velocity and heading angle control schemes from known laws that account for heading and velocity rate constraints of the UAV. A parameter adaptation technique is utilized to estimate autopilot parameters that are not known (Ren & Atkins, 2005). Gavilan et al. developed a two layer guidance and control system, which uses a robust L1 navigation law that ensures a solution to the nonlinear optimization problem by successive linearization. The top level guidance system uses an iterative model predictive scheme to precompute references which outputs the airspeed, flight path and bank angle. These are then fed into the controller that utilizes an adaptive back-stepping scheme for longitudinal dynamics and an integral-LQR for the lateral one.

A different approach developed by (Yamasaki et al., 2007) which consists of a proportioanl navigation (Pro-Nav) guidance law for tracking. A dynamic inversion technique was employed for guidance force generation to achieve high maneuverability. A cubic spline interpolation provides virtual waypoints across the desired trajectory by using flight distance. The use of proportional navigation is beneficial to avoid control saturation or divergence in large tracking error situations, making the system more robust than using tracking error corrections. (de Marina et al., 2017) presented an algorithm for trajectory tracking of smooth curves with constant airspeed under a constant wind disturbance. Their methodology is

based on following a vector field constructed from the implicit function describing the trajectory. The algorithm output can be directly expressed as a bank angle and can be tuned offline to set saturation limits on critical physical constraints. A guidance system linked to a nonlinear model predictive controller, which solves at each sampling time, a finite horizon optimal control problem to track the reference path, was proposed by (De Filippis et al., 2014). This tracking system successfully accomplishes good tracking performance and effective control actions for a smooth and safe flight path. Another nonlinear MPC tracking method was implemented by (Stastny et al., 2017) for lateral-directional fixed wing trajectory tracking. Model identification is done on closed loop low-level roll channel dynamics, which then produces a low order equivalent of low level autopilot response to high level commands.

(Adami & Zhu, 2011) used a trajectory linearization controller that combines the open loop dynamic inverse with a regulator for the tracking error. This system provides robustness to modeling errors, disturbances or excitation of internal dynamics. Feedback gains are obtained as a function of nominal trajectory, which negates the use of gain scheduling. A Lyapunov theory based controller was proposed for trajectory tracking while flying in non-optimal wind conditions and adaptive techniques are developed for wind identification (Brezoescu et al., 2015). This control system is applied to light fixed wing UAVs, and straight line paths between geo-referenced waypoints are obtained, which are used to calculate the dynamic error with respect to the reference trajectory by using the lateral airplane equations of motion. This error is then used to derive control inputs required to track

the given trajectory by applying the tuning functions method, guaranteeing the closed loop adaptive system to be minimal.

Any system in real world scenarios experiences disturbances, either external or mechanical (e.g vibrational, aeroelastic etc.). An ideal control system should be able to mitigate these unwanted inputs while continuing to perform the tasks required. Disturbance rejection becomes a challenge while utilizing classical control techniques such as PID. This issue was highlighted by (Han, 2009), which also details the workings of active disturbance rejection control (ADRC) and its advantages in performance and practicality over PID. ADRC was applied to a micro rlectro-mechanical system gyroscope to compensate for imperfections in manufacturing and disturbances in control effort caused by its small size; this process was detailed by (Zheng et al.,2008). (Zheng et al., 2007) analyzed the stability characteristics of ADRC for nonlinear time varying systems and proved asymptotic stability for unknown dynamics. (Alonge et al., 2017) used a robust sliding mode based ADRC controller that was used to deal with the dynamic and steady state behavior of an induction motor, where the external and internal disturbances were estimated and compensated for by using extended state observers. Dinh et. al. presented a novel application of the ADRC for integrated guidance and control of missiles using an enhanced feedback linearization based control law (Dinh et al., 2017).

A robust multiple sliding mode controller was applied to a hovercraft tracking trajectories with external disturbances (Jeong & Chwa, 2018). Coupled multiple sliding surfaces were introduced to track the error between pseudo and actual control variables and the controller was then applied to the sliding surfaces for convergence within finite time.

(Cabecinhas et al., 2014) developed a nonlinear adaptive state feedback tracking controller to steer a quadrotor along a given trajectory while under constant force disturbances. The closed loop system was shown to be asymptotically stable and experimental verification was presented for the same. Wang et. al. presented an analysis of a novel adaptive algorithm to a linearized system. In this work, the stability controller was augmented with an adaptive controller to enhance the performance of trajectory tracking/disturbance rejection (Wang et al., 1991). (Shahnazi & Akbarzadeh-T., 2008) developed a PI-adaptive fuzzy controller for uncertain nonlinear systems that provides robustness in the presence of large and fast uncertainties and disturbances that are bounded but unknown. A Lyapunov theory based proof of asymptotic stability is also provided.

3. Objective and Methodology

The objective of this research is to find a robust solution to the problem of UAV control system development, focusing on the aspects of trajectory following while rejecting persistent external disturbances. Details of the dynamic modeling of the UAV and the development of a simulation will be highlighted followed by a mathematical proof of stability of the proposed adaptive control system. The various assumptions made to insure closed-loop stability and details of the controller implementation are discussed.

3.1   6-DoF Dynamic Modeling and Simulation

The dynamics model used for trajectory generation is a linearized, state-space model derived from a 6 degree-of-freedom (6-DoF) nonlinear model of a typical general aviation aircraft. This specific flight dynamics model was chosen for the well-behaved, open-loop dynamics of the aircraft and the similarity in handling characteristics to many small and medium-scale UAVs. The model treats the aircraft as a rigid body and includes the following 12 states:

$$X = [u, v, w, p, q, r, \phi, \theta, \psi, X_N, Y_E, h]^T \tag{3.1}$$

where u, v, w denote the body-referenced velocity components, p, q, r represent the body-referenced angular velocity components, ϕ, θ, ψ are the roll, pitch, and yaw angles, and X_N, Y_E, h denote the inertial (North, East, altitude) position. The aircraft model includes the following control inputs:

$$U = [\delta_e, \delta_t, \delta_a, \delta_T]^T \tag{3.2}$$

where δ_e is the elevator deflection, δ_T represents the thrust control, δ_a is the aileron deflection, and δ_r is the rudder deflection. The mass and geometry properties of this aircraft model and the aerodynamic coefficients are provided in Tables 1 and 2.

The nonlinear aircraft model was linearized about a wings-level, constant-altitude trim condition corresponding to:

$$X^* = \{u^*, v^*, w^*, p^*, q^*, r^*, \varphi^*, \theta^*, \psi^*, X_N^*, Y_E^*, h^*\}^T$$
$$= \{176.4\,\text{ft/s}, 0, -0.244\,\text{ft/s}, 0, 0, 0, 0, 0.08\,\text{deg}, 0, 0, 0, 0\}^T$$

(3.3)

Table 3.1. Aircraft Geometry and Mass Properties

Description	Symbol	Value	Units
Wing Area	S	184	ft^2
Wing Span	b	33.4	ft.
Mean Aerodynamic Chord	$\bar{c}$	5.7	ft.
Weight	W	2750	lb.
Moment of Inertia about X-axis	Ixx	1048	slug-ft^2
Moment of Inertia about Y-axis	Iyy	3000	slug-ft^2
Moment of Inertia about Z-axis	Izz	3500	slug-ft^2
Product of Inertia – XZ	Ixz	0	slug-ft^2

This trim condition corresponds to sea level altitude with the aircraft at close to zero angle of attack. The trim control inputs are:

$$U = [\delta_e, \delta_t, \delta_a, \delta_T]^T = [0.0573\,deg, 0.5406, 0, 0]^T$$

(3.4)

The trim thrust control corresponds to 54.06 percent of the maximum available power from the engines. The linear model used for trimming the aircraft is obtained by using the

linearization tools built into MATLAB. During this process, an input point was placed at the vector input for elevator, aileron, rudder and throttle; the output of the system was designated at the output of the Euler angles describing the aircraft attitude.

Table 3.2. Aircraft Aerodynamic Coefficients

Longitudinal			Lateral		
Coefficient	**Value**	**Units**	**Coefficient**	**Value**	**Units**
$C_{L\alpha}$	4.44	/rad	$C_{l\beta}$	-0.074	/rad
C_{Lq}	3.8	s/rad	C_{lp}	-0.41	s/rad
$C_{L\delta e}$	0.355	/rad	C_{lr}	0.107	s/rad
C_{L0}	0.41	/rad	$C_{l\delta a}$	-0.134	/rad
			$C_{l\delta r}$	0.107	/rad
$C_{D\alpha}$	0.33	/rad	$C_{Y\beta}$	-0.564	/rad
C_{D0}	0.05	/rad	$C_{Y\delta r}$	0.157	/rad
			$C_{n\beta}$	0.071	/rad
$C_{M\alpha}$	-0.683	/rad	C_{np}	-0.0575	s/rad
$C_{M\delta e}$	-0.923	/rad	C_{nr}	-0.125	s/rad
$C_{M\dot{\alpha}}$	-4.36	s/rad	$C_{n\delta a}$	-0.0035	/rad
C_{Mq}	-9.96	s/rad	$C_{n\delta r}$	-0.072	/rad

The linearization process yielded decoupled longitudinal and lateral state-space models of the form:

$$\Delta \dot{X}_{long} = A_{long}\Delta X_{long} + B_{long}\Delta U_{long}$$

$$\Delta \dot{X}_{lat} = A_{lat}\Delta X_{lat} + B_{lat}\Delta U_{lat}$$

(3.5)

where ΔX and ΔU represent changes in the state and control variables from the trim state.

These vectors are defined as:

$$
\begin{aligned}
\Delta X_{long} &= \{\Delta h, \Delta u, \Delta w, \Delta \theta, \Delta q\}^T \\
\Delta U_{long} &= \{\Delta \delta_e, \Delta \delta_T\}^T \\
\Delta X_{lat} &= \{\Delta v, \Delta \varphi, \Delta \psi, \Delta p, \Delta r\}^T \\
\Delta U_{lat} &= \{\Delta \delta_a, \Delta \delta_r\}^T
\end{aligned}
\tag{3.6}
$$

The specific longitudinal and lateral linear models are given by

$$
\begin{bmatrix} \Delta \dot{h} \\ \Delta \dot{u} \\ \Delta \dot{w} \\ \Delta \dot{\theta} \\ \Delta \dot{q} \end{bmatrix}
=
\begin{bmatrix}
0 & -1.4e^{-3} & -1 & 176.4 & 0 \\
0 & -6.76e^{-2} & 3.08e^{-2} & -32.2 & 0.23 \\
0 & -0.36 & -2.02 & 0.04 & 171.5 \\
0 & 0 & 0 & 0 & 1 \\
0 & 0 & -0.05 & 0 & -2.08
\end{bmatrix}
\begin{bmatrix} \Delta h \\ \Delta u \\ \Delta w \\ \Delta \theta \\ \Delta q \end{bmatrix}
+
\begin{bmatrix}
0 & 0 \\
-0.03 & 7.30 \\
-28.28 & 0 \\
0 & 0 \\
-11.93 & 0
\end{bmatrix}
\begin{bmatrix} \Delta \delta_e \\ \Delta \delta_T \end{bmatrix}
$$

$$
\begin{bmatrix} \Delta \dot{v} \\ \Delta \dot{\phi} \\ \Delta \dot{\psi} \\ \Delta \dot{p} \\ \Delta \dot{r} \end{bmatrix}
=
\begin{bmatrix}
-0.27 & 32.2 & 0 & -0.24 & -176.4 \\
0 & 0 & 0 & 1 & -1.4e^{-3} \\
0 & 0 & 0 & 0 & 1 \\
-0.091 & 0 & 0 & -8.41 & 2.19 \\
0.0261 & 0 & 0 & -0.35 & -0.76
\end{bmatrix}
\begin{bmatrix} \Delta v \\ \Delta \phi \\ \Delta \psi \\ \Delta p \\ \Delta r \end{bmatrix}
+
\begin{bmatrix}
0 & 12.5 \\
0 & 0 \\
0 & 0 \\
-29.05 & 23.20 \\
-0.22 & -4.67
\end{bmatrix}
\begin{bmatrix} \Delta \delta_a \\ \Delta \delta_r \end{bmatrix}
$$

The longitudinal and lateral eigenvalues associated with these linear state-space models are listed in Tables 3.3 and 3.4. The longitudinal dynamics are characterized by stable short period and long period modes. There is also a zero (neutrally stable) eigenvalue associated with the altitude state. The lateral dynamics are characterized by stable dutch roll, roll convergence, and spiral modes. Similar to the longitudinal model, there is a zero eigenvalue associated with the yaw state, which is neutrally stable.

Table 3.3. Open-Loop UAV Longitudinal Modes

Longitudinal Modes	
Short Period	$\lambda_{SP} = -2.06 \pm 2.93j$ $\zeta_{SP} = 0.575, \omega_{SP} = 3.58 rad/s$
Long Period	$\lambda_{LP} = -0.027 \pm 0.21j$ $\zeta_{LP} = 0.126, \omega_{LP} = 0.215 rad/s$
	$\lambda_5 = 0$

Table 3.4. Open-Loop UAV Lateral Modes

Lateral Modes	
Dutch Roll	$\lambda_{DR} = -0.498 \pm 2.36j$ $\zeta_{DR} = 0.206, \omega_{DR} = 2.41 rad/s$
Roll Convergence	$\lambda_R = -8.45$
Spiral	$\lambda_S = -0.0085$
	$\lambda_5 = 0$

3.2 Disturbance Accommodating Control

A Disturbance Accommodating Controller (DAC) (Johnson, 1986), (Balas, 2016) was designed to enable the UAV to track reference trajectories while rejecting persistent external disturbances u_D. The plant is represented as a linear model of the form:

$$\dot{x} = Ax + Bu + \Gamma u_D$$
$$y = Cx$$

(3.7)

The DAC is designed to reject disturbances of known frequency with unknown magnitude. Therefore, the DAC implementation requires that the general form of the disturbance is known and can be modeled as a disturbance generator state-space system as follows:

$$\dot{z}_D = F z_D$$
$$u_D = \Theta z_D$$

(3.8)

where z_D represents the disturbance state. The DAC is designed to enable the system to track reference trajectories that are generated from a linear model:

$$\dot{x}_{ref} = A_{ref} x_{ref} + B_{ref} u_{ref}$$
$$y_{ref} = C_{ref} x_{ref}$$

(3.9)

3.2.1 Disturbance Accommodation Control Formulation

In general, the reference model can be different from the system model, but the reference output y_{ref} is required to have the same dimension as the system output y. In this

work, the reference trajectories represent lateral and longitudinal maneuvers that were generated from the linear system models discussed in Section 2.1. Therefore, in this case, $A_{ref} = A$ and $B_{ref} = B$. Given the system model and the disturbance generator model, ideal trajectories can be defined for the system so that:

$$\dot{x}_* = Ax_* + Bu_* + \Gamma u_D$$

$$y_* = Cx_{ref}$$

(3.10)

The ideal trajectories are assumed to take the general form

$$x_* = S_{11}x_{ref} + S_{12}u_{ref} + S_{13}z_D$$

$$u_* = S_{21}x_{ref} + S_{22}u_{ref} + S_{23}z_D$$

$$y_* = y_{ref} = Cx_{ref}$$

(3.11)

This leads to the following set of matching conditions that must be satisfied:

$$S_{11}A_{ref} = AS_{11} + BS_{21}$$

$$S_{11}B_{ref} = AS_{12} + BS_{22}$$

$$S_{13}F = AS_{13} + BS_{23} + \Gamma\Theta$$

$$CS_{12} = 0$$

$$CS_{11} = C$$

$$CS_{13} = 0$$

(3.12)

Since, in this case, $A_{ref} = A$ and $B_{ref} = B$, the matching conditions reduce to

$$S_{11} = I, S_{12} = 0, S_{13} = 0, S_{21} = 0$$
$$S_{22} = I, BS_{23} = -\Gamma\Theta \tag{3.13}$$

Assuming B is full rank, the ideal trajectories are given by:

$$x_* = x_{ref}$$
$$u_* = u_{ref} - S_{23}z_D \tag{3.14}$$
$$y_* = y_{ref} = Cx_{ref} = Cx_*$$

The control law for the DAC takes the form given below

$$u = u_{ref} + G_x\left(x - x_{ref}\right) + G_D z_D$$
$$= u_{ref} + G_x\Delta x + G_D z_D \tag{3.15}$$

Defining $\Delta x = x - x_*$ and $\Delta u = u - u_*$, we obtain

$$\Delta u = u_{ref} + G_x\left(\Delta x + x_*\right) + G_D z_D - u_*$$
$$= G_x\left(\Delta x + S_{11}z_D\right) + G_D z_D - S_{23}z_D \tag{3.16}$$
$$= G_x\Delta x + \left(G_D - S_{23} + G_x S_{11}\right)z_D$$

Then, if the gain G_D is selected as $G_D = S_{23} - G_x S_{11}$, the state error dynamics will be given by:

$$\Delta\dot{x} = A\Delta x + B\Delta u = \left(A + BG_x\right)\Delta x \tag{3.17}$$

Assuming that $R(B) \subseteq R(\Gamma)$, where $R(B)$ and $R(\Gamma)$ denote the range of B and Γ respectively, it can be shown that a unique G_D exists. This G_D has to satisfy the equation $BG_D + \Gamma\Theta = 0$ (M. Balas, 2016, April). Therefore, the state error dynamics will be stable (i.e., the state will converge to the ideal state trajectory) if G_x is chosen so that the eigenvalues of $(A + BG_x)$ are stable with G_D chosen as follows:

$$\begin{aligned} G_D &= S_{23} - G_x S_{11} \\ &= -\left(B^T B\right)^{-1} B^T \Gamma\Theta - G_x \end{aligned} \tag{3.18}$$

State and disturbance estimators can then be developed, which take the form:

$$\begin{aligned} \dot{\hat{x}} &= A\hat{x} + Bu + K_x(y - \hat{y}) \\ \hat{y} &= C\hat{x} \\ \dot{\hat{z}}_D &= F\hat{z}_D + K_D(y - \hat{y}) \\ \hat{u}_D &= \Theta\hat{z}_D \end{aligned} \tag{3.19}$$

Defining $e_x = x - \hat{x}$ and $e_D = z_D - \hat{z}_D$, an estimation error system can then be defined as

$$\begin{bmatrix} \dot{e}_x \\ \dot{e}_D \end{bmatrix} = \bar{A} \begin{bmatrix} e_x \\ e_D \end{bmatrix} - \bar{K}(y - \hat{y}) = \left[\bar{A} - \bar{K}\bar{C}\right] \begin{bmatrix} e_x \\ e_D \end{bmatrix} \tag{3.20}$$

$$\bar{A} = \begin{bmatrix} A & \Gamma\Theta \\ 0 & F \end{bmatrix} \quad \bar{C} = \begin{bmatrix} C & 0 \end{bmatrix} \quad \bar{K} = \begin{bmatrix} K_x \\ K_D \end{bmatrix}$$

The state and disturbance estimation errors will then converge to zero if K_x and K_D are chosen such that the eigenvalues of $\left[\bar{A} - \bar{K}\bar{C}\right]$ are stable. The architecture of the disturbance accommodating controller with reference trajectory tracking is depicted in Figure 3.1.

3.2.2   Disturbance Accommodating Control Implementation
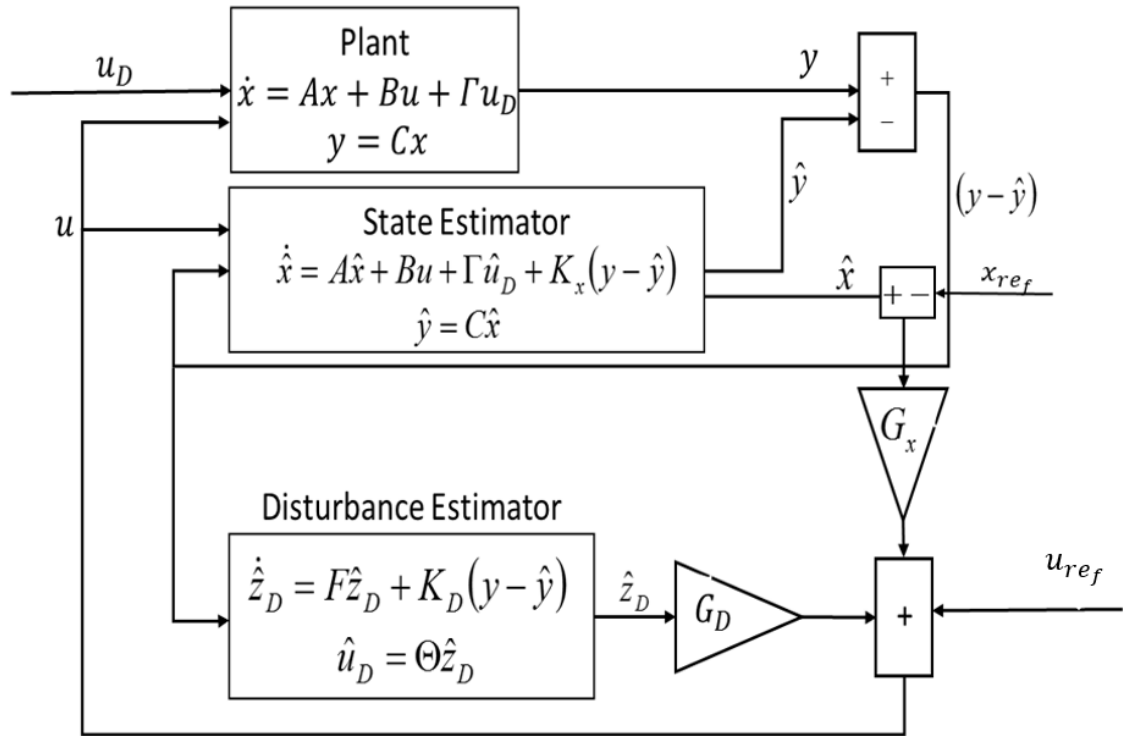
Figure 3.1. Schematic Diagram of Disturbance Accommodating Controller

The disturbance accommodating controller (DAC) was implemented on the linear lateral and longitudinal UAV dynamic models for the case in which there was a persistent 5

Hz sinusoidal disturbance. In the lateral case, this disturbance was modeled as a sinusoidal aileron input with an amplitude of 0.1 rad, while in the longitudinal case, the disturbance was modeled as a sinusoidal elevator input with amplitude of 0.1 rad. In this example, these sinusoidal inputs represent persistent, high-frequency external disturbances to the system, and the control objective was to regulate the UAV back to its lateral and longitudinal trim states in the presence of the disturbances. The lateral and longitudinal performance of the disturbance accommodating controller is depicted in Figures 3.2 and 3.3. For comparison purposes, an LQR controller was also implemented on the lateral and longitudinal models for the same case, the results of which are also shown in Figures 3.2 and 3.3. The results show that the disturbance accommodating controller successfully regulates the UAV back to trim, rejecting the disturbance inputs. In contrast, the standard LQR controller fails to reject the persistent disturbances.
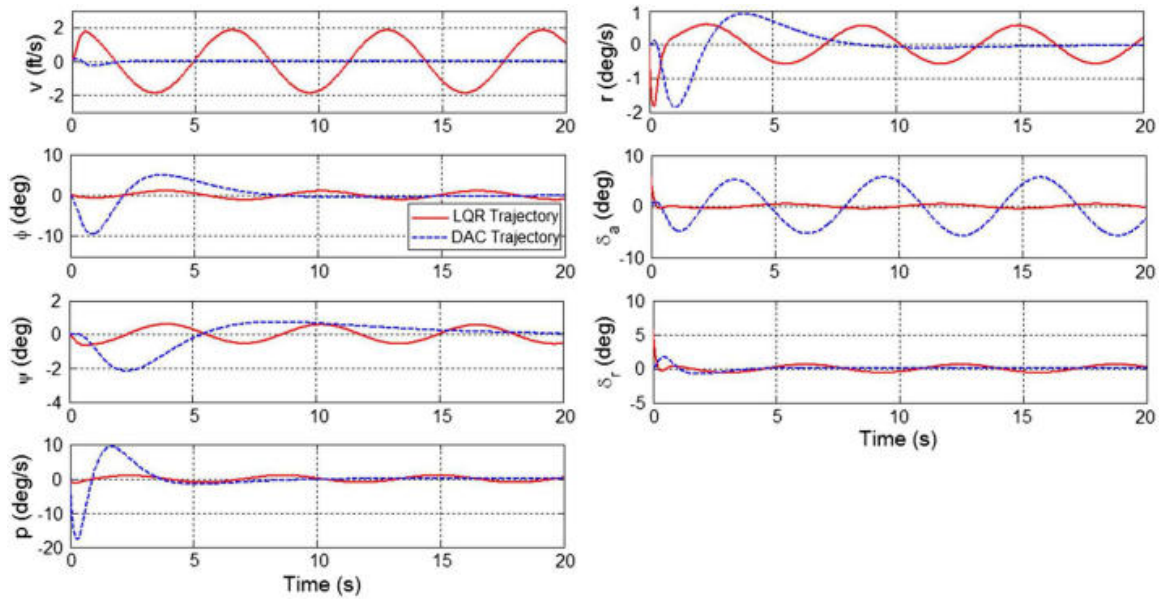
Figure 3.2. Lateral UAV Model Output for Sinusoidal Disturbance Case (DAC and LQR)
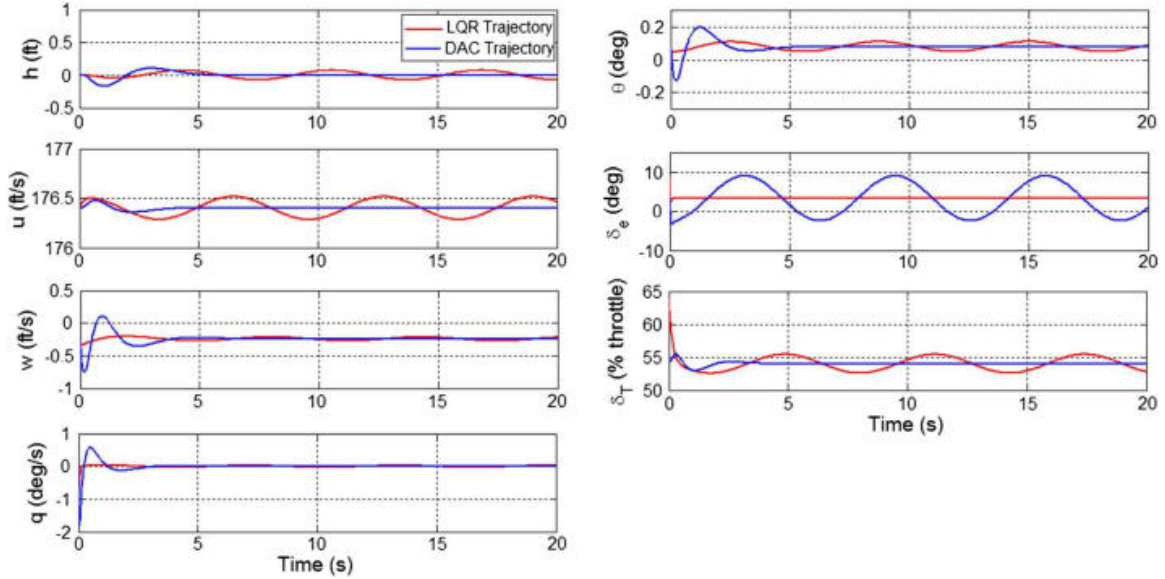
Figure 3.3. Longitudinal UAV Model Output for Sinusoidal Disturbance Case (DAC and LQR)

Figure 3.4 represents the results obtained from a longitudinal model using a disturbance accommodating controller for rejecting a persistent disturbance while tracking a reference trajectory. The states are tracked with minimal error and the elevator control deflection is within an acceptable range. Minimal change in the throttle is used to achieve these control objectives. Similar observations can be made from Figure 3.5 which depicts the results obtained from a lateral model using DAC with tracking capabilities.
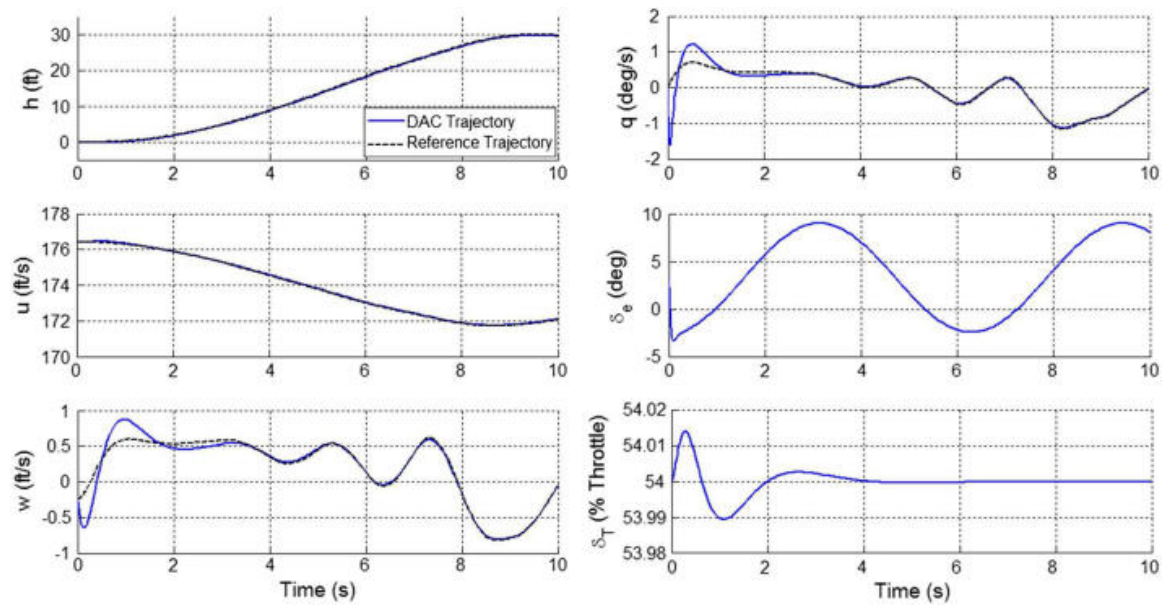
Figure 3.4. Longitudinal DAC: Tracking a Reference Climb Trajectory while Rejecting a Persistent Sinusoidal Disturbance
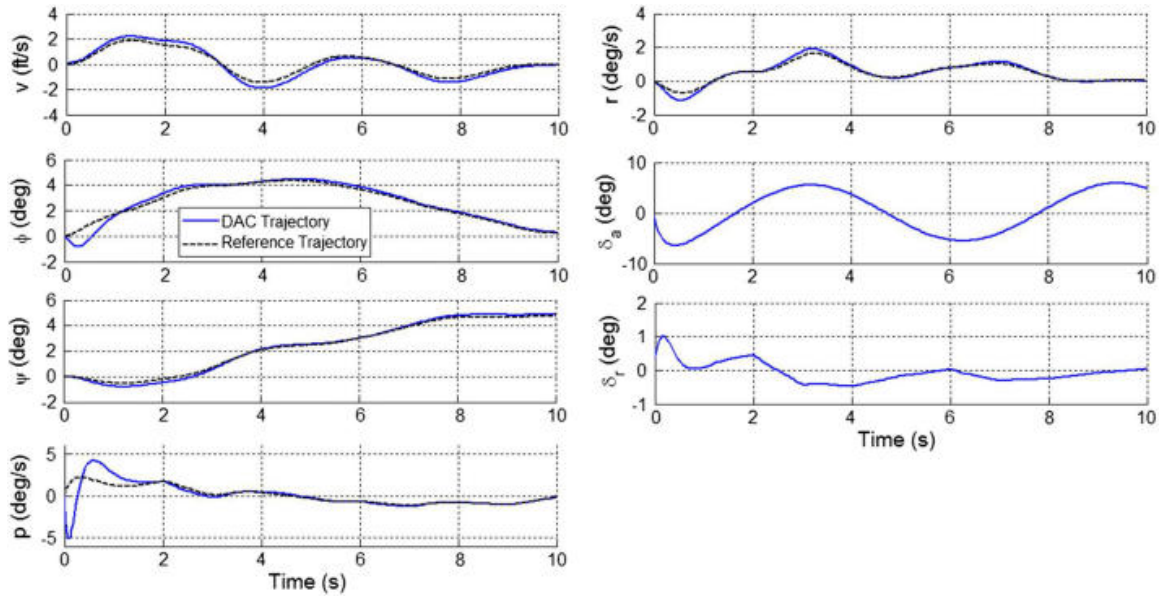
Figure 3.5. Lateral DAC: Tracking a Reference Turn Trajectory while Rejecting a Persistent Sinusoidal Disturbance

3.3 Direct Adaptive Controller for Trajectory Tracking and Disturbance Rejection

Although Disturbance Accommodating Control can provide a suitable solution to the UAV tracking application under certain conditions, as shown in Section 2.2, it does not solve all of the problems previously discussed. Specifically, the DAC requires substantial knowledge of the dynamics of the aircraft system to solve the matching conditions and find control gains for implementation. It also requires the matching conditions to be solved for different disturbance scenarios. There is no provision to account for any modeling error in the matching conditions; these limitations are detrimental to the implementation of this method to a UAV system.

Adaptive controllers use gains that adapt based on the changes in parameters or states of the system. Direct adaptive control is a direct feedback controller where the gains follow a highly nonlinear adaptation scheme depending on only the output of the system. The adaptation laws used in this research are derivatives of the algorithms developed by Fuentes et al (Fuentes & Balas, 2002). The adaptive control law can be represented as:

$$u = G_e e_y + G_m x_r + G_r u_r + G_D z_D \tag{3.21}$$

where the matrices G_e, G_m, G_r, and G_D are updated using the following adaptation laws

$$
\begin{aligned}
\dot{G}_e &= -e_y e_y^T \sigma_e; \sigma_e > 0 \\
\dot{G}_r &= -e_y x_r{}^T \sigma_u; \sigma_u > 0 \\
\dot{G}_u &= -e_y u_r^T \sigma_r; \sigma_r > 0 \\
\dot{G}_D &= -e_y z_D^T \sigma_D; \sigma_D > 0
\end{aligned}
\tag{3.22}
$$

Note that this implementation requires the input and output to have the same dimension. Therefore, the outputs chosen for the adaptive control implementation must match the control inputs.

We assume there exists an ideal linear plant that the UAV has to follow. The only requirement for the ideal model is that it must have of outputs as the linear UAV model.

The states of the ideal model are known whereas only the output of the UAV model is used in this implementation. Consider the linear UAV model:

$$\dot{x}(t) = Ax(t) + Bu(t) + \Gamma u_D; \quad y(t) = Cx(t) \tag{3.23}$$

and a reference model used to generate ideal trajectories:

$$\dot{x}_r = A_r x_r + B_r u_r; \quad y_r(t) = C_r x_r(t) \tag{3.24}$$

The objective of the controller is to achieve asymptotic output tracking (i.e $e_y \longrightarrow 0$ as $t \longrightarrow \infty$) while under the effect of persistent disturbances. To achieve this goal, ideal trajectories are introduced; the ideal trajectories $x_*(t)$ are generated via application of a pre specified ideal control $u_*(t)$. If the ideal trajectories exist, they will generate zero output tracking error e_y (Wen & Balas, 1989). The ideal trajectories are represented by:

$$\begin{bmatrix} x_* \\ u_* \end{bmatrix} = \begin{bmatrix} S_{11}^* & S_{12}^* & S_{13}^* \\ S_{21}^* & S_{22}^* & S_{23}^* \end{bmatrix} \begin{bmatrix} x_r \\ u_r \\ z_D \end{bmatrix} \tag{3.25}$$

Here, the ideal control generates these trajectories:

$$\dot{x}_*(t) = Ax_*(t) + Bu_*(t) + \Gamma u_D; \quad y_*(t) = Cx_*(t) = y_r \tag{3.26}$$

Substituting Equation 3.25 to Equation 3.26, the linear matching conditions are obtained,

$$AS_{11}^* + BS_{21}^* = S_{11}^* A_r$$

$$AS_{12}^* + BS_{22}^* = S_{12}^* F_r + S_{11}^* B_r$$

$$CS_{11}^* = C_r$$

$$CS_{12}^* = 0 \tag{3.27}$$

$$AS_{13}^* + BS_{23}^* + \Gamma\theta = S_{13}^* F$$

$$CS_{13}^* = 0$$

where, θ and F are the same values defined in equation 3.8.

Defining, $S_1 = \begin{bmatrix} S_{11}^* & S_{12}^* & S_{13}^* \end{bmatrix}$, $S_2 = \begin{bmatrix} S_{21}^* & S_{22}^* & S_{23}^* \end{bmatrix}$, $H_1 = \begin{bmatrix} 0 & 0 & -\Gamma\theta \end{bmatrix}$,

$H_2 = \begin{bmatrix} C_r & 0 & 0 \end{bmatrix}$ and $L_r = \begin{bmatrix} A_r & B_r & 0 \\ 0 & F_r & 0 \\ 0 & 0 & F \end{bmatrix}$. The matching conditions can be rewritten as:

$$AS_1 + BS_2 = S_1 L_r + H_1 \tag{3.28}$$

$$CS_1 = H_2$$

Equation 3.28 provides necessary and sufficient conditions for the existence of ideal trajectories in the form of 3.27. Solutions for the matching conditions must exist for the development of the direct adaptive controller, but in order to gurantee stablility to these conditions explicit solutions are not needed for controller design. If CB is nonsingular, per Balas et al (M. Balas & Fuentes, 2004), there exists an invertible linear operator W that is bounded

which can be used to convert the linear system into normal form. $W = \begin{bmatrix} C \\ (W_2)^T P_2 \end{bmatrix}$, where W_2 forms an orthonormal basis for the null space of C, N(C). The coordinate transformations $\bar{A} = WAW^{-1}$, $\bar{B} = WB$ and $\bar{C} = CW^{-1}$ results in converting the system into the normal form, which can be represented by:

$$\begin{aligned} \dot{y} &= \bar{A}_{11}y + \bar{A}_{12}z_2 + CBu \\ \dot{z}_2 &= \bar{A}_{21}y + \bar{A}_{22}z_2 \end{aligned}$$

(3.29)

The subsystem $(\bar{A}_{22}, \bar{A}_{12}, \bar{A}_{21})$ is called the zero dynamics systems of a linear state space system, and the eigenvalues of $\bar{A}_{22}$ are the transmission zeros of (A, B, C) (M. J. Balas & Frost, 2016). (M. J. Balas, 1995) rewrote the matching conditions Equation (27), multiplying them by W and substituting the normal form into the matching conditions to obtain:

$$\begin{aligned} S_2 &= (CB)^{-1}[H_2 L_r + \overline{H}_a - (\overline{A}_{11}H_2 + \overline{A}_{12}\overline{S}_b)] \\ \overline{S}_b L_r &= \overline{A}_{22}\overline{S}_b + (\overline{A}_{21}H_2 - \overline{H}_b) \end{aligned}$$

(3.30)

where $\bar{S}_1 = W S_1 = \begin{bmatrix} \bar{S}_a \\ \bar{S}_b \end{bmatrix}$ and $\bar{H}_1 = W H_1 = \begin{bmatrix} \bar{H}_a \\ \bar{H}_b \end{bmatrix}$. Equation 3.30 can be solved for a unique solution of S_b if and only if there are no shared eigenvalues between A_{22} and A_r, F_r and F (M. J. Balas, 1995). Considering the state tracking error $e_* \equiv x - x_*$, we also define $\Delta u \equiv u - u_*$. Using these definitions and Equations 3.23 and 3.26 the following results can be obtained:

$$\dot{e}_* = Ae_* + B\Delta u \tag{3.31}$$

A fixed gain controller ($u_p = u_* + G_e^* e_y$) is defined for analysis. Using the controller gains in Equation 3.23 combined with the ideal trajectories and output error vector e_y, we obtain the following:

$$\dot{e}_* = (A + BG_e^*C)e_* \tag{3.32}$$

For an adaptive system the gain G_e^* can change; therefore the only assumptions to be made about the system being controlled is controllability and observability. If the (A, B, C) system forms a controllable, observable pair, the eigenvalues of the closed loop system can be placed anywhere on the left half of the $j\omega$ axis, guaranteeing asymptotic tracking of the output.

Assume the system (A, B, C) is almost strictly dissipative (i.e. there exists a gain G_e^* that gives a strictly dissipative closed loop system[1] (A_c, B, C), where $A_c = A + BG_e^*C$) (Balas & Fuentes, 2004) and the disturbance basis ϕ_d is bounded. Then substituting Eq. 3.21 for u and 3.25 for u_* the following results are obtained:

$$
\begin{aligned}
\Delta u = u - u_* &= (G_r x_r + G_u u_r + G_e e_y + G_D z_D) - (S_{21}^* x_r + S_{22}^* u_r + S_{23}^* z_D) \\
&= G_e^* e_y + \Delta G_e e_y + \begin{bmatrix} \Delta G_r & \Delta G_u & \Delta G_D \end{bmatrix} \begin{bmatrix} x_r \\ u_r \\ z_D \end{bmatrix} = G_e^* e_y + \Delta G \eta
\end{aligned}
\tag{3.33}
$$

Here, we define $\Delta G = G - G_*$; $G = \begin{bmatrix} G_e & G_r & G_u & G_D \end{bmatrix}$; $G_* = \begin{bmatrix} G_e^* & S_{21}^* & S_{22}^* & S_{23}^* L \end{bmatrix}$ and $\eta = \begin{bmatrix} e_y & x_r & u_r & z_D \end{bmatrix}^T$. Then the tracking error system becomes $\dot{e}_* = A_c e_* + B\Delta G \eta$

---

[1]A strictly dissipative is defined as a system which dissipates its internal energy. For finite dimensional linear systems, strict dissipativity and strictly positive real can be used interchangeably (Balas & Frost, 2015)

and $e_y = Ce_*$. This system with the adaptive gain law $\dot{G} = -e_y\eta^T\sigma$ will produce asymptotic tracking, which is illustrated below by using the Lyapunov functions and Barbalat lemma below, here $\sigma = \begin{bmatrix} \sigma_e & 0 & 0 & 0 \\ 0 & \sigma_r & 0 & 0 \\ 0 & 0 & \sigma_u & 0 \\ 0 & 0 & 0 & \sigma_D \end{bmatrix}$.

To determine the closed loop stability of the adaptive system, Lyapunov theory is employed and two positive definite functions are formed. Let $V_1(e_*) \equiv \frac{1}{2}e_*^T P e_*$ and $V_2(\Delta G) = \frac{1}{2}tr(\Delta G\sigma^{-1}\Delta G^T)$, where $P > 0$ is the solution to the Kalman-Yakubovich-Popov Conditions, which are specified as:

$$
\begin{aligned}
\dot{V}_1(e_*) &= \frac{1}{2}e_*^T P[A_c e_* + Bw] + \frac{1}{2}[A_c e_* + Bw]^T P e_* \\
&= \frac{1}{2}e_*^T[PA_c + A_c^T P]e_* + e_*^T \underbrace{PB}_{C^T} w \\
&= -\frac{1}{2}e_*^T Q e_* + e_*^T w, C^T = 1.
\end{aligned}
\tag{3.34}
$$

where, $w = \Delta G\eta$. The derivative of V_2 gives the following results along the trajectory:

$$
V_2(\Delta G) = \frac{1}{2}tr(\Delta G\sigma^{-1}\Delta G^T)
\tag{3.35}
$$

$$
\dot{V}_2(\Delta G) = \frac{1}{2}tr(\Delta\dot{G}\sigma^{-1}\Delta G^T + \Delta G\sigma^{-1}\Delta\dot{G}^T) = tr(\Delta\dot{G}\sigma^{-1}\Delta G^T)
\tag{3.36}
$$

From the structure of the adaptive system, we know that $\dot{G} = -e_y\eta^T\sigma$; therefore:

$$
\dot{V}_2(\Delta G) = tr(-e_*\eta^T\sigma\sigma^{-1}\Delta G^T) = -tr(-e_*\underbrace{\eta^T\Delta G^T}_{w^T}) = -tr(-e_* w^T)
\tag{3.37}
$$

using the properties of trace tr(a b)=tr(b a) we can rewrite the above result as $-tr(w^T e_*)$

which is a scalar quantity, and therefore the above equation takes the form:

$$\dot{V}_2(\Delta G) = -w^T e_* = -e_*{}^T w \tag{3.38}$$

Adding the results of Equations 3.34 and 3.38 it can be proven that the Lyapunov The-

ory guarantees the stability of the zero equilibrium point of Equation 3.32 and that all

trajectories of the system will be bounded. This also guarantees the boundedness of e_* and

ΔG.

$$V = V_1 + V_2 \equiv \dot{V} = \dot{V}_1 + \dot{V}_2 \tag{3.39}$$

$$\dot{V} = -\frac{1}{2} e_*{}^T Q e_* \rightarrow \dot{V} \leq 0 \tag{3.40}$$

3.4   Sensor Blending of Non-Minimum Phase Systems

There are a few assumptions made in proving the stability of the direct adaptive con-

troller in the previous section. They are as follows:

- $CB \geq 0$

- (A, B, C) is almost strictly positive real (i.e. all transmission zeros of the system

  are stable). This implies that $P(s) = C(sI - A_c)^{-1}B$ is strictly positive real or

  minimum phase system.

- Eigenvalues of the reference model and disturbance model do not coincide with the

  transmission zeros (eigenvalues of A_{22}) of the system.

- Basis functions of the disturbance z_D are bounded.

- The reference model A_r is stable.

- All reference trajectories are bounded.

The stability of the closed loop system has already been proven, which guarantees the boundedness of the trajectories and tracking. Further, Barbalat's Lemma can be applied to the system to prove asymptotic tracking of the errors, $e_* \to 0$ and $e_y \to 0$ as $t \to \infty$ (Frost et al., 2009).

One of the main requirements for implementation of the adaptive control system is the realization of minimum phase. Aircraft systems however are generally categorized as non-minimum phase systems (i.e. they have neutrally stable or unstable transmission zeros). To mitigate this problem (Balas and Frost, 2017) developed a systematic approach to stabilize the unstable transmission zeros of a non-minimum phase system known as Sensor Blending.

3.4.1 Sensor Blending Formulation

The lateral and longitudinal UAV models employed in this research, and aircraft models in general, are non-minimum phase systems. Therefore, the UAV models do not satisfy an important condition required for the stability of the adaptive controller. In order to address non-minimum phase systems, the sensor blending process entails generating a new system

output $y_\Delta \in \Re$ corresponding to a linear combination of the original outputs $y \in \Re$ (i.e., the sensor measurements):

$$y_\Delta = C_\Delta x = (C + \Delta C)x \tag{3.41}$$

The blended output is designed so that the resulting transfer function $P(s) = C_\Delta (sI - A)^{-1}$ is minimum phase, making it possible to guarantee the stability of the adaptive control system.

The sensor blending process entails first transforming the linear time-invariant UAV models into normal form. (M. Balas & Fuentes, 2004) showed that if CB is nonsingular, then there exists a projection $P_1 = B(CB)^{-1}C$ onto the range of B along the null space of C. A projection $P_2 = (I - P_1)$ can then be defined as the complement of the projection P_1. The transformation to the normal form is then defined in terms of the nonsingular matrix W:

$$z = \begin{bmatrix} y \\ z_2 \end{bmatrix} = Wx, \ W = \begin{bmatrix} C \\ W_2{}^T P_2 \end{bmatrix} \tag{3.42}$$

where $W_2 = Q_2{}^T P_2$ and the columns of Q_2 form a basis for the null space of C. The normal form is then defined as

$$\dot{z} = \bar{A}z + \bar{B}u, \ y = \bar{C}z \tag{3.43}$$

where the transformed system matrices are given by

$$\bar{A} = WAW^{-1} = \begin{bmatrix} \bar{A}_{11} & \bar{A}_{12} \\ \bar{A}_{21} & \bar{A}_{21} \end{bmatrix}$$

$$\bar{B} = WB = \begin{bmatrix} CB \\ 0 \end{bmatrix} \tag{3.44}$$

$$\bar{C} = CW^{-1} = \begin{bmatrix} I_p & 0 \end{bmatrix}$$

The state equation in normal form can then be written as

$$\dot{y} = \bar{A}_{11}y + \bar{A}_{12}z_2 + CBu$$

$$\dot{z}_2 = \bar{A}_{21}y + \bar{A}_{22}z_2 \tag{3.45}$$

Eq. 3.45 represents the zero dynamics of the LTI system, which are invariant under transformation. The transmission zeros $Z(A, B, C)$ of an LTI system are given by (Kailath, n.d.):

$$Z(A, B, C) = \left\{ \lambda \mid H(\lambda) \equiv \begin{bmatrix} A - \lambda I & B \\ C & 0 \end{bmatrix} \ is \ singular \right. \tag{3.46}$$

The transmission zeros correspond to the eigenvalues of the sub matrix $\bar{A}_{22}$ in the normal form (M. J. Balas & Frost, 2016). That is, $Z(A, B, C) = \sigma(\bar{A}_{22})$. It should be emphasized that the transmission zeros cannot be altered using output feedback. Therefore, (M. J. Balas & Frost, 2017) showed that, for cases in which there are unstable or neutrally stable trans-

mission zeros, a blended output $y_\Delta = C_\Delta x = (C + \Delta C)x$ can be derived that yields stable

transmission zeros of the form:

$$Z(A, B, C) = \left\{ \lambda \mid H(\lambda) \equiv \begin{bmatrix} A - \lambda I & B \\ C + \Delta C & 0 \end{bmatrix} = H(\lambda) + \begin{bmatrix} 0 & 0 \\ \Delta C & 0 \end{bmatrix} \right. \tag{3.47}$$

This is accomplished by first decomposing the second equation in the normal form given

in Eq. 3.45 into stable and unstable subsystems:

$$\begin{bmatrix} \dot{z}_2^s \\ \dot{z}_2^u \end{bmatrix} = \begin{bmatrix} \bar{A}_{22}^s & 0 \\ 0 & \bar{A}_{22}^u \end{bmatrix} + \begin{bmatrix} \bar{A}_{21}^s \\ \bar{A}_{21}^u \end{bmatrix} y \tag{3.48}$$

where $\sigma(\bar{A}_{22}) = \sigma(\bar{A}_{22}^s) \cup \sigma(\bar{A}_{22}^u)$ with $\sigma(\bar{A}_{22}^s)$ denote the stable eigenvalues of $\bar{A}_{22}$ (i.e,

the stable transmission zeros) and $\sigma(\bar{A}_{22}^u)$ represent the stable eigenvalues (i.e, the unstable

transmission zeros). In Theorem 6 from (M. J. Balas & Frost, 2017), the authors show that

if CB is nonsingular and the pair $(\bar{A}_{22}^u, \bar{A}_{21}^u)$ is controllable, then there exists a ΔC such

that for all $Re(\lambda) \geq 0$, $H_\Delta(\lambda)$ as defined in Eq. 3.47 is invertible. In other words, under

these conditions, a blended output $y_\Delta = C_\Delta x = (C + \Delta C)x$ exists such that the resulting

transmission zeros $Z(A, B, C + \Delta C)$ are all stable. A blended output can then be derived

by computing a feedback matrix K_Δ such that $\sigma(\bar{A}_{22}^u - \bar{A}_{21}^u K_\Delta)$ is stable. The blending

matrix ΔC can then be computed as $\Delta C = K_\Delta Q_2^T P_2$. It should be noted that the blending

process does not alter CB (i.e., $C_\Delta B \equiv (C + \Delta C)B = CB$).

3.4.2 Implementation of Sensor Blending to the UAV model

Both the lateral and longitudinal LTI models employed in this work have $m = 2$ control inputs; therefore, the lateral and longitudinal adaptive control design required $p = m = 2$ outputs. These sensor outputs, which were selected to ensure that CB is nonsingular in each case, corresponded to the side velocity Δv and roll rate Δp in the lateral case and the forward velocity Δu and the pitch rate Δq in the longitudinal case:

$$\begin{bmatrix} \Delta v \\ \Delta p \end{bmatrix} C_{lat} = \begin{bmatrix} 1 & 0 & 0 & 0 & 0 \\ 0 & 0 & 0 & 1 & 0 \end{bmatrix} \begin{bmatrix} 12.51 & 0 \\ -29.06 & 23.20 \end{bmatrix} \tag{3.49}$$

$$\begin{bmatrix} \Delta u \\ \Delta q \end{bmatrix} C_{long} = \begin{bmatrix} 0 & 1 & 0 & 0 & 0 \\ 0 & 0 & 0 & 0 & 1 \end{bmatrix} \begin{bmatrix} -0.04 & 7.30 \\ -11.93 & 0 \end{bmatrix} \tag{3.50}$$

Given these sensor outputs, the transmission zeros for the lateral and longitudinal systems are given by

$$Z_{lat}(A_{lat}, B_{lat}, C_{lat}) = 0, -0.0002, -86.10 \tag{3.51}$$

$$Z_{long}(A_{long}, B_{long}, C_{long}) = 0, 0, -1.909 \tag{3.52}$$

Clearly, neither system is minimum phase due to the presence of transmission zeros at 0. In the lateral case, there are 2 stable transmission zeros and 1 neutrally stable transmission zero; therefore, sensor blending is required to relocate the neutrally stable zero into the left-half (stable) plane. In the longitudinal case, there is 1 stable transmission zero and 2 neutrally stable transmission zeros, both of which need to be moved to the left-half plane

using the sensor blending process. In both the lateral and longitudinal cases, the Bass-Gura

numerical algorithm (Nelson, 2008) is employed to generate the feedback matrices required

to place the neutrally stable zeros into the left-half plane. In the lateral case, the 1 neutrally

stable zero is placed at $\bar{z}_1 = -1$ while in the longitudinal case, the 2 neutrally stable zeros

are placed at $\bar{z}_1 = \bar{z}_2 = -1$. This results in the following blended output equations:

$$y_{\Delta lat} = C_{\Delta lat}\Delta x_{lat} = \begin{bmatrix} 1.012 & 0.007 & -0.032 & 0.005 & 0.0246 \\ -0.033 & 1 & 0.0024 & 0.986 & -0.069 \end{bmatrix} \begin{bmatrix} \Delta v \\ \Delta \phi \\ \Delta \psi \\ \Delta p \\ \Delta r \end{bmatrix} \quad (3.53)$$

$$y_{\Delta long} = C_{\Delta long}\Delta x_{long} = \begin{bmatrix} 0.0025 & 1 & -0.0013 & 1.1011 & 0.0031 \\ 0.0057 & 0 & 0.003 & 2.524 & 1.007 \end{bmatrix} \begin{bmatrix} \Delta h \\ \Delta u \\ \Delta w \\ \Delta \theta \\ \Delta q \end{bmatrix} \quad (3.54)$$

It is easily confirmed that the CB matrices are unaltered by the sensor blending process. The

blended outputs result in minimum phase lateral and longitudinal systems; however, the

use of blended outputs results in the adaptive control system tracking the blended outputs

instead of the original reference outputs. As a final implementation note, CB_{long} in Eq.

3.50 is not positive definite. This is addressed by employing an equivalent input matrix $\hat{B}_{long} = B_{long}(CB)_{long}^{-1}$, which results in $C\hat{B} = I$, which clearly is positive definite.

The controllability and observability of the system are important metrics in determining what states can be stabilized. The direct adaptive control implementation does not effect the B matrix; therefore the controllability of the system is not effected. Observability of the system can be affected, however, by the sensor blending process as there are changes in the C matrix (even though the changes are small). A check needs to be put into place to account for any such occurrence; during this implementation both the longitudinal and lateral observability matrices remained full rank.

3.5 Stability Margins and Robustness w.r.t Aircraft Dynamics

In order to analyze the relationship between the aircraft dynamics and stability of the direct adaptive controller a symbolic approach was devised. The 6 DoF nonlinear aircraft equations were derived but the aerodynamic stability coefficients were left as variables. The nonlinear model was then linearized at the trim conditions provided in Equation 3.4 and the lateral and longitudinal models were separated, providing two state space matrices with variable aero-coefficients. It should be noted that only the A matrix in this state space model is in the variable form. The B and the C matrices are assumed to be constant as they represent the sensors and actuators, which are well defined. Only the magnitudes of the aero-coefficients are chosen as variables, the signs are kept as designated by standard aircraft design (e.g $C_{M\alpha}$ is input as $-'C_{M\alpha}'$ to account for the negative pitching moment). The longitudinal A matrix is defined as follows:

$$\left[A_{Longitudinal}\right] = \begin{bmatrix} A_{11} & A_{12} & A_{13} & A_{14} & A_{15} \end{bmatrix}$$

$$\text{where, } \left[A_{11}\right] = \begin{bmatrix} 1.253e^{-3}C_{D\alpha} + 1.739e^{-6}C_{L\alpha} - 1.289e^{-6}C_{L\delta e} - 6.807e^{-2} \\ 1.253e^{-3}C_{L\alpha} - 1.739e^{-6}C_{D\alpha} - 9.286e^{-9}C_{L\delta e} - 3.703e^{-1} \\ 8.979e^{-9}C_{D\alpha} - 6.471e^{-6}C_{L\alpha} + 4.794e^{-6}C_{L\delta e} + 1.912e^{-3} \\ 0 \\ -0.001388 \end{bmatrix}$$

$$\left[A_{12}\right] = \begin{bmatrix} 4.643e^{-4}C_{L\delta e} - 1.253e^{-3}C_{L\alpha} - 0.4517C_{D\alpha} + 1.852e^{-1} \\ 1.253e^{-3}C_{D\alpha} - 0.4517C_{L\alpha} - 6.443e^{-7}C_{L\delta e} - -2.284e^{-1} \\ 2.33e^{-3}C_{L\alpha} - 6.471e^{-6}C_{D\alpha} + 3.326e^{-9}C_{L\delta e} - 0.0732 * C_{M\alpha} + 1.1e^{-5} \\ 0 \\ -1 \end{bmatrix}$$

$$\left[A_{13}\right] = \begin{bmatrix} 0.2448 - 0.001786C_{Lq} \\ 176.4 - 1.287C_{Lq} \\ 0.006646C_{Lq} - 0.2089C_{Mq} - 0.9107 \\ 1 \\ 0 \end{bmatrix}$$

$$\left[A_{14}\right] = \begin{bmatrix} -32.2 \\ 0.04468 \\ -0.0002307 \\ 0 \\ 176.4 \end{bmatrix} \quad \left[A_{15}\right] = \begin{bmatrix} 0 \\ 0 \\ 0 \\ 0 \\ 0 \end{bmatrix}$$

Note: $C_{L\delta e}$ appears in this formulation as a part of a C_{Ltrim} term that is part of the linear longitudinal model.

The lateral state space matrix is given below:

$$\left[A_{Lateral}\right] = \begin{bmatrix} -0.4517C_{Y\beta} & -0.2448 & 7.543C_{Yr}-176.4 & 32.2 & 0 \\ -1.229C_{l\beta} & -20.53C_{lp} & 20.53C_{lr} & 0 & 0 \\ 0.365C_{n\beta} & -6.095C_{np} & -6.095C_{nr} & 0 & 0 \\ 0 & 1.0 & -0.001388 & 0 & 0 \\ 0 & 0 & 1.0 & 0 & 0 \end{bmatrix}$$

The C matrix is then chosen in accordance with the conditions discussed in Section 3.4. The following mathematical operations are then performed to transform these state space systems into the normal form.

$$Q_2 = N(C) = sp(\phi_1, \phi_2, \phi_3) \tag{3.55}$$

The null space of C is calculated which is later used to define the transformation matrix. The next step is to define a non-orthogonal projection P_1 onto the range of B along with the null space of C.

$$P_1 = B(CB)^{-1}C; P_2 = I - P_1 \tag{3.56}$$

Here $R^n = R(B) \oplus N(C)$. The transformation matrix W is then defined as:

$$W = \begin{bmatrix} C \\ W_2 \end{bmatrix} \tag{3.57}$$

where, $W_2 = Q_2^T P_2$. If CB is nonsingular then the transformation matrix W satisfies $W^{-1} = \begin{bmatrix} Q_1 & Q_2 \end{bmatrix} \ni WB = \begin{bmatrix} CB \\ 0 \end{bmatrix}$ and $CW^{-1} = \begin{bmatrix} I_m & 0 \end{bmatrix}$. This is then used to transform the system into the normal form which is given by:

$$\dot{y} = \bar{A}_{11}y + \bar{A}_{12}z_2 + CBu$$
$$\dot{z}_2 = \bar{A}_{21}y + \bar{A}_{22}z_2 \tag{3.58}$$

This is achieved by the following operations:

$$\bar{A}_{11} = CAQ_1, \ \bar{A}_{12} = CAQ_2, \ \bar{A}_{21} = W_2AQ_1, \ \bar{A}_{22} = W_2AQ_2 \tag{3.59}$$

$(\bar{A}_{22}, \bar{A}_{12}, \bar{A}_{21})$ becomes the zero dynamics system for the initial state space system. This implies that the eigenvalues of $\bar{A}_{22}$ are the transmission zeros of the (A,B,C) system as previously discussed in Section 3.4. According to the requirements to guarantee stability of the direct adaptive system the transmission zeros of the state space system should be stable; as previously discussed the eigenvalues of $\bar{A}_{22}$ are the transmission zeros. These eigenvalues for the longitudinal and the lateral system are given below:

$$\lambda_{Long_1} = 0.001269C_{D\alpha} - 0.4573C_{L\alpha} - 6.522*10^{-7}C_{L\delta e} + 0.1759C_{M\alpha} - 0.02312 \quad (3.60)$$

$$\lambda_{Long_2} = 0.2715C_{L_q} - 0.1044C_{M_q} \pm 0.5(0.2949C_{L_q}^2 - 0.2269C_{L_q}C_{M_q}$$
$$+0.04363C_{M_q}^2 + 31.09C_{M_q} + 5539)^{1/2} - 37.21 \quad (3.61)$$

$$\lambda_{Lat_1} = 1.452C_{Yr} - 0.07959C_{lr} - 3.048C_{nr} \pm 0.5(8.431C_{Yr}^2 - 0.9244C_{Yr}C_{lr} -$$

$$35.4C_{Yr}C_{nr} - 394.4*C_{Yr} + 0.02534C_{lr}^2 + 1.94C_{lr}C_{nr} + 21.62C_{lr} + 37.15C_{nr}^2 +$$

$$827.8C_{nr} + 4611.0)^{1/2} - 33.95$$

$$(3.62)$$

$$\lambda_{Lat_2} = 0.02476C_{l_b} - 0.4517C_{Y_b} + 0.9481C_{n_b} \quad (3.63)$$

$$\lambda_{Lat_3} = 393.1C_{n_p} - 10.27C_{l_p} - \pm 0.5(421.5C_{l_p}^2 - 32288C_{l_p}C_{n_p} -$$
$$499C_{l_p} + 6.18x10^5C_{n_p}^2 + 19111C_{n_p} - 6247)^{1/2} + 6.076 \quad (3.64)$$

Different choices of the output matrix C which correspond to different combination of

outputs, yield different transmission zeros. There are two different C values that produce

a positive definite CB for the longitudinal case and three values of C for the lateral case. Although there are five different transmission zero values for this system, they all follow one of two patterns: one is a linear combination of stability derivatives, whereas the other is a polynomial nonlinear combination. Only the non-zero transmission zeros are discussed here. There are two zero eigenvalues for the linear combination (Eq. 3.60, 3.63) and one for the nonlinear one (Eq. 3.61, 3.62, 3.64). The zero eigenvalues can be placed into the left half of the real axis to make them stable by designing a state feedback controller for the pair $(\bar{A}_{22}, \bar{A}_{12})$ using the Bass Gura method to compute the gain matrix given that the $(\bar{A}_{22}, \bar{A}_{12}, \bar{A}_{21})$ system forms a controllable, observable pair. The robustness and stability can therefore be determined from evaluating Equations 3.60 - 3.64.

Since the linear equations already have two zero transmission zeros, the sensor blending technique needs to performed to stabilize those zeros. Since sensor blending does not affect the other zeros of the system the stability of the longitudinal system can solely be determined by Equations 3.60 and 3.63. The criteria for stability of the longitudinal system therefore is met as long as the output of the equation is less than zero, since the other two transmission zeros have already been stabilized. Meanwhile the nonlinear polynomial equations only have one eigenvalue at zero, which needs to be stabilized. Equations 3.61, 3.62, and 3.64 are of the form $A \pm \sqrt{B}$ which extends into two possibilities, if $B < 0$ or $B > 0$. For the first case $B < 0$, the eigenvalues come out to be a complex conjugate pair, but the complex part can be neglected as the real part of the eigenvalue dictates their stability measure. Therefore, the only consideration in this case would be to check if $A < 0$. On the other hand, if $B > 0$ the whole equation needs to considered.

3.5.1   Augmenting Handling Capabilities of Poorly Handling UAVs

The Cooper-Harper handling capabilities (Cooper & Harper Jr, 1969) are a qualitative assessment of the dynamic behavior of an aircraft being controlled by a pilot. Pilot input was used to create a range of optimal flight characteristics for various longitudinal and lateral modes. The idea behind this analysis is to augment the qualitative characteristics of a poorly handling aircraft by the use of a linear reference system that satisfies the required handling characteristics. This will generate an ideal trajectory for the adaptive control system to follow.

As an example, the coupled lateral-directional oscillation of an aircraft, also known as dutch roll is considered. Dutch roll is a combination of rolling and yawing motion; it is one of the main dynamical modes of the lateral system (spiral and roll convergence being the others). According to the Cooper-Harper criteria, to attain a Level 1 flight category for a small general aviation aircraft, the minimum dutch roll damping should be ≥ 0.19 and the natural frequency should be ≥ 1 rad/sec (Cooper & Harper Jr, 1969). Let us assume an aircraft with lateral dynamic behavior that is not up to this standard. This assumption can be enacted by using a value of C_{nr} that is 70% of its original value. This change in the magnitude of C_{nr} makes the aircraft lose its Level 1 handling characteristics as can be observed from the damping value of 0.05479 from Table 3.5. The previous section described the transmission zeros and how they relate to the stability coefficients. These equations can now be used to determine the stability of the controller in this case where there is a change in C_{nr}.

Table 3.5. Dutch Roll Characteristics with Changing C_{nr}

C_{nr}	Eigenvalues	Damping	Frequency
-0.125	$-0.498 \pm 2.36i$	0.206	2.41 rad/s
-0.09	$-0.128 \pm 2.34i$	0.0547	2.34 rad/s
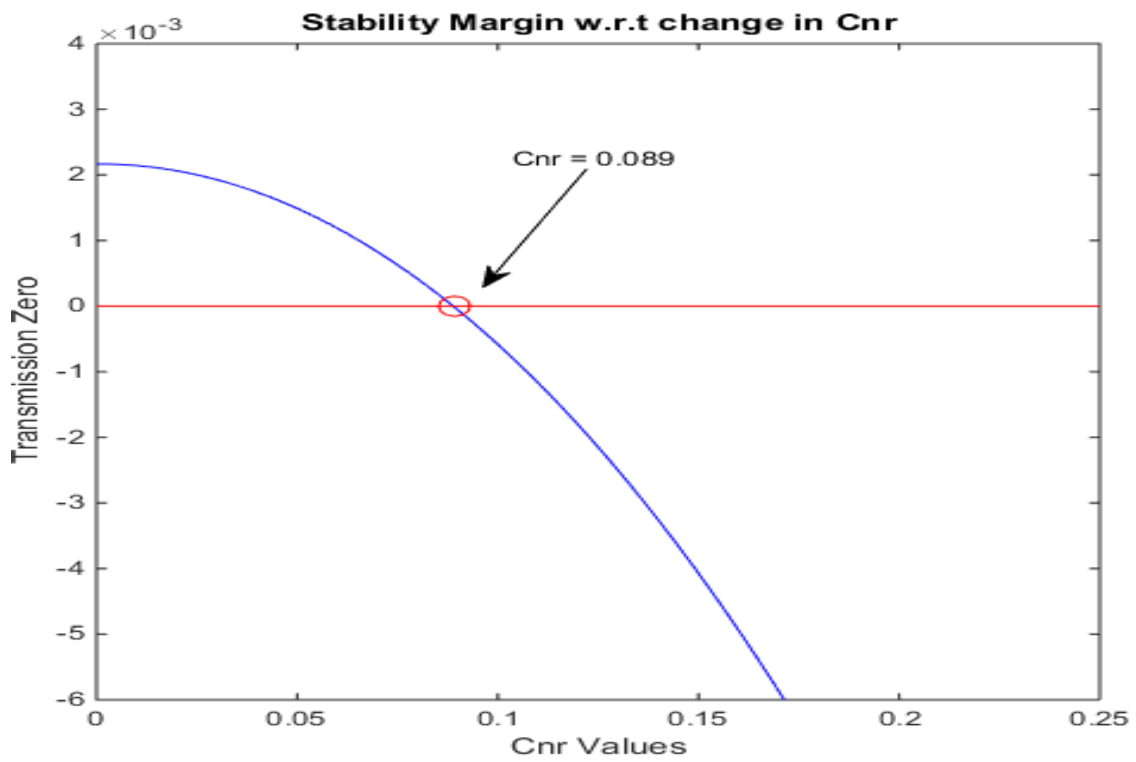
Figure 3.6. Stability of Transmission Zeros w.r.t varying C_{nr}

Using Equation 3.62, which corresponds to the output matrix C used during the sensor blending, a stability margin can be developed. This margin will quantify the stability of the adaptive system taking into account the erroneous value of C_{nr}. Using the values

of C_{Yr} and C_{lr} from Table 3.2 and varying the values of C_{nr} to sweep a 200% range in magnitude, a graph for the change in transmission zeros can be plotted. This graph can then be used to find a range of C_{nr} that attains a stable transmission zero. Figure 3.6 provides an example of this method while using Equation 3.62. It can be observed that any value of $C_{nr} > 0.089$ will result in a stable transmission zero, which in turn guarantees stability of the adaptive system. This method can be extended for creating a Monte-Carlo simulation for determining the range of stability derivatives that will confine the transmission zeros to be stable. This example shows the potential of direct adaptive control to augment the perceptive dynamics of an aircraft.

The example used above can be illustrated by simulating an aircraft with low C_{nr} as described in Table 3.5. A linear aircraft simulation is set up and a joystick is used to simulate pilot input. Aileron, elevator, and rudder doublets are applied to the system, which generate the ideal trajectories that the adaptive controller is made to follow. The adaptive controller follows this reference while the system is injected with a persistent disturbance (simulating gusts/disturbance). Figure 3.7 is a depiction of the persistent disturbance that is being induced into the system. It is modeled as a dynamic change encountered by the aircraft states equivalent to a sinusoidal wave of 1.5 degrees deflection on the elevator and a complex pulse superimposed with a sinusoidal wave on the aileron.

Pilot inputs, depicted by Figure 3.8 are sent as control inputs to the reference model. This reference model outputs an ideal trajectory which is used to generate the output error e_y as defined in Equation 3.21. The adaptive system then uses this output error to calculate the adaptive gains. In this simulation, three doublets are introduced into the system at 10
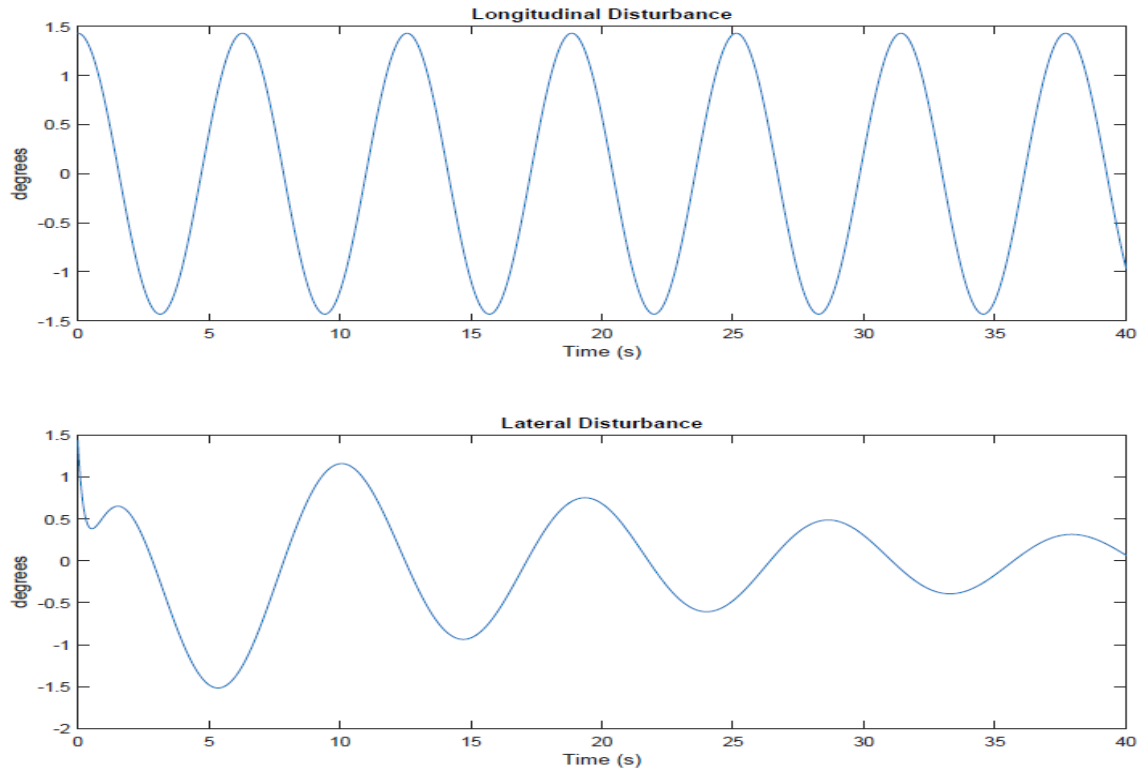
Figure 3.7. Disturbance Models for Persistent Disturbances Injected into the System

second intervals. This is done to excite all the underlying modes of the aircraft. The final results showcasing the performance of the controller are shown in Figures 3.9 and 3.10.

As can be observed from the figures, the adaptive system is able to track the given reference (Level 1 handling quality). This implies that the poor dutch roll mode of the aircraft was augmented by the adaptive system, while guaranteeing the stability of the system. The difference between the pilot inputs and the control effort generated by the adaptive controller can be observed by comparing Figure 3.8 and Figure 3.12 and 3.12.
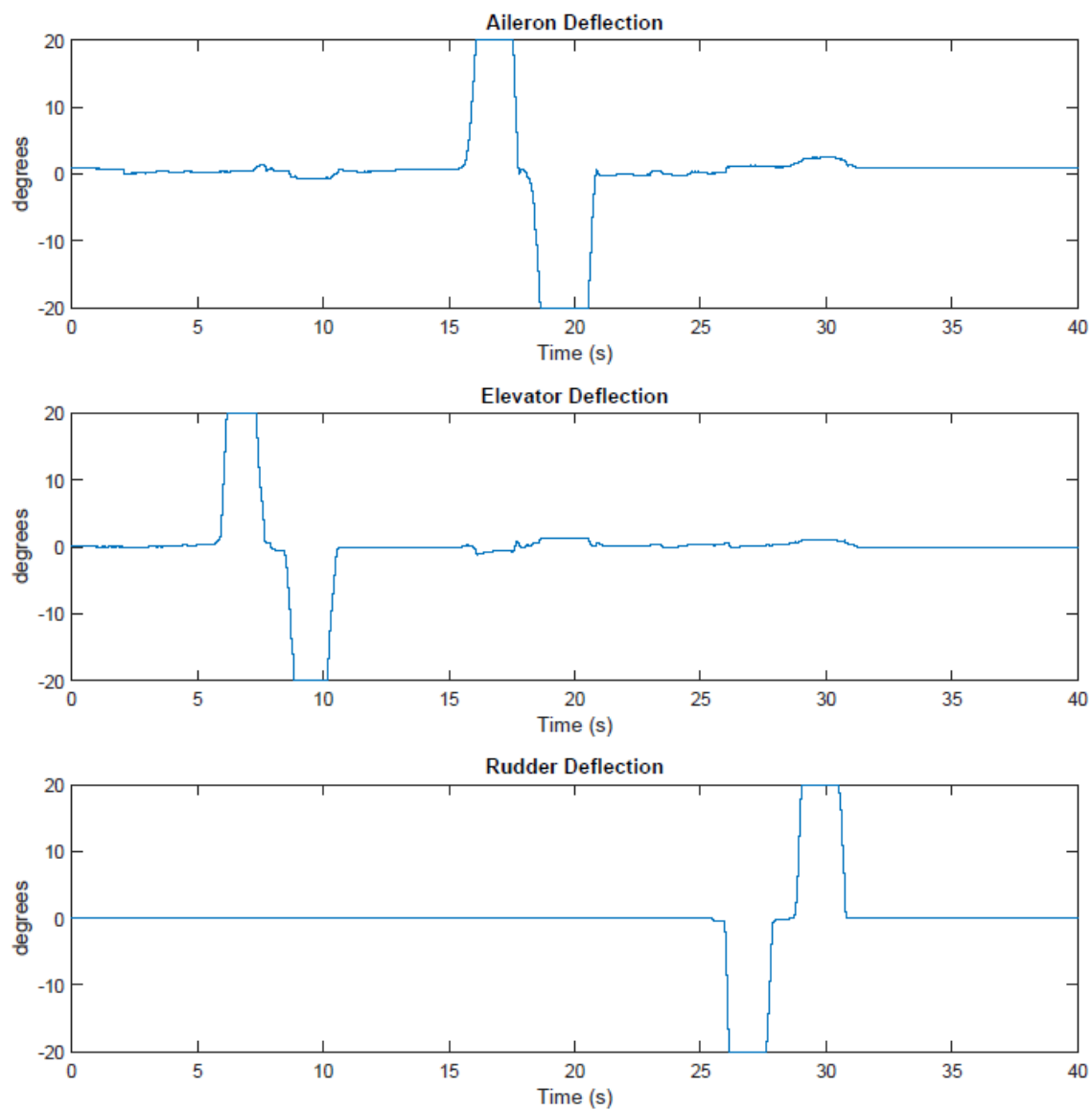
Figure 3.8. Pilot Input for Reference Trajectory Generation
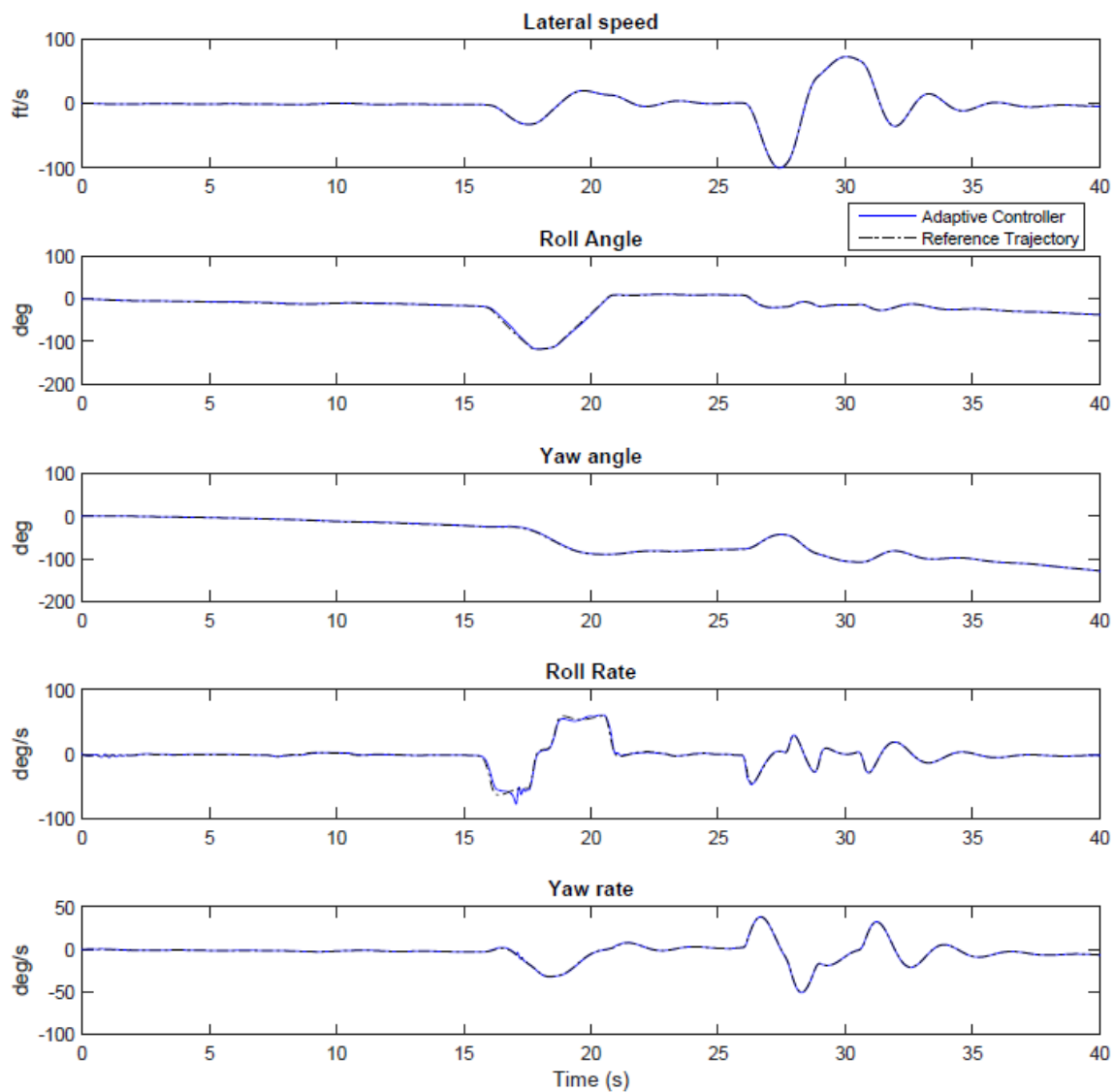
Figure 3.9. Lateral States while Following Reference Trajectory
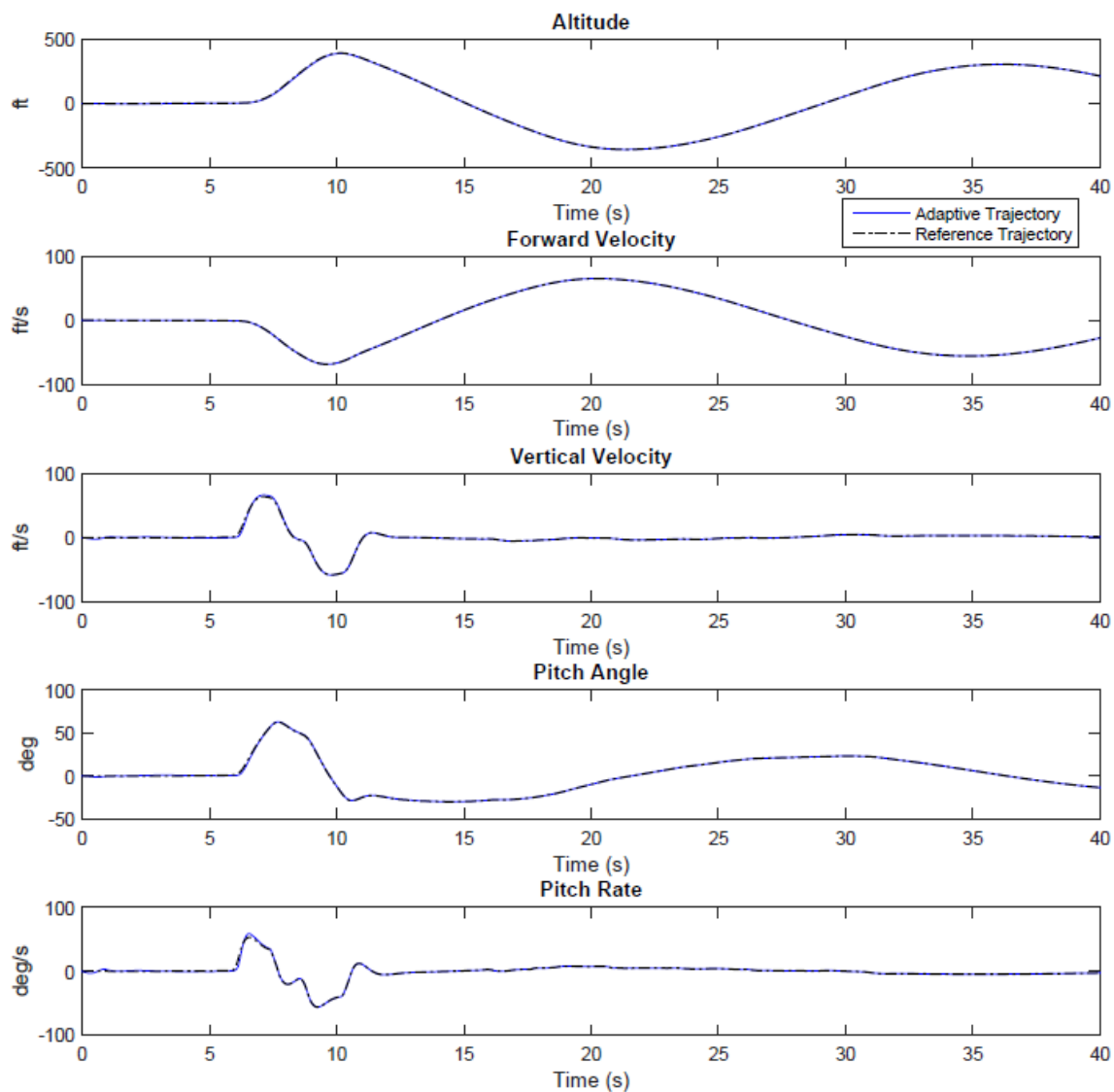
Figure 3.10. Longitudinal States while Following Reference Trajectory
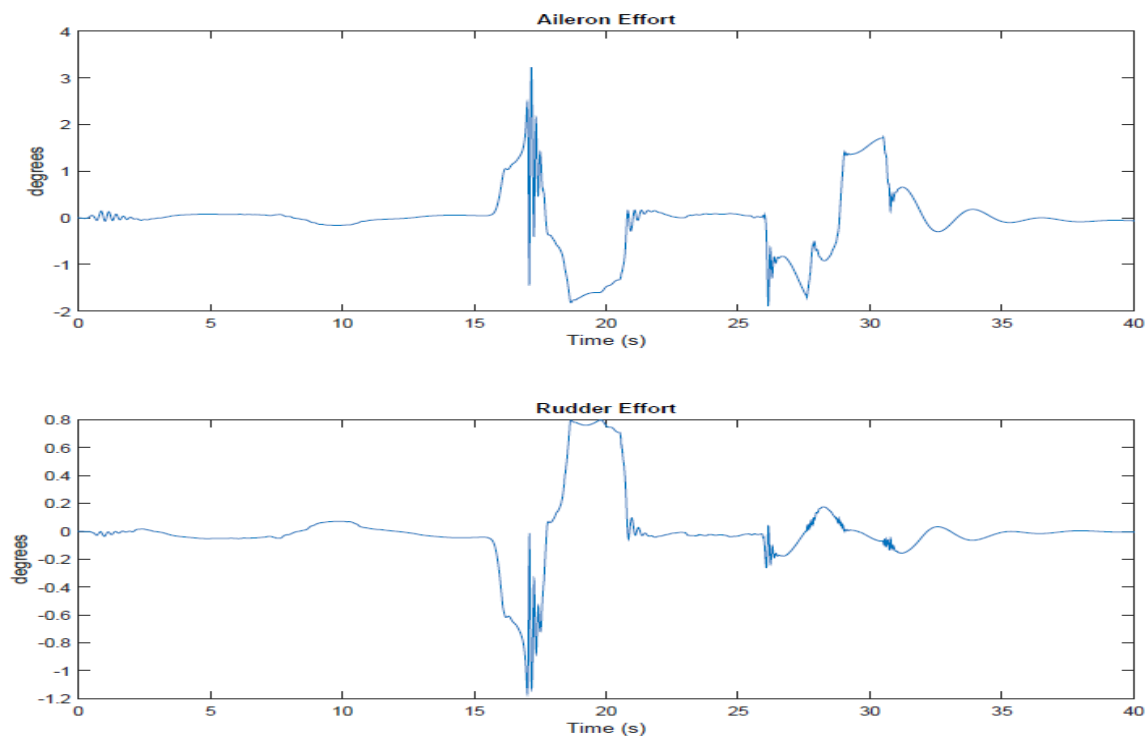
Figure 3.11. Lateral Control Effort while Following Reference Trajectory
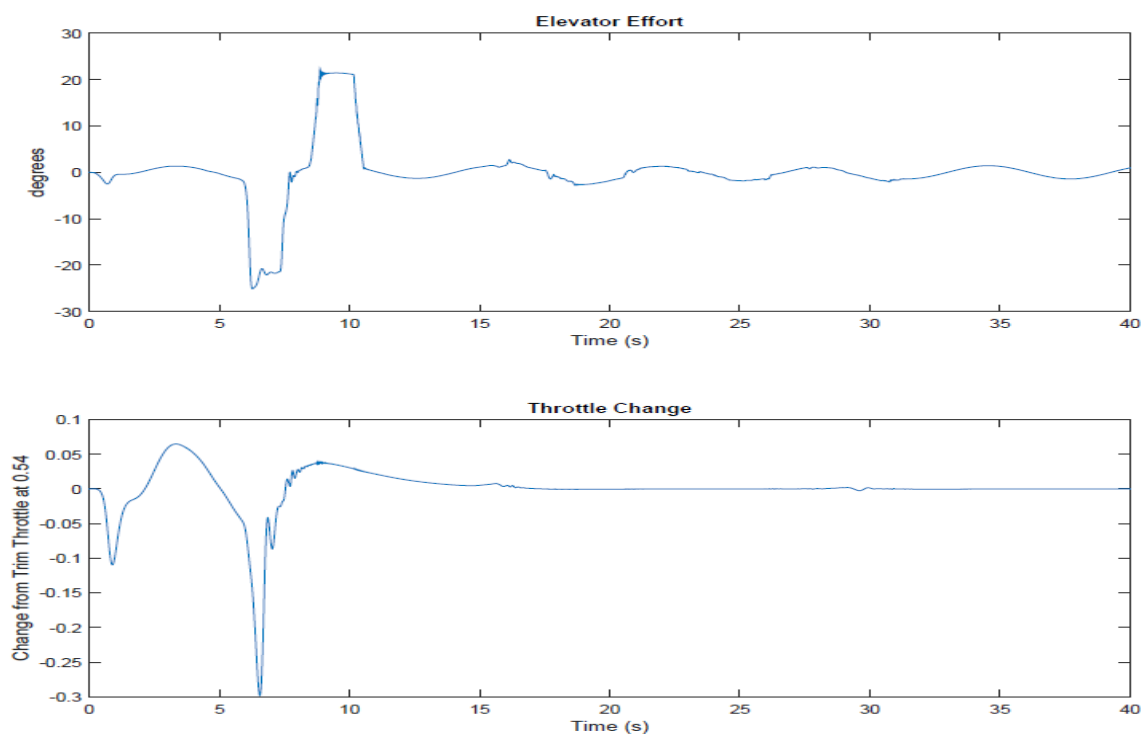
Figure 3.12. Longitudinal Control Effort while Following Reference Trajectory

4. Implementation and Results

In this chapter the implementation of the adaptive controller will be highlighted and the simulation results of the various modeling scenarios will be presented. Adaptive implementation will be tested on various linear and nonlinear aircraft models with different trajectories and external persistent disturbances. This will facilitate the analysis of stability and performance of the direct adaptive controller under various circumstances. Modeling error will also be simulated and studied to generate a broader understanding of robustness of the adaptive scheme. Various modeling and signal noise that are encountered in hardware in loop simulations will also be tested and the performance of the controller will be assessed. The final section will include a study of various solvers that are used to run simulations and how they effect the simulation and the stability of the system and the controller.

4.1   Linear Analysis

The adaptive controller was applied to the lateral and longitudinal UAV models for the case in which the objective was to track a reference trajectory in the presence of a persistent disturbance. Similar to the DAC simulations presented in Section 3.2, the lateral and longitudinal disturbance were applied as sinusoidal inputs of amplitude 0.1 rad with a frequency of 1 rad/s (0.16 Hz) to the aileron and elevator, respectively. As in the DAC implementation, the adaptive controller uses the disturbances models in Eq. 3.8, which describe the frequency of excitation but do not assume knowledge of the amplitude. The adaptive con-

trol structure given in Eq. 3.21 was implemented with the following parameters for the lateral and longitudinal cases:

$$\sigma_{e,lat} = \begin{bmatrix} 100 & 0 \\ 0 & 100 \end{bmatrix} \quad \sigma_{r,lat} = \begin{bmatrix} 1 & 0 \\ 0 & 1 \end{bmatrix} \quad \sigma_{u,lat} = \begin{bmatrix} 10 & 0 \\ 0 & 10 \end{bmatrix} \quad \sigma_{D,lat} = \begin{bmatrix} 10 & 0 \\ 0 & 10 \end{bmatrix}$$

$$\sigma_{e,long} = \begin{bmatrix} 100 & 0 \\ 0 & 100 \end{bmatrix} \quad \sigma_{r,long} = \begin{bmatrix} 0.01 & 0 \\ 0 & 0.01 \end{bmatrix} \quad \sigma_{u,long} = \begin{bmatrix} 1 & 0 \\ 0 & 1 \end{bmatrix} \quad \sigma_{D,long} = \begin{bmatrix} 1 & 0 \\ 0 & 1 \end{bmatrix}$$

These parameters were selected through a manual tuning process. Since the open-loop lateral and longitudinal LTI models are both nonminimum phase systems, the sensor blending process described in Section 3.4 was applied to generate the blended outputs defined in Eqs. 3.53 and 3.54; these blended outputs result in minimum phase systems.

Figures 4.1 and 4.2 show the lateral states and controls that were obtained using the adaptive controller to track a reference trajectory corresponding to a 5° heading change while subjected to the persistent sinusoidal disturbance. The results in Figure 4.1 show that the adaptive system is able to reject the disturbance and track the reference trajectory with minimal error. An initial overshoot can be observed in the roll and yaw rates, but the amplitude of these overshoots is low and they damp out within the first second of the maneuver. The results in Figure 4.2 show that the aileron and rudder control deflections for this maneuver are bounded in magnitude by 2.5° and 0.5°, respectively, while the actuation frequency is on the order of 5 Hz or less. These values are well within the control surface deflection and rate limits. The aileron deflection has a sinusoidal characteristic, which is

associated with the disturbance rejection. The adaptive control gains, which are plotted in Figure 4.3, are clearly bounded for the duration of the maneuver.
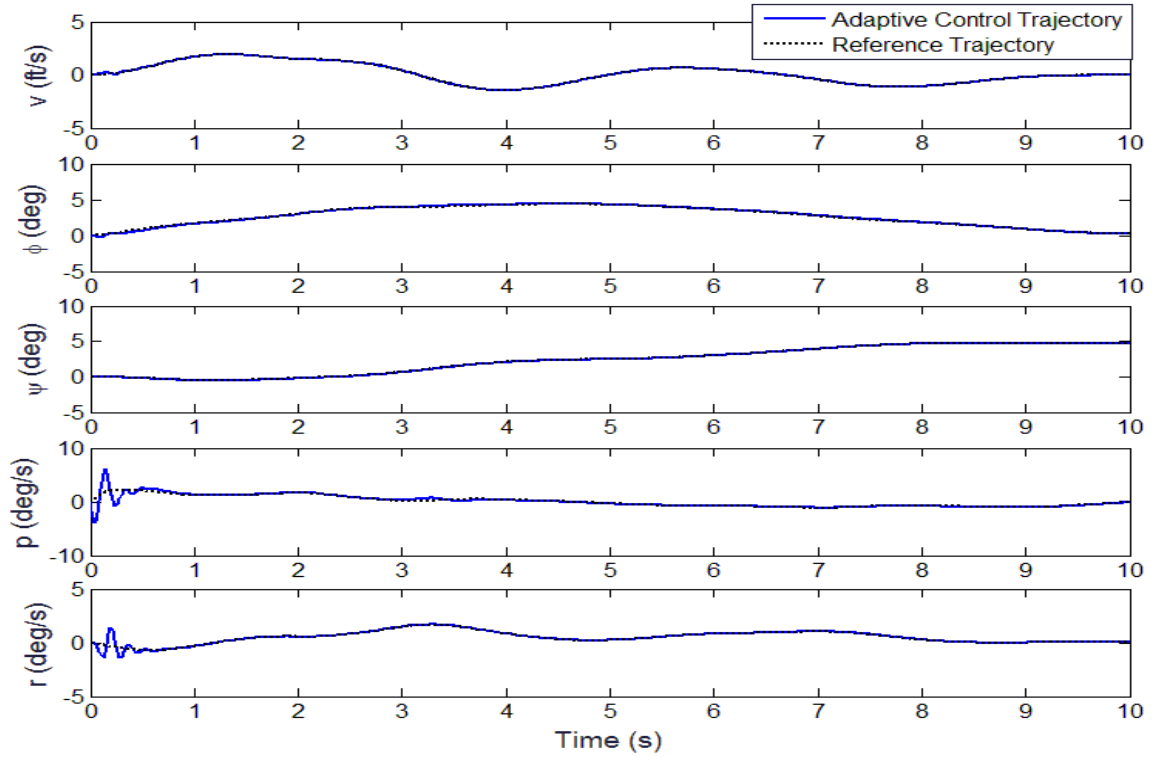

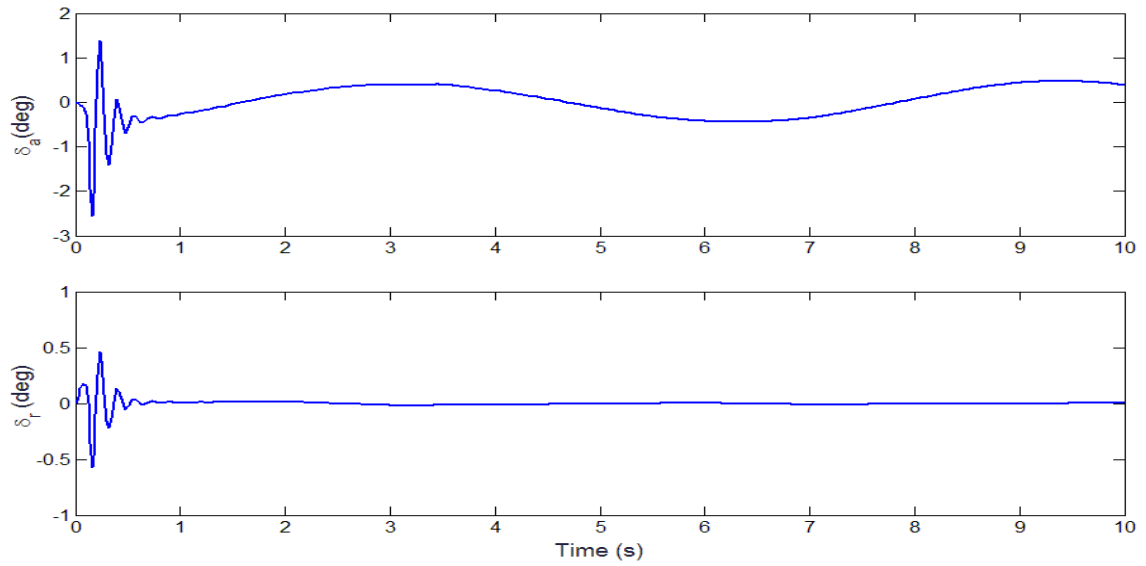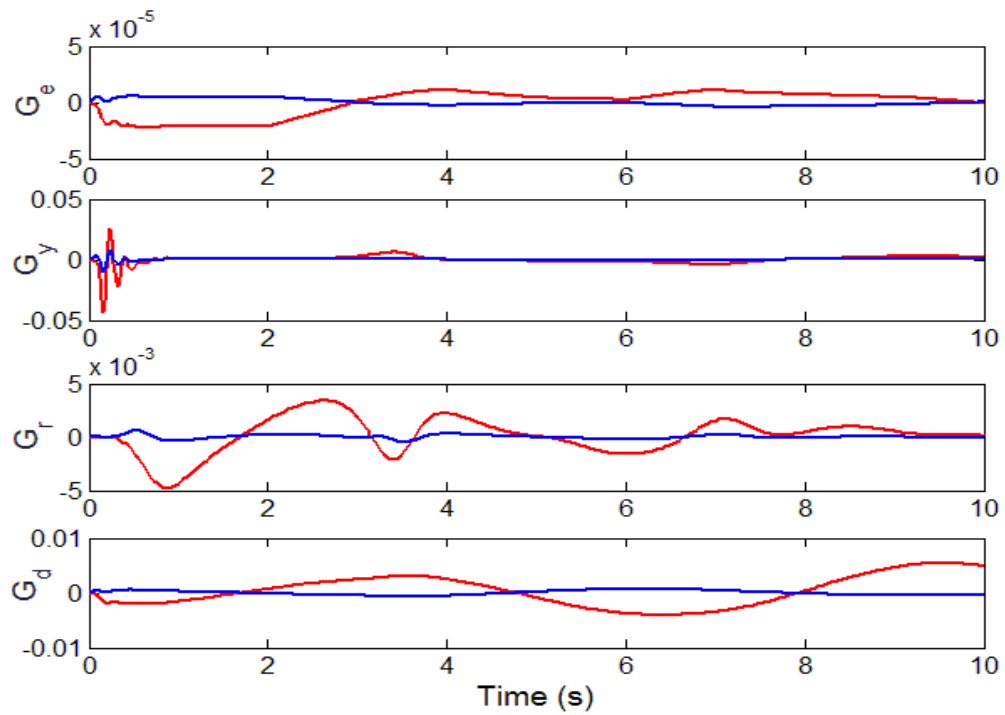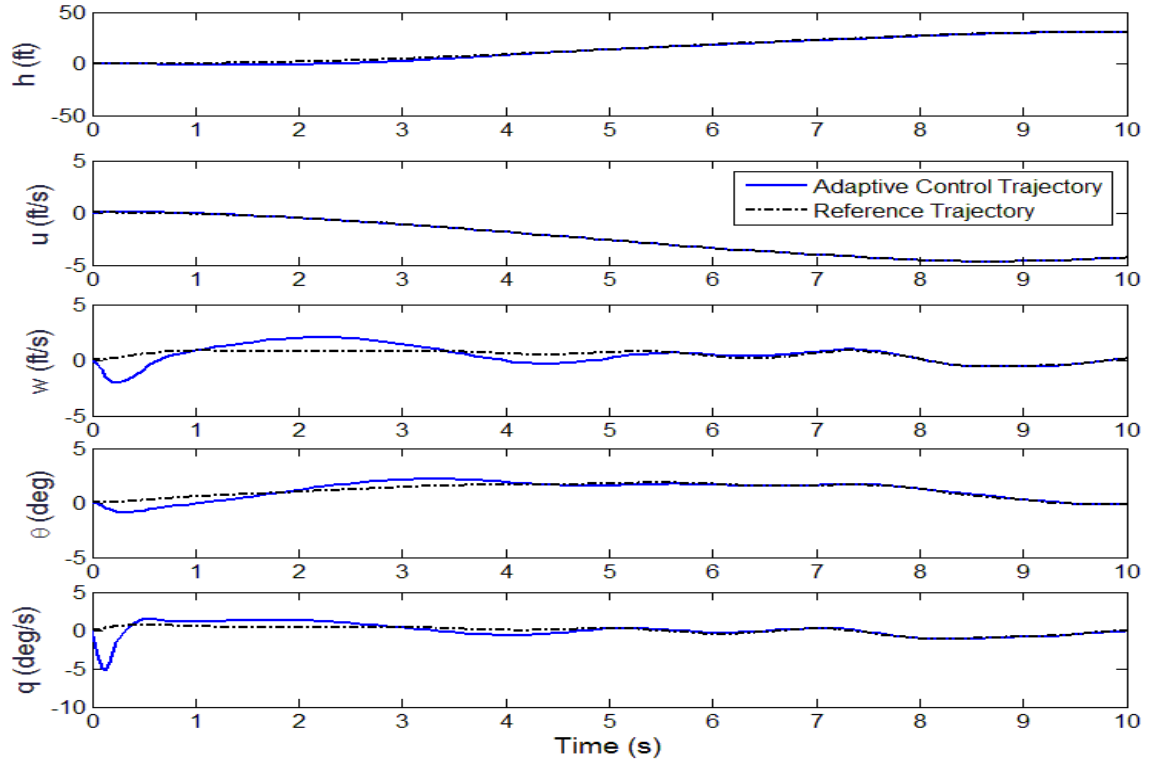Figure 4.1. Lateral Adaptive Control States: Tracking a Reference Heading Change Trajectory while Rejecting a Sinusoidal Disturbance.

Figures 4.4 and 4.5 show the longitudinal states and controls that were obtained using the adaptive controller to track a reference trajectory corresponding to a 30 ft altitude change while subjected to the persistent sinusoidal disturbance. The results in Figure 4.4 show that, just as in the lateral case, the adaptive system is able to reject the disturbance and track the reference trajectory with minimal error. An initial overshoot can be observed in the pitch rate and the body-referenced downward velocity w, but the amplitude of the overshoot is low and quickly attenuates. Figure 4.5 show that the elevator deflection and

Figure 4.2. Lateral Adaptive Control Inputs: Tracking a Reference Heading Change Trajectory while Rejecting a Sinusoidal Disturbance.
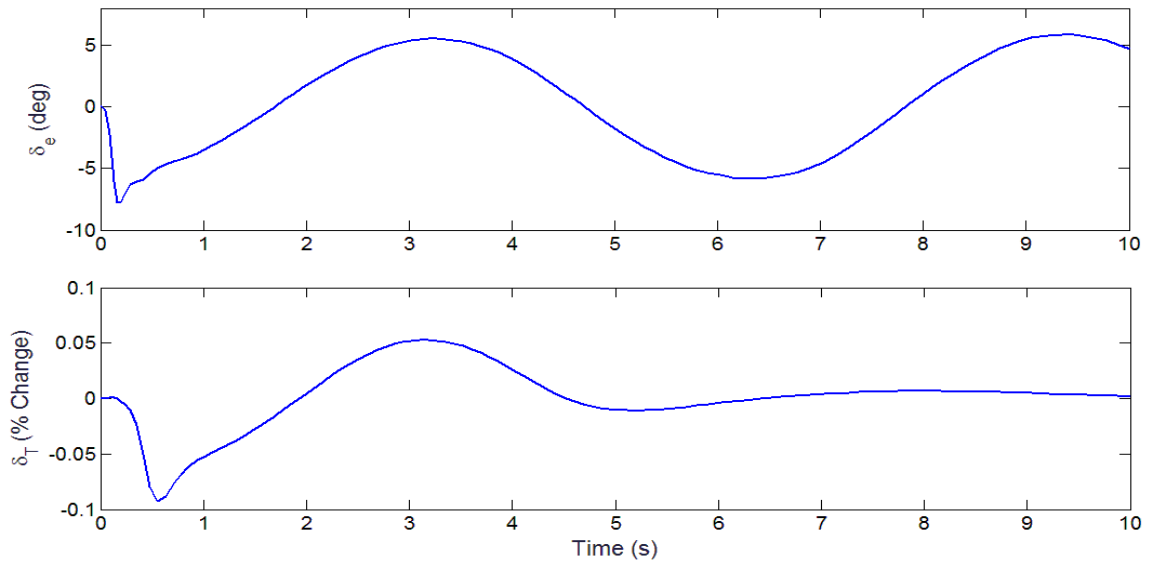

Figure 4.3. Lateral Adaptive Control Gains: Tracking a Reference Heading Change Trajectory while Rejecting a Sinusoidal Disturbance.

throttle control for this maneuver are bounded in magnitude by 7.5° and 10% (relative to the trim throttle setting), respectively, which are well within the control limits. The elevator deflection has a sinusoidal characteristic, which is associated with the disturbance rejection.

Figure 4.4. Longitudinal Adaptive Control States: Tracking a Reference Altitude Change Trajectory while Rejecting a Sinusoidal Disturbance.

It should be noted that, as shown in Section 3.2, the Disturbance Accommodating Controller (DAC) is also able to provide tracking of a reference trajectory in the presence of persistent disturbances. In contrast to the adaptive controller, however, the DAC requires the solution of the matching conditions on a case-to-case basis for various disturbances, making it difficult to implement in practice. The adaptive system, on the other hand, only requires a disturbance model that provides basis functions that describe the disturbances,

Figure 4.5. Longitudinal Adaptive Control Inputs: Tracking a Reference Heading Change Trajectory while Rejecting a Sinusoidal Disturbance.

without requiring the solution of the matching conditions. Another distinct advantage of the adaptive controller over the DAC is that, because the adaptive controller does not explicitly make use of a system model, it is naturally better suited to accommodate modeling error. As an example, Figure 4.6 presents results in which the lateral adaptive controller and the DAC were applied to track a reference trajectory while subjected to a persistent sinusoidal disturbance. In this example, a 20% error is introduced into the A_{lat} matrix (i.e., the model A_{lat} matrix corresponds to $1.2A_{lat}$), which directly affects the performance of the DAC. The results in Figure 4.6 show that the performance of the DAC degrades significantly in the presence of modeling error, while the adaptive controller is unaffected since it does not depend directly on the system model. More modeling error analysis will be performed in the sections below.
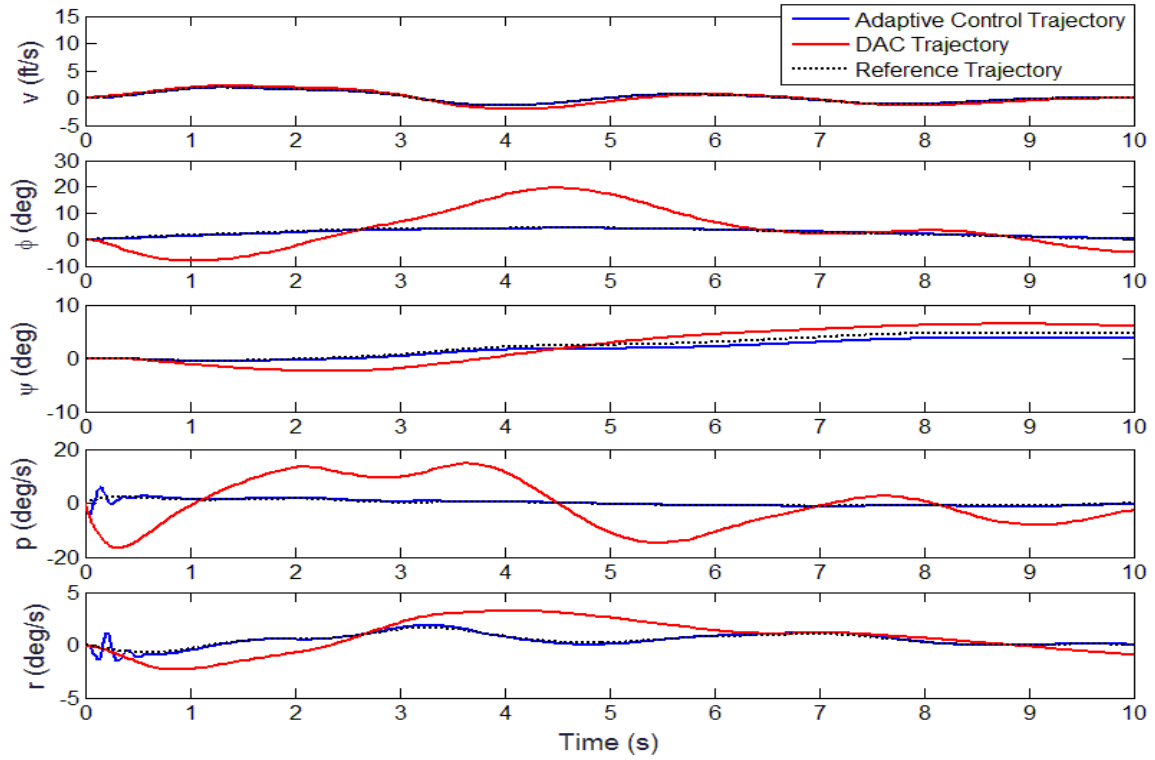
Figure 4.6. Lateral Adaptive Control and DAC States: Tracking a Reference Heading Change Trajectory with a Sinusoidal Disturbance and 20% Modeling Error.

4.1.1 Effect of Persistent Disturbances on Linear Direct Adaptive Control

Disturbance rejection is an important function of the direct adaptive controller. This section provides elaboration on the modeling and analysis of the disturbance models used in this dissertation. The adaptive controller is capable of rejecting any linear combination of the basis functions that represents the disturbance model. Various frequencies and types of disturbances that can be modeled using basis functions to form a disturbance model; all the frequencies represented in the model will be rejected by the disturbance adaptive gain. More complex disturbance models like the 'pulse' and 'riddle' models are presented. These models represent a more realistic version of a real-world disturbance.

All the results presented in the previous section have been derived with a single sinusoidal persistent disturbance with a frequency of 1 rad/s. This section will elaborate on the effects that various types of disturbance models have on the performance of this adaptive controller. The amplitude of these disturbance models is unknown to the system but frequency information is part of the generation model. Therefore, the first step to studying the effects of disturbances on the performance will be to analyze the effects of errors in the modeling frequency. Various simulations are performed where the disturbance frequency induced into the system is different from the one used in the disturbance generators. Simulation results are presented below: The first case results, where the frequency in the linear
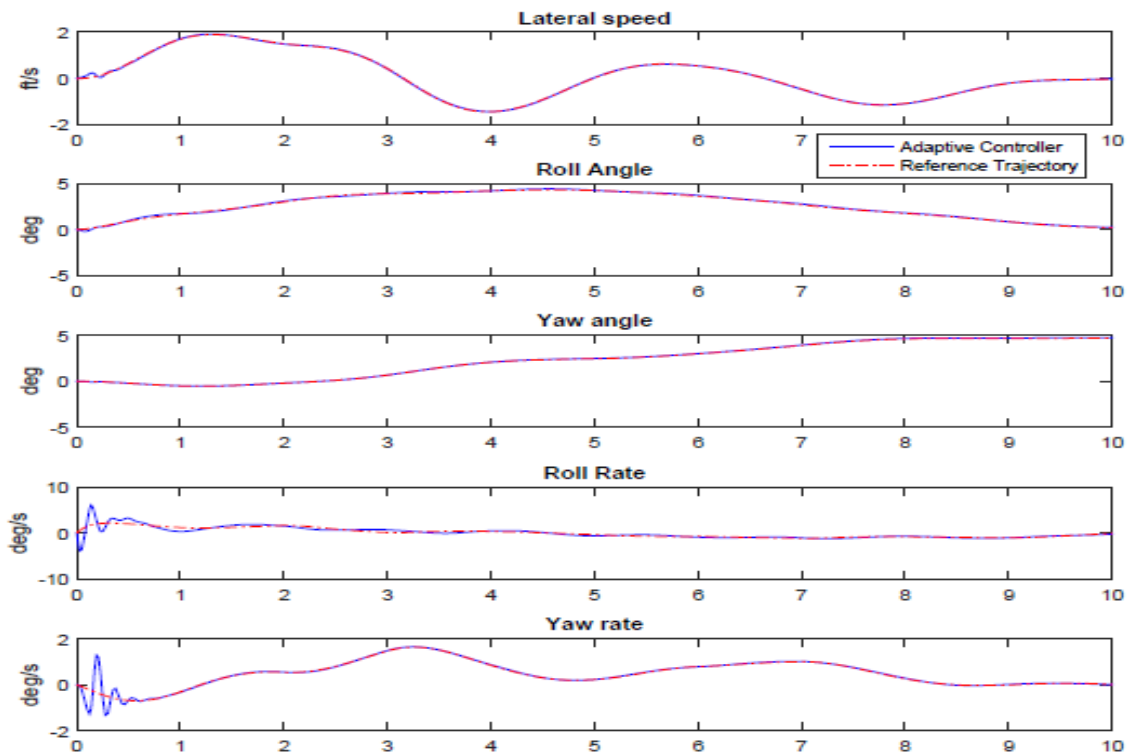
Figure 4.7. Lateral Adaptive Control: Controller performance with error in the Disturbance Frequency(5rad/s)

disturbance model is 1 rad/s but the frequency fed into the simulation as persistent distur-
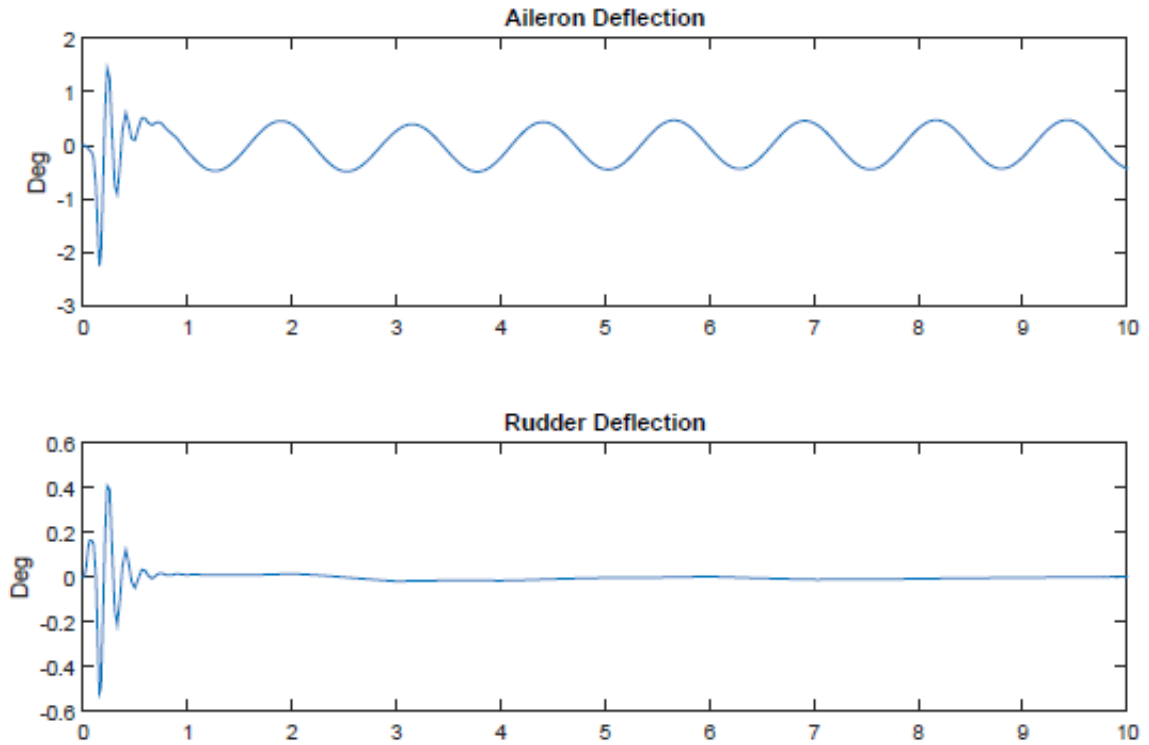
Figure 4.8. Lateral Adaptive Control: Control Deflections with error in the Disturbance Frequency (5 rad/s)

bance is 5 rad/s are depicted in Figures 4.7 and 4.8. It can be inferred that the direct adaptive controller was able to accommodate for a 5x change in frequency between the linear distur- bance model and the actual frequency of the persistent disturbance. The aileron deflection in Figure 4.8 shows a high frequency sinusoidal oscillation after the initial deflection used to mitigate this change in the disturbance.

For the second case, the disturbance generator is modified to produce different com- binations of disturbances. This is done to test the boundaries of the kind of persistent disturbances the direct adaptive controller can handle. Two combinations of disturbances are simulated and the results are presented in Figure 4.9. The first generator superimposes two sine waves with different frequencies while the second test includes a combination of

a step input and a sine wave. Figures 4.9 and 4.10 depict the states and control deflections
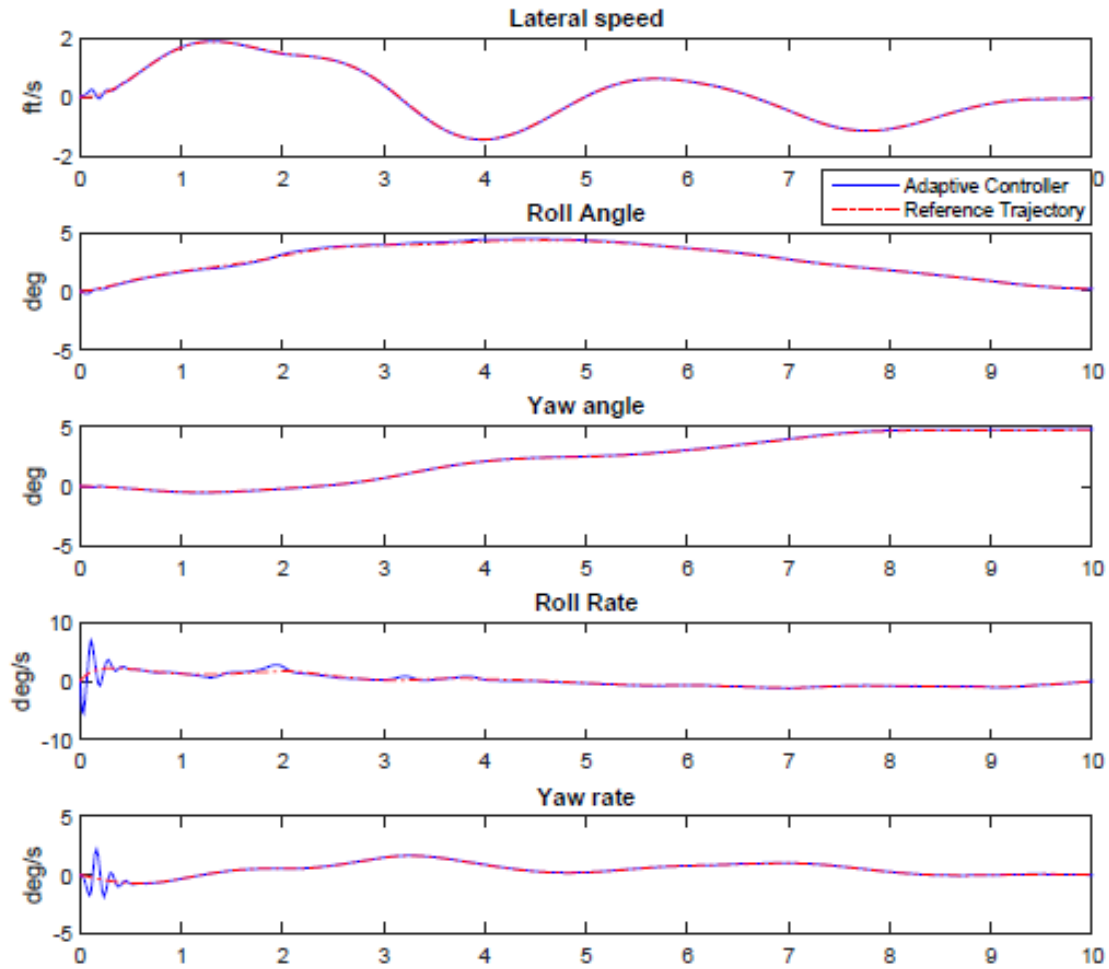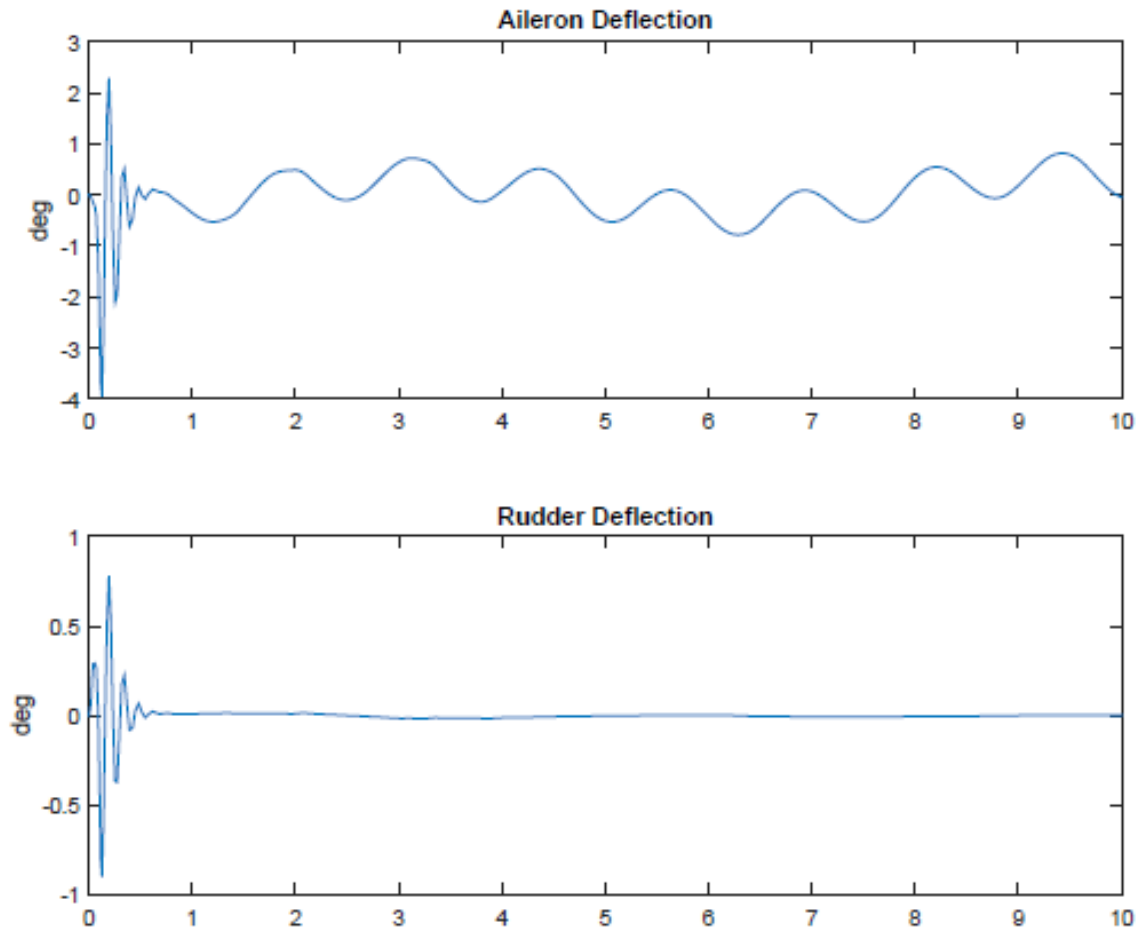

Figure 4.9. Lateral Adaptive Control: Controller performance with a distur-
bance generator producing two superimposed sine waves with frequencies of
1 rad/s and 5 rad/s

that the adaptive controller applies to mitigate the persistent disturbance shown in Figure

4.11. The states closely follow the reference trajectory and the aileron deflection pattern

resembles the superimposed sine wave disturbance.

Figures 4.12 and 4.13 represent the states and control deflections of the direct adaptive

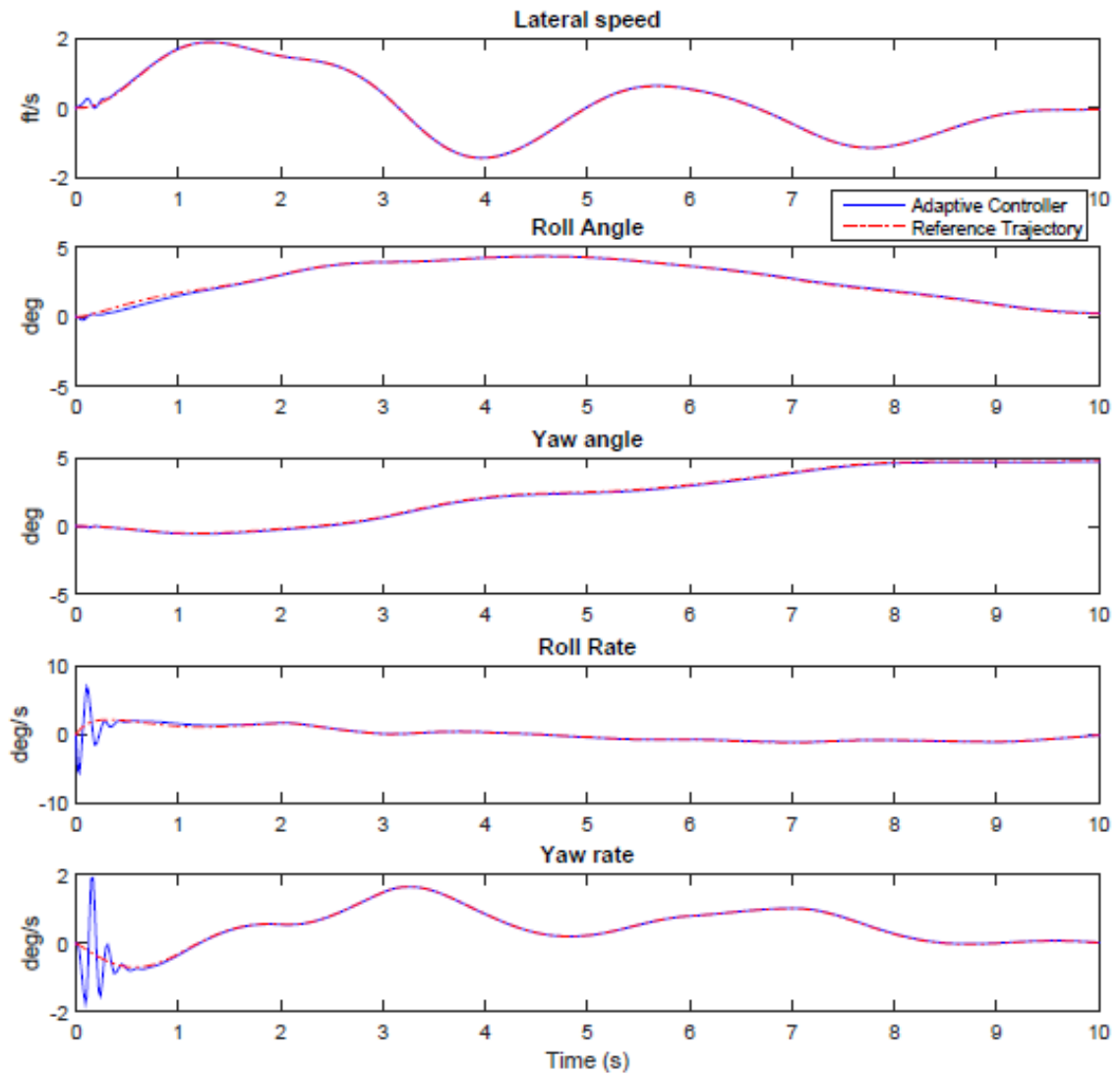controller when the disturbance generator superimposes a step and a sinusoid of frequency

Figure 4.10. Lateral Adaptive Control: Control Deflections with a disturbance generator producing two superimposed sine waves with frequencies of 1 rad/s and 5 rad/s

1 rad/s which is shown in Figure 4.14. It can be observed in both these given cases that the adaptive controller responds to the given disturbance and is able to track the given reference trajectory, which corresponds to following a $5°$ heading change.

The previously modeled persistent disturbances are simple trigonometric functions or derivatives of these functions. More complex disturbances were modeled to represent realistic scenarios like wind gusts. Some of the simulation results performed using these disturbance models are presented here.
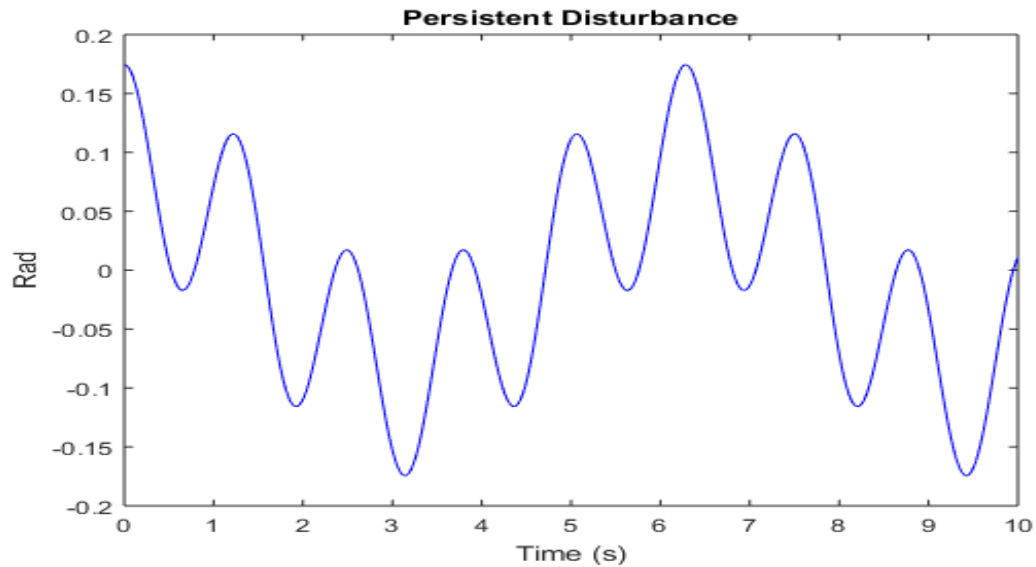
Figure 4.11. Persistent Disturbance with superimposed sine waves with frequencies of 1 rad/s and 5 rad/s

Figures 4.15-4.20 represent the results obtained from a lateral simulation using a complex disturbance generators (referred to as a pulse and riddle, named for their resemblance to the namesake). As can be observed from the disturbance shapes, it is non-uniform and is much likely to resemble a real-world gust/disturbance that might be experienced by a UAV. It is imperative to note that the actual disturbance the UAV encounters is akin to the change in states this pulse will cause if this disturbance shape was an aileron deflection, this causes the disturbance propagation to be more complex than what can be simulated by a continuous system model. The propagation of the disturbance into the states can be observed in the figure 4.21 below. The results obtained in this section are representative of the ability of an adaptive control scheme to mitigate persistent disturbances.

Figure 4.12. Lateral Adaptive Control: Controller performance with a disturbance generator producing a superimposed step and sinusoid waves with a frequency of 1 rad/s
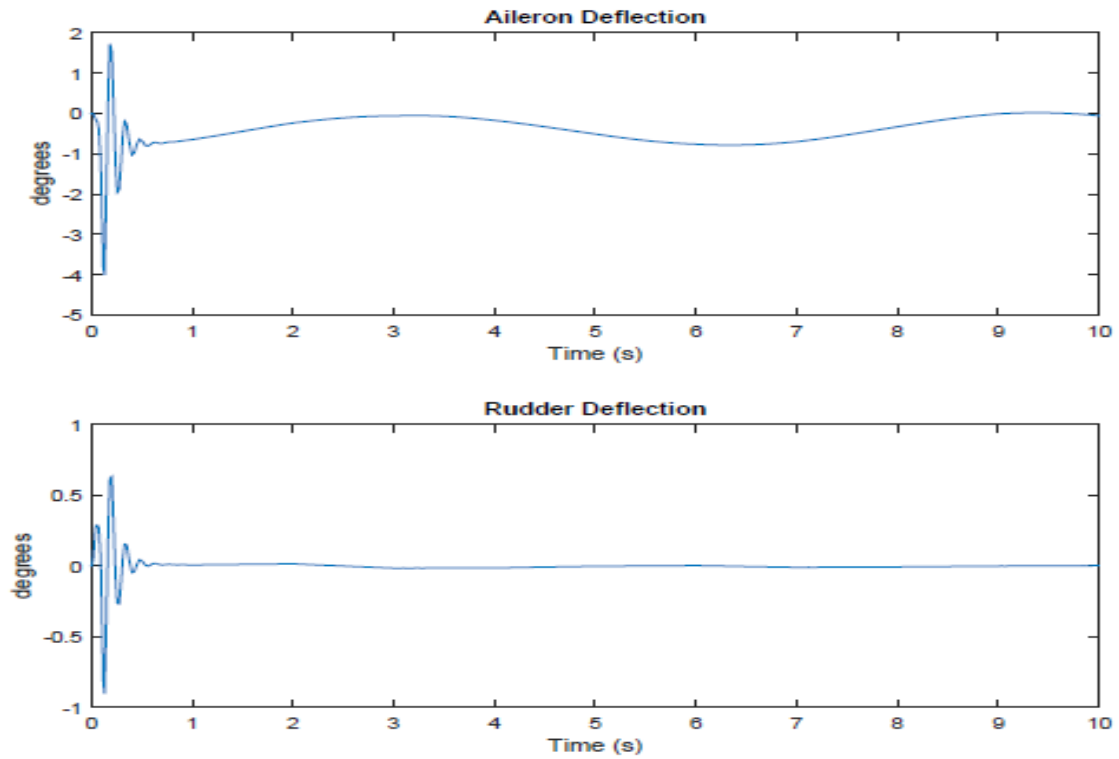
Figure 4.13. Lateral Adaptive Control: Control Deflections with a disturbance generator producing a superimposed step and sinusoid waves with a frequency of 1 rad/s
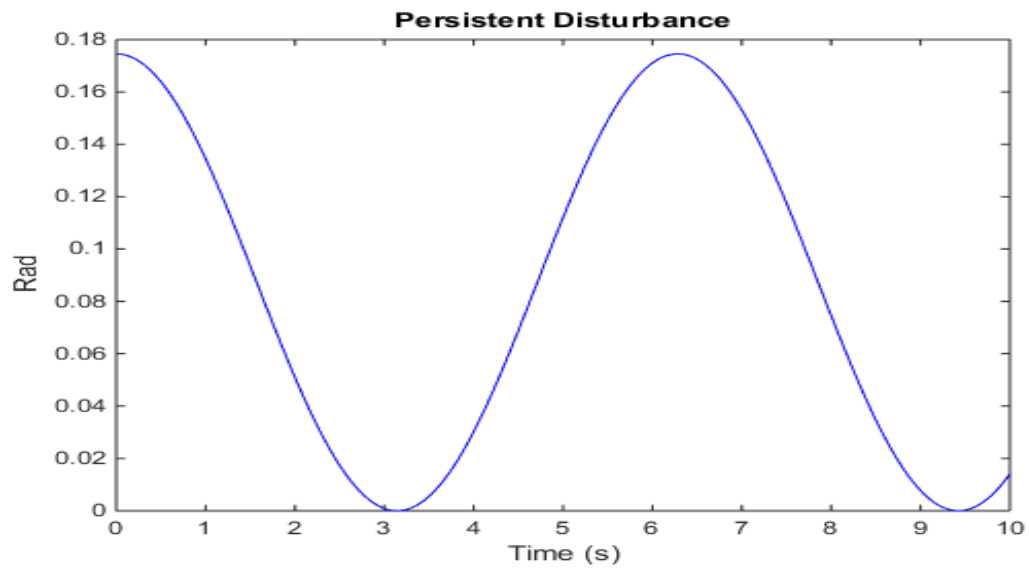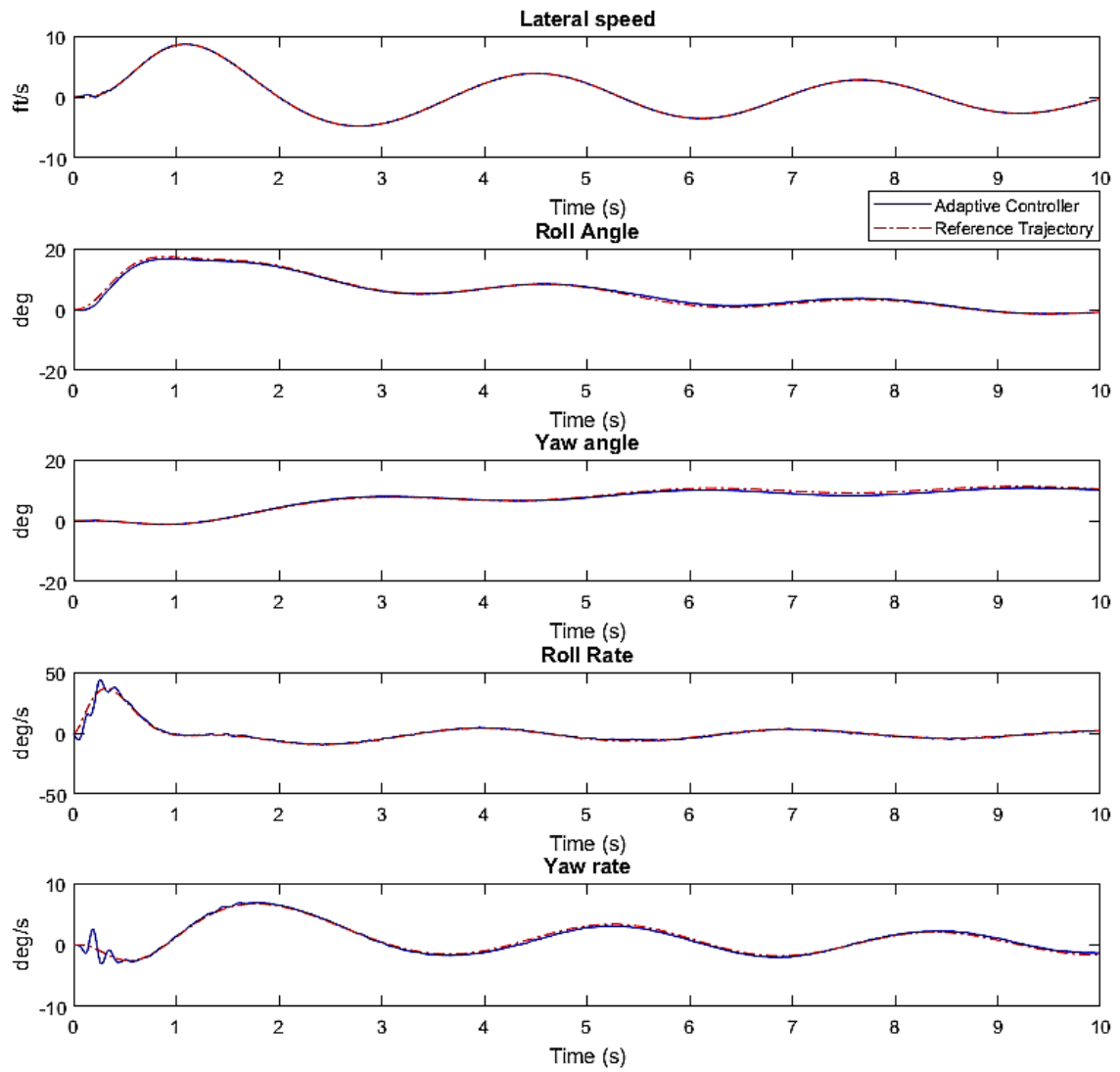

Figure 4.14. Persistent Disturbance with a disturbance generator producing a superimposed step and sinusoid waves with a frequency of 1 rad/s

Figure 4.15. Lateral Adaptive Control: states with a complex persistent distur-
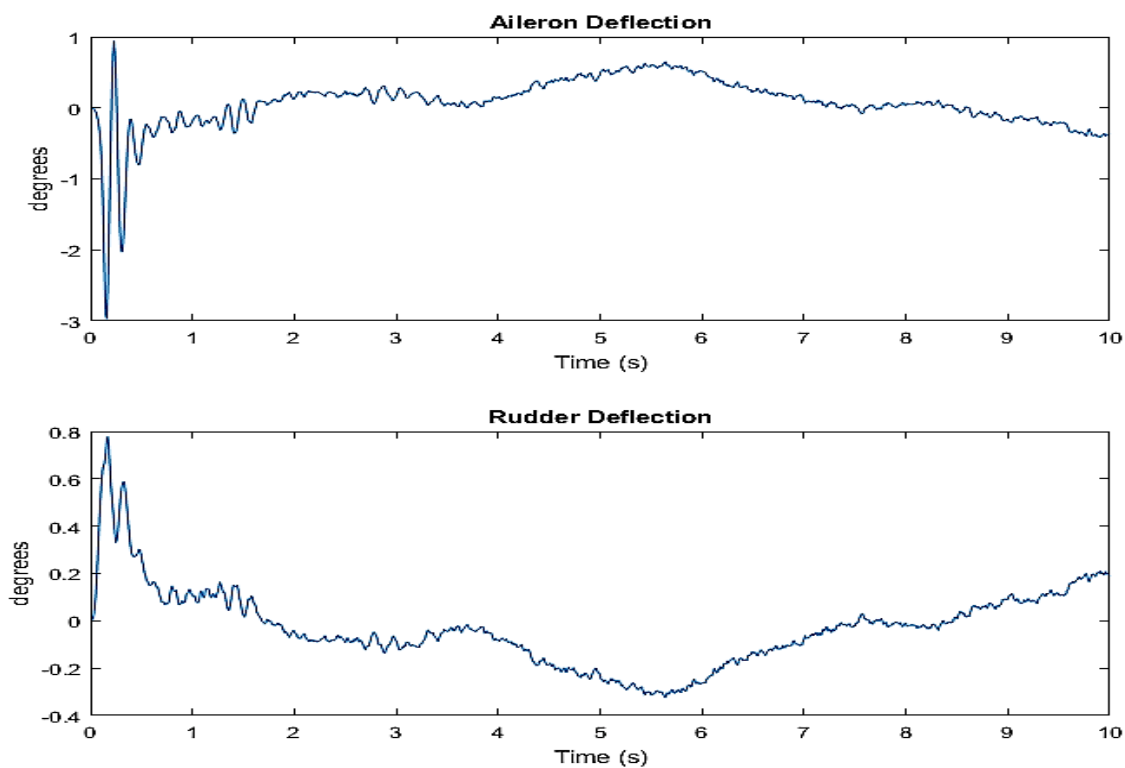bance generator 'Pulse'

Figure 4.16. Lateral Adaptive Control: Control effort with a complex persistent disturbance generator 'Pulse'
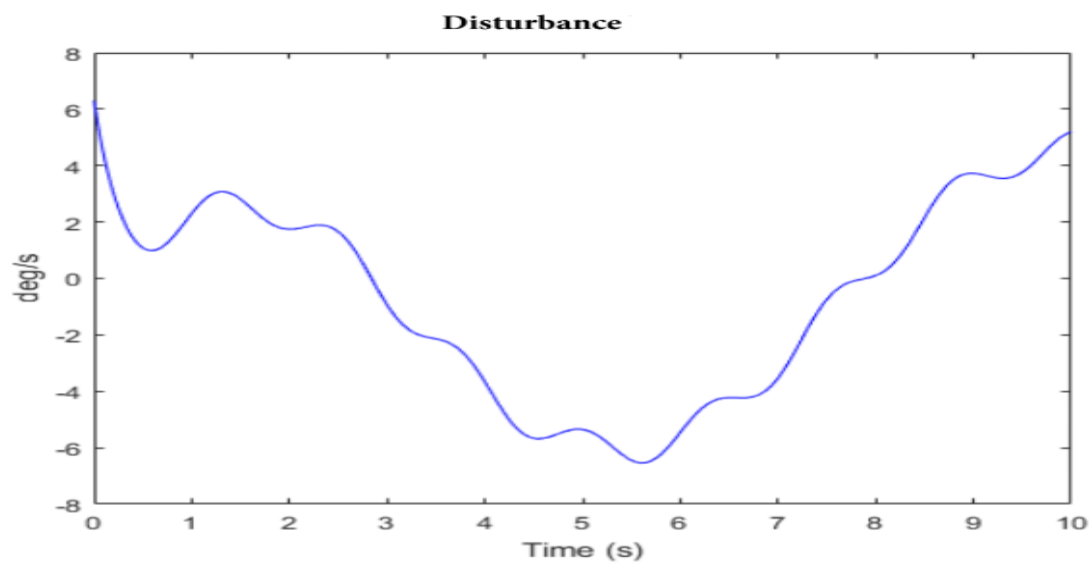

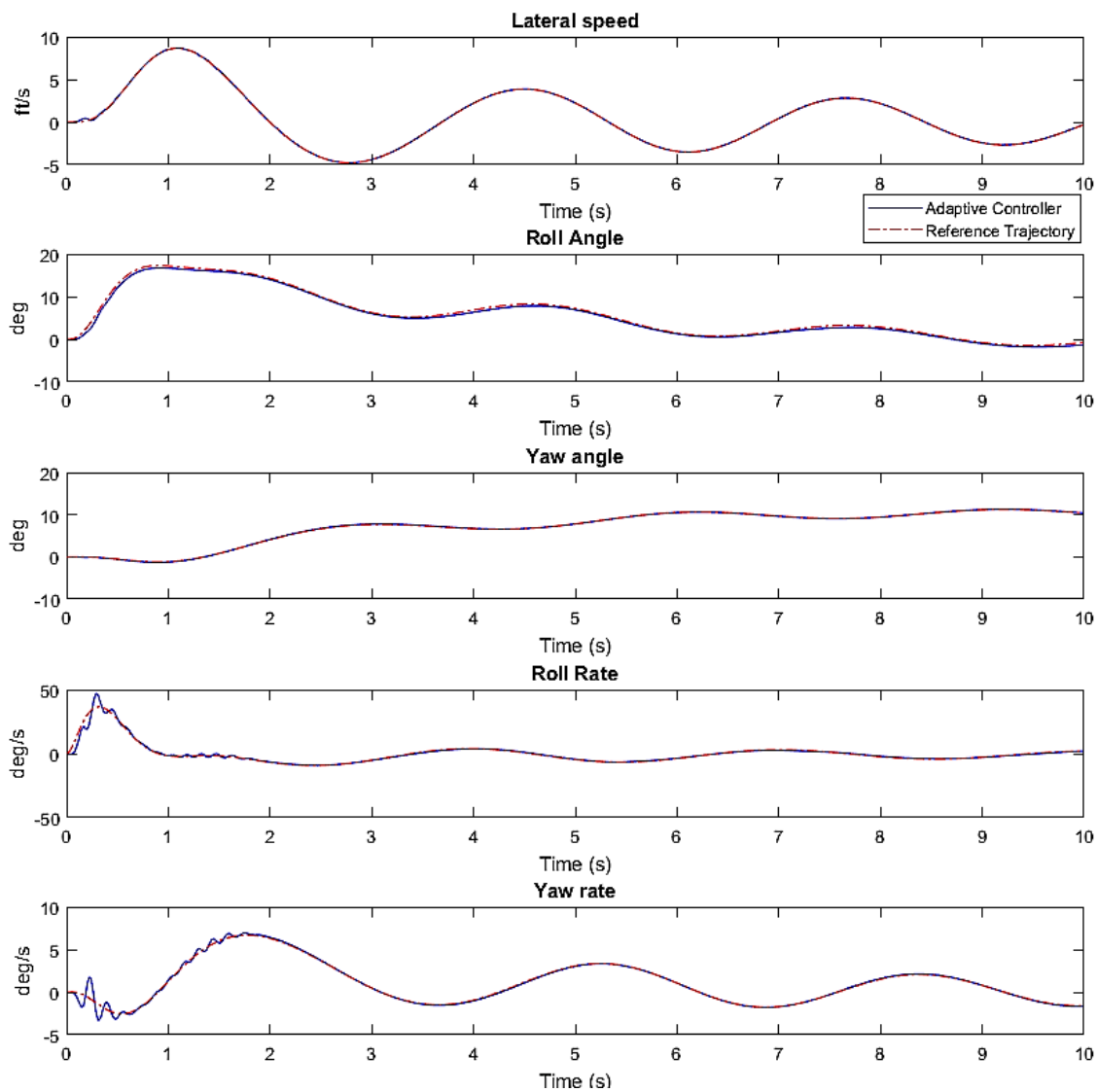Figure 4.17. Complex persistent disturbance 'Pulse'

Figure 4.18. Lateral Adaptive Control: states with a complex persistent disturbance generator 'Riddle'
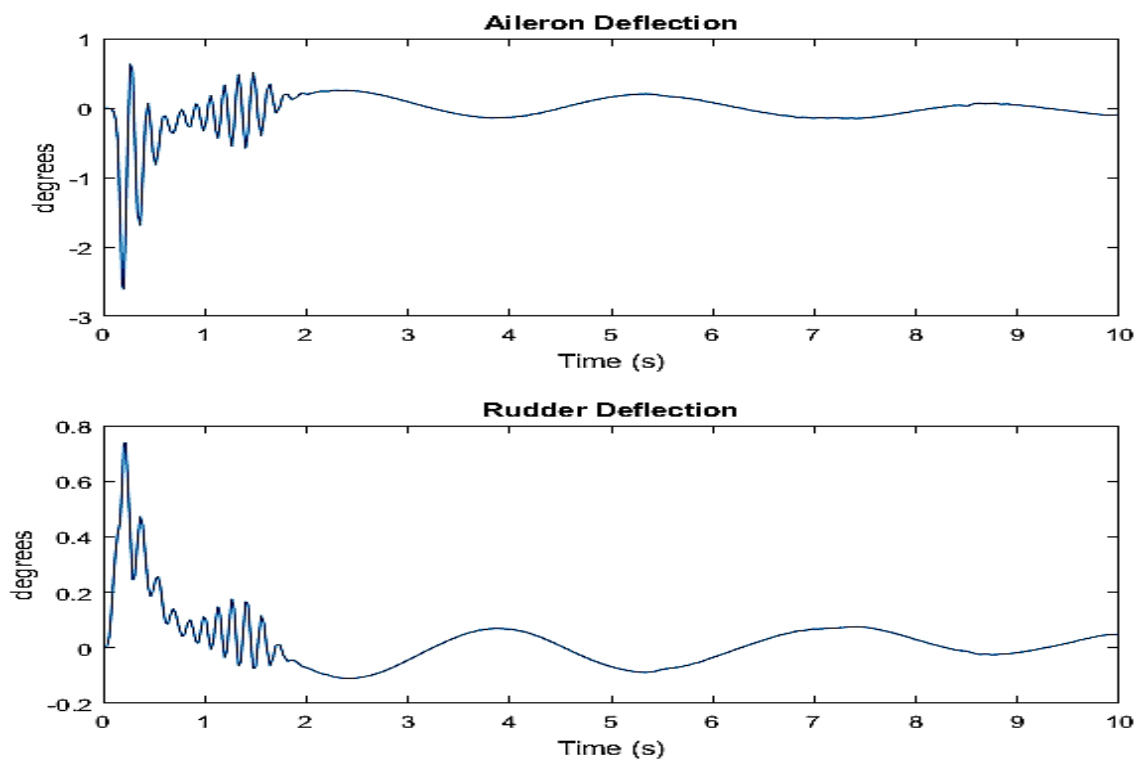
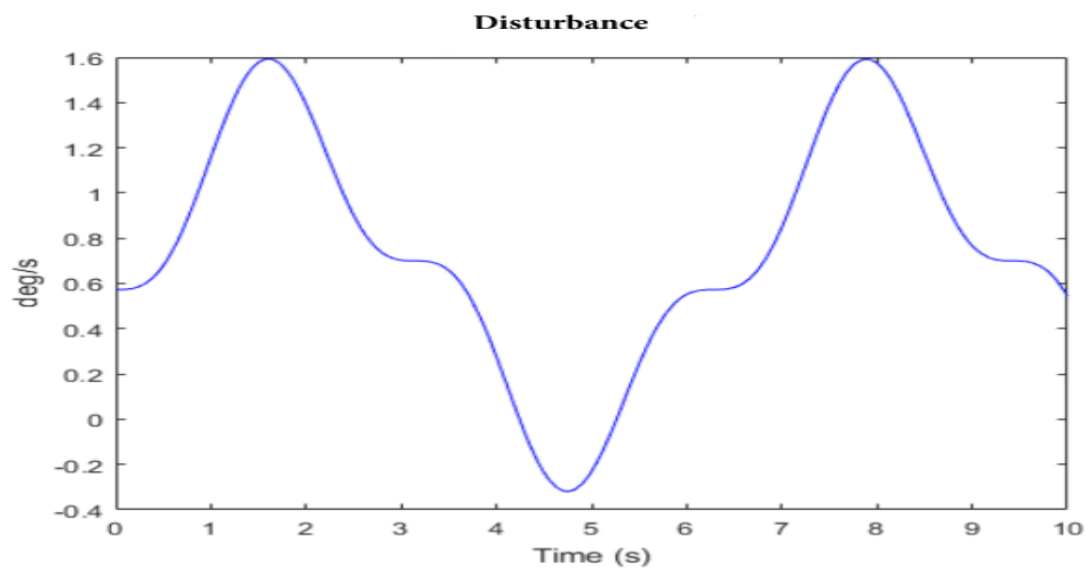Figure 4.19. Lateral Adaptive Control: Control effort with a complex persistent disturbance generator 'Riddle'

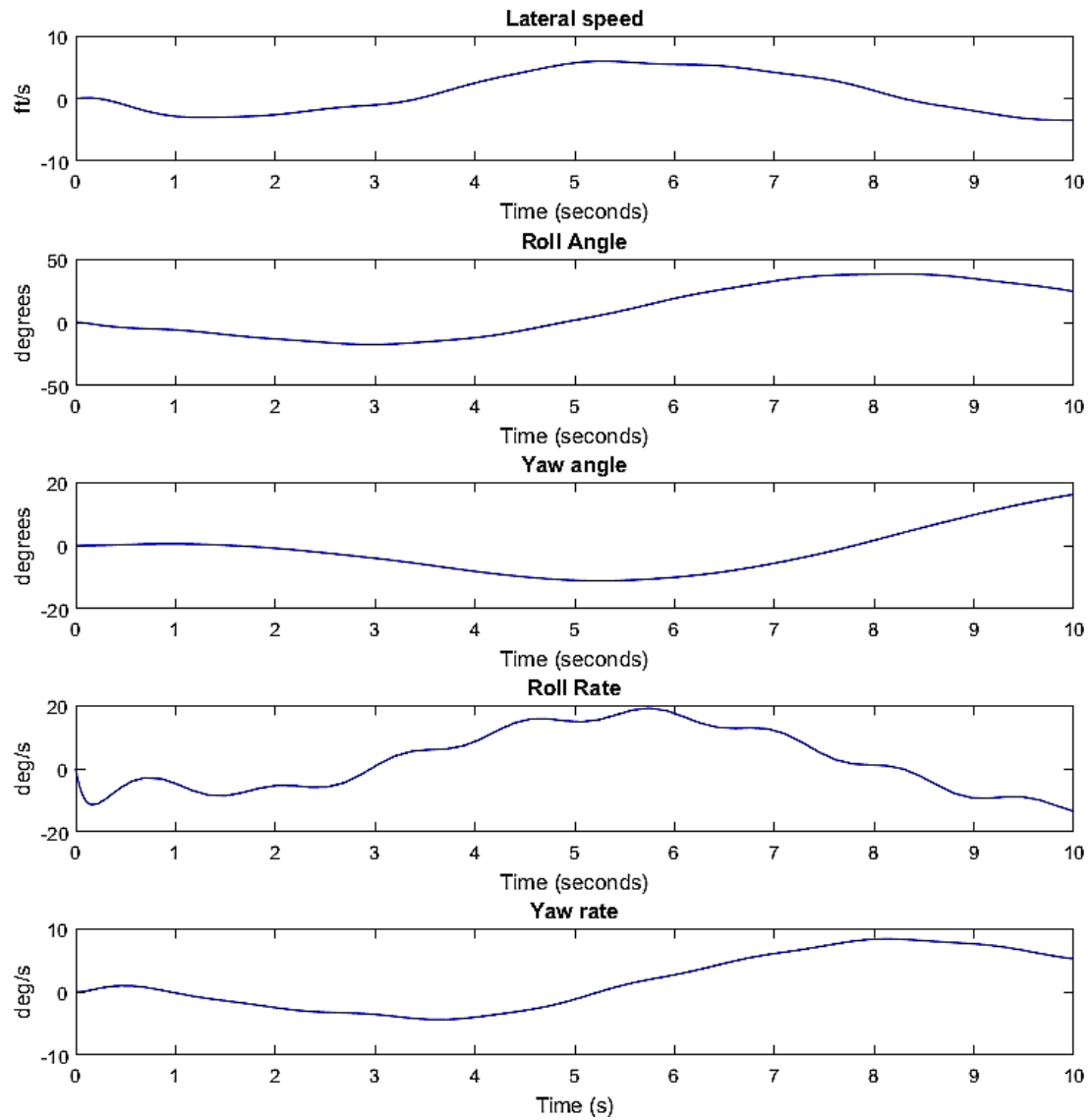Figure 4.20. Complex persistent disturbance 'Riddle'

Figure 4.21. Propagation of complex disturbance 'Pulse' through to the lateral states

4.1.2 Complex Trajectory Tracking

In previous sections simple 10 second long dynamically separated maneuvers like change in yaw or a climb have been simulated but to study the effectiveness of a direct adaptive scheme more complex maneuvers need to be analyzed. A rudimentary PID controller is
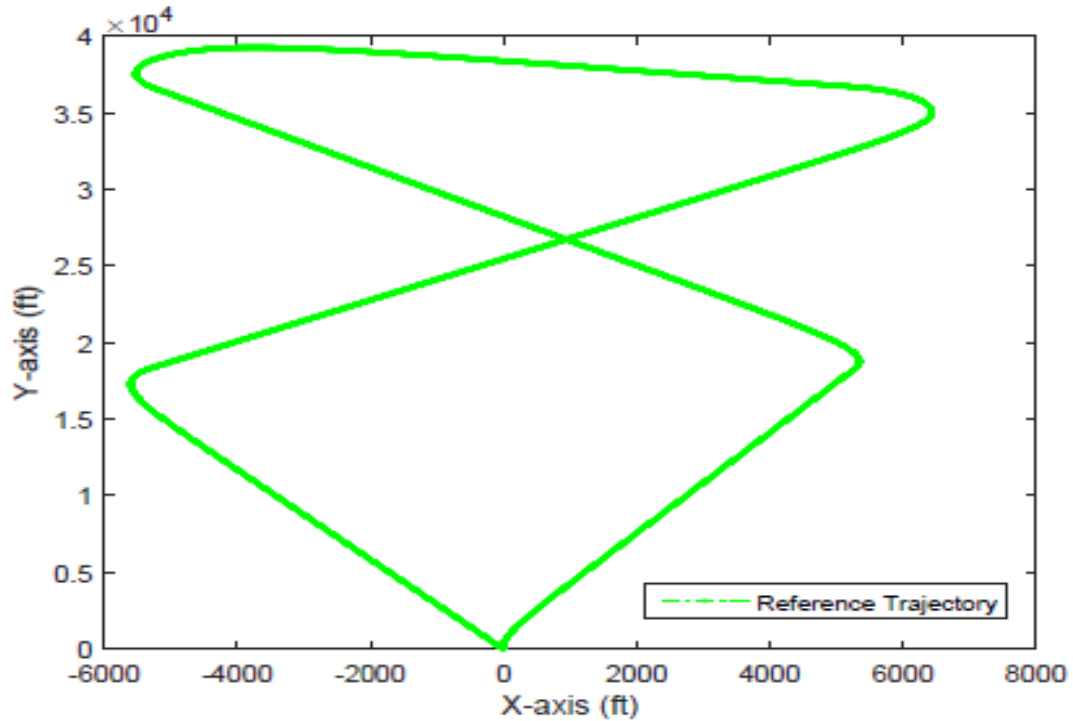

Figure 4.22. Figure 8 Trajectory used as a reference

developed for the purpose of making a nonlinear aircraft model follow a figure 8 trajectory as shown in figure 4.22, while limiting a change in altitude. The control effort and the states obtained from these simulations are recorded and further used as references in the adaptive scheme. The results of one such case is shown below: The first 500 seconds of the figure 8 maneuver is cut and the control deflections generated are used as references to a linear lateral model of the UAV, the linear model is linearized at the same trim conditions
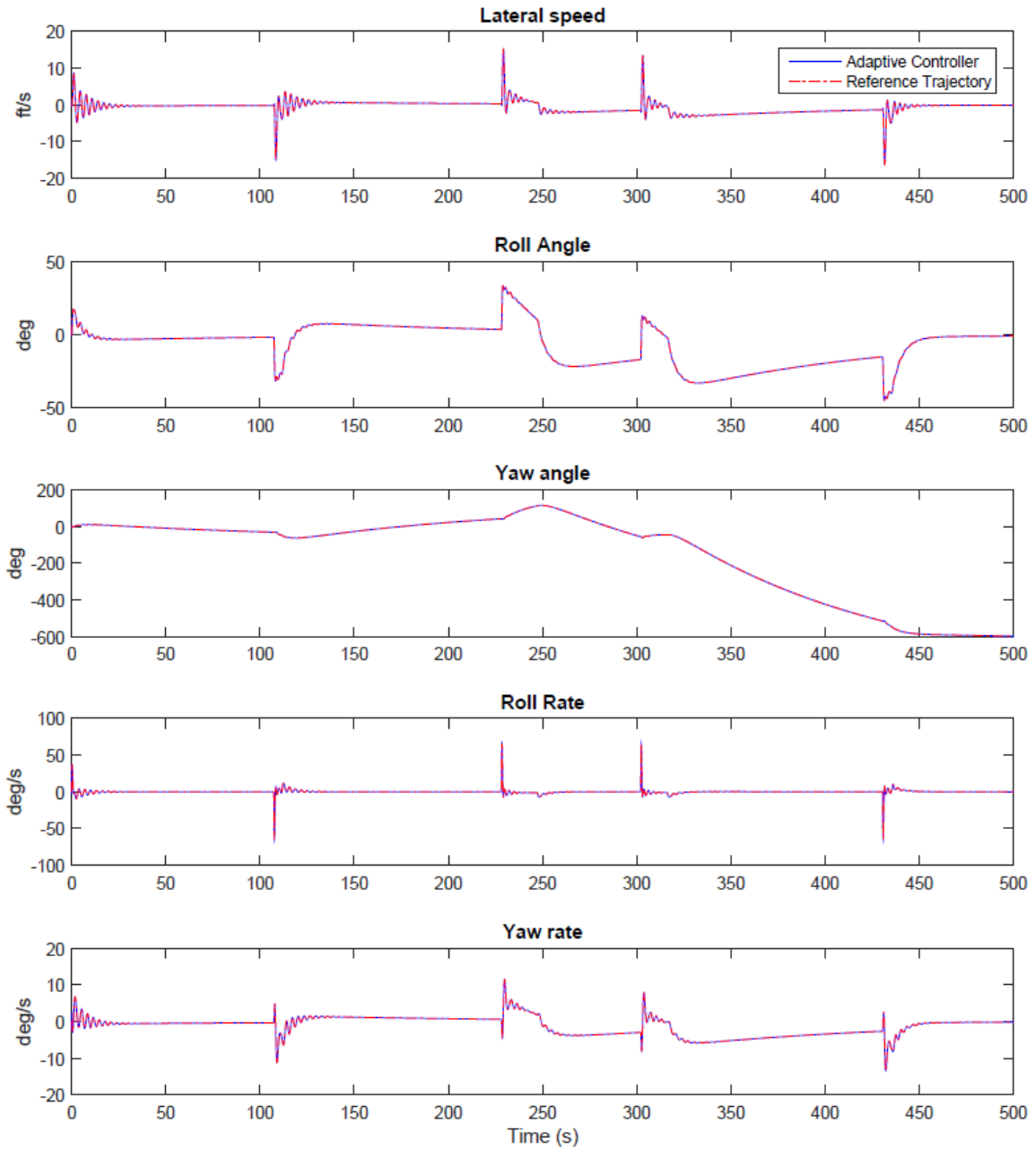
Figure 4.23. Lateral Adaptive Control: Controller performance while tracking a figure 8 trajectory

as the nonlinear model. As can be observed from figure 4.23 the direct adaptive controller

closely tracks the required trajectory with minimal overshoots or steady state error. Figure

4.24 depicts the control effort required by the controller to track the given maneuver, both
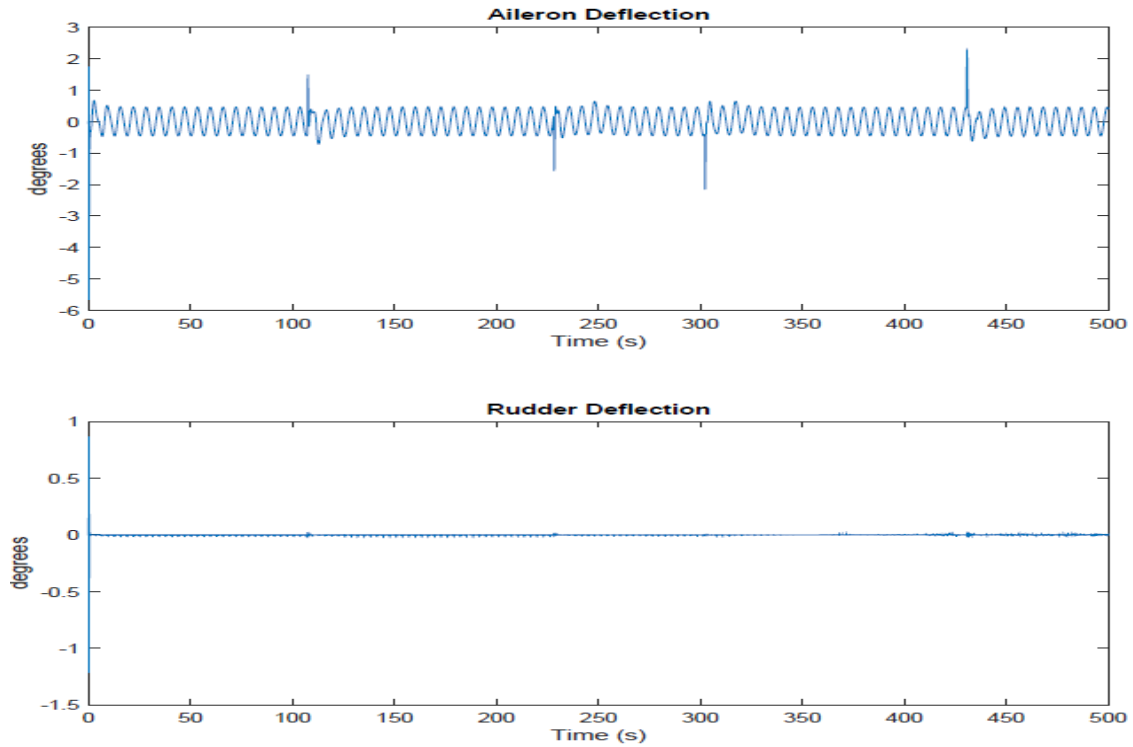
Figure 4.24. Lateral Adaptive Control: Control Deflections while tracking a figure 8 trajectory

the rudder and aileron lie well within the limits of the actuators. The persistent disturbance used in this case is a sinusoidal wave fed into the aileron with a constant frequency of 1rad/s. For completeness another case with the figure 8 tracking is run with the superimposed sinusoidal persistent disturbance as represented in figure 4.11. The results are presented below, it can be seen from figure 4.25 and figure 4.26 that the adaptive system is able to track these trajectories while in contrast the aileron deflections from figure 4.24 and figure 4.26 depict the changes in control deflection that occur due to the change in the persistent disturbance. Figure 4.27 represents the first 10 seconds of this maneuver and the superimposed sinusoidal pattern of different frequencies can be observed in detail.
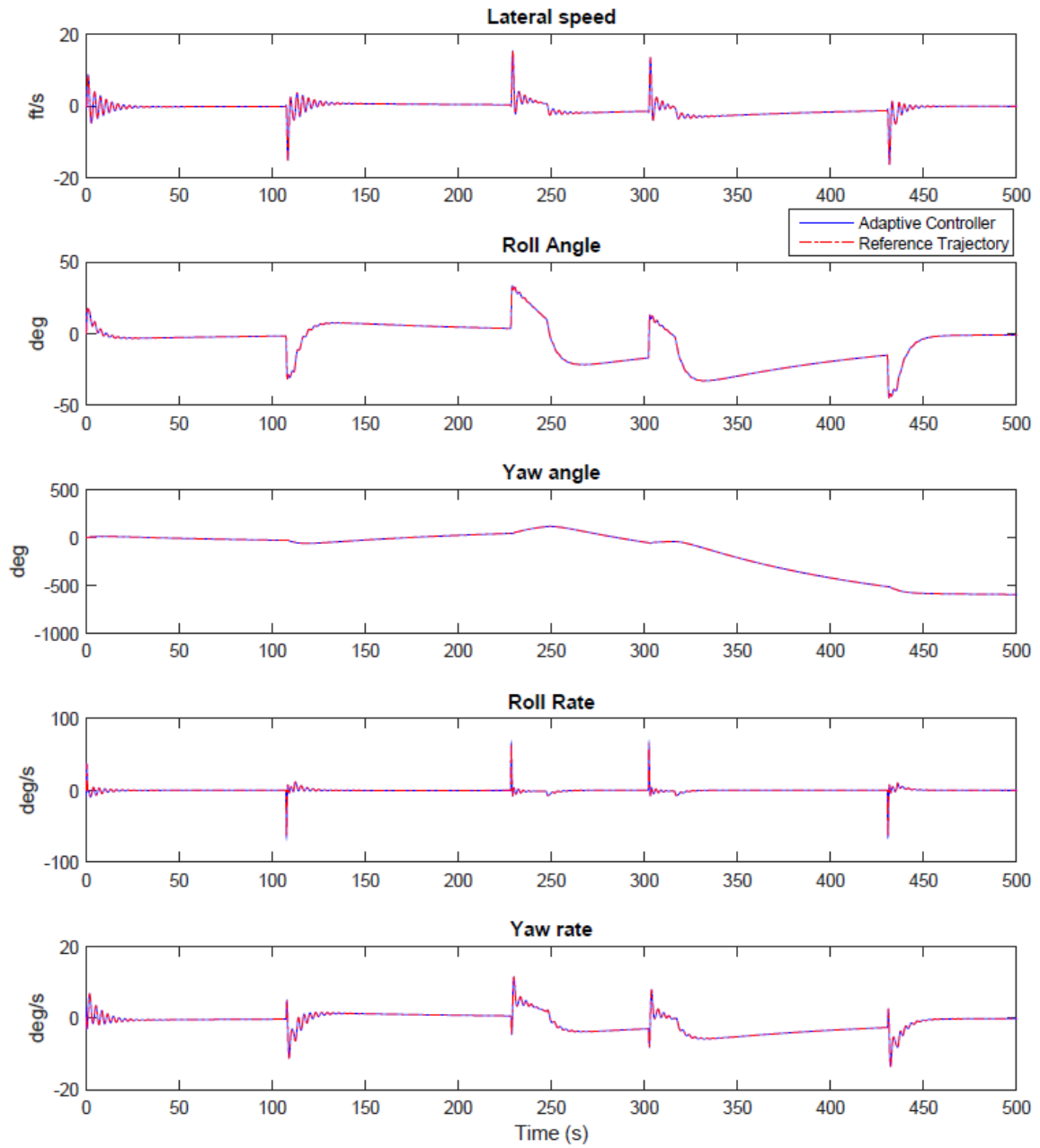
Figure 4.25. Lateral Adaptive Control: Controller performance while tracking a figure 8 trajectory with superimposed sinusoidal persistent disturbances
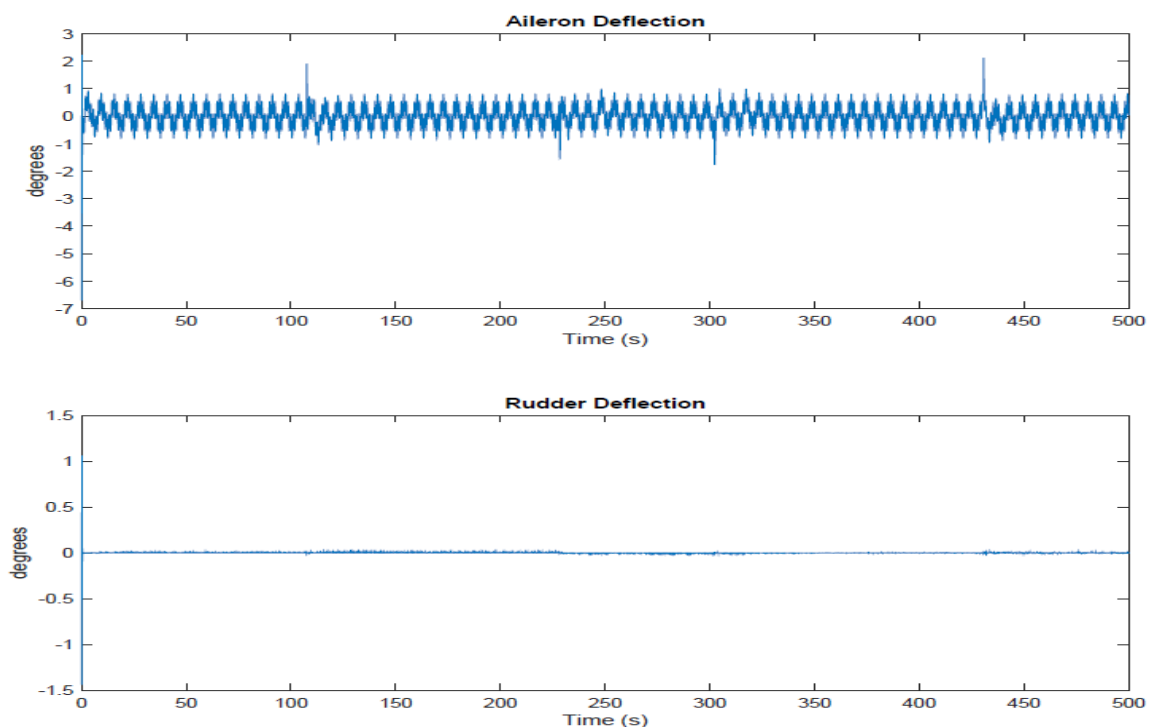
Figure 4.26. Lateral Adaptive Control: Control Deflections while tracking a figure 8 trajectory with superimposed sinusoidal persistent disturbances
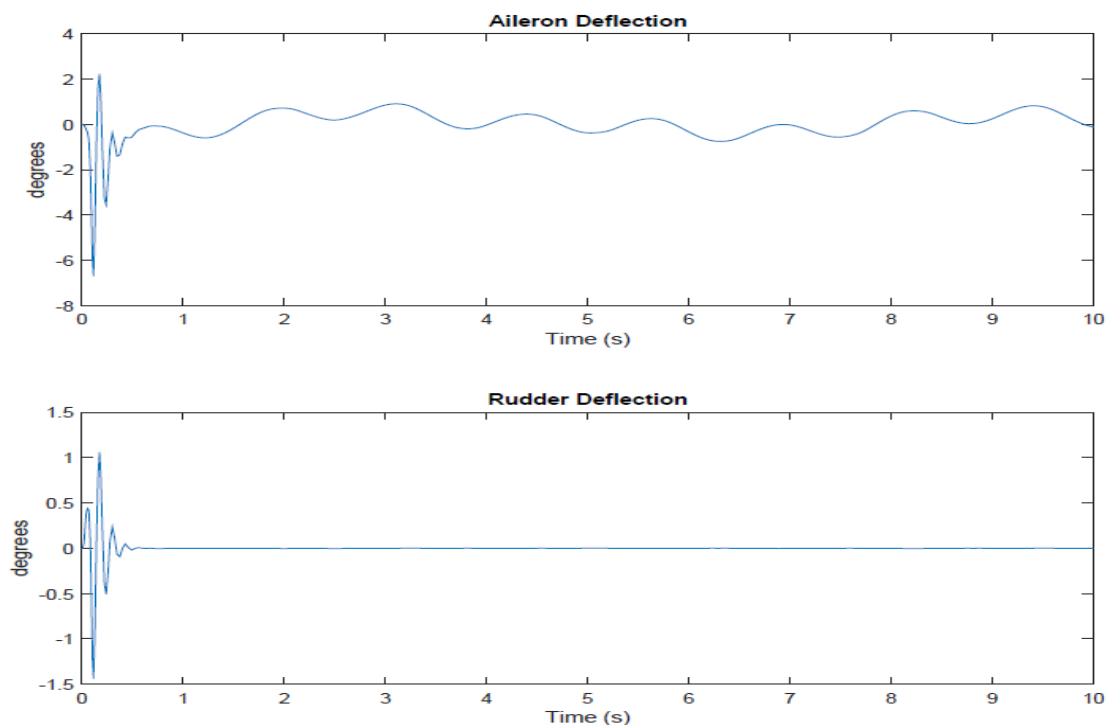

Figure 4.27. Lateral Adaptive Control: Control Deflections while tracking a figure 8 trajectory with superimposed sinusoidal persistent disturbances cut to the first 10 seconds
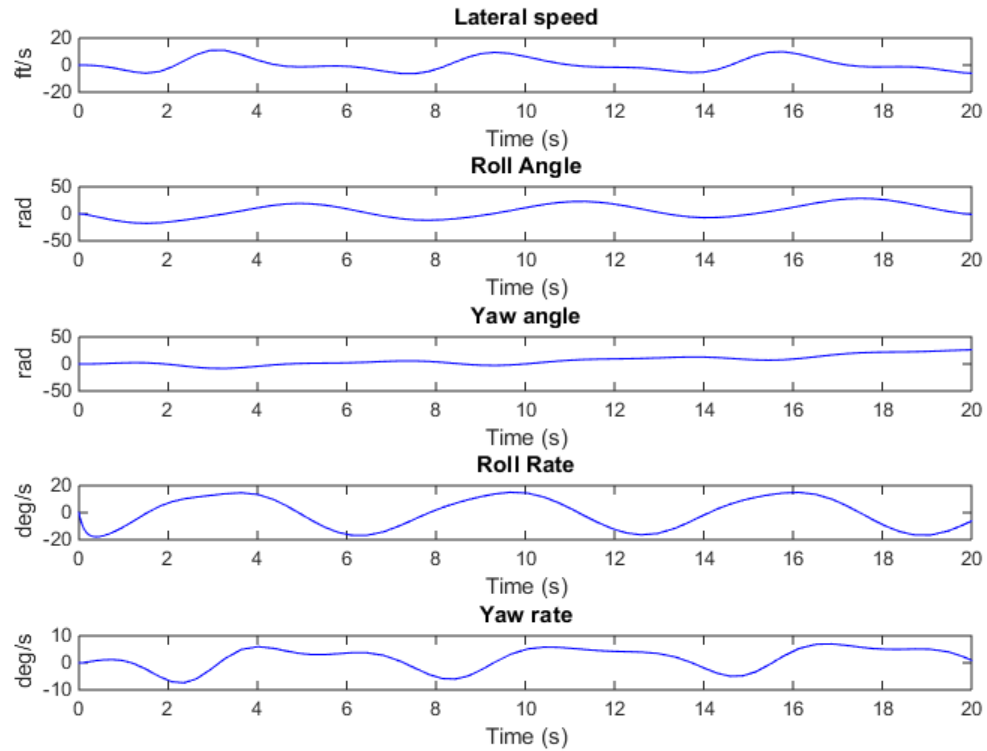
Figure 4.28. Open-loop response of nonlinear system to persistent disturbance – Lateral States.

4.2 Nonlinear Analysis

A 6-DoF nonlinear aircraft model developed in accordance with the aircraft aerody-namic coefficients provided in Table 3.2 is used to to test the performance of the adaptive control scheme mentioned in equation 3.21. The open loop nonlinear system is stable in the vicinity of a steady, wings-level trim condition but is unable to maintain steady state when acted upon by a persistent sinusoidal disturbance, this can be observed in Figure 4.28.

In order for the adaptive controller to track a reference trajectory there are two require-ments, the linear states and, the linear control inputs that are used to generate these linear
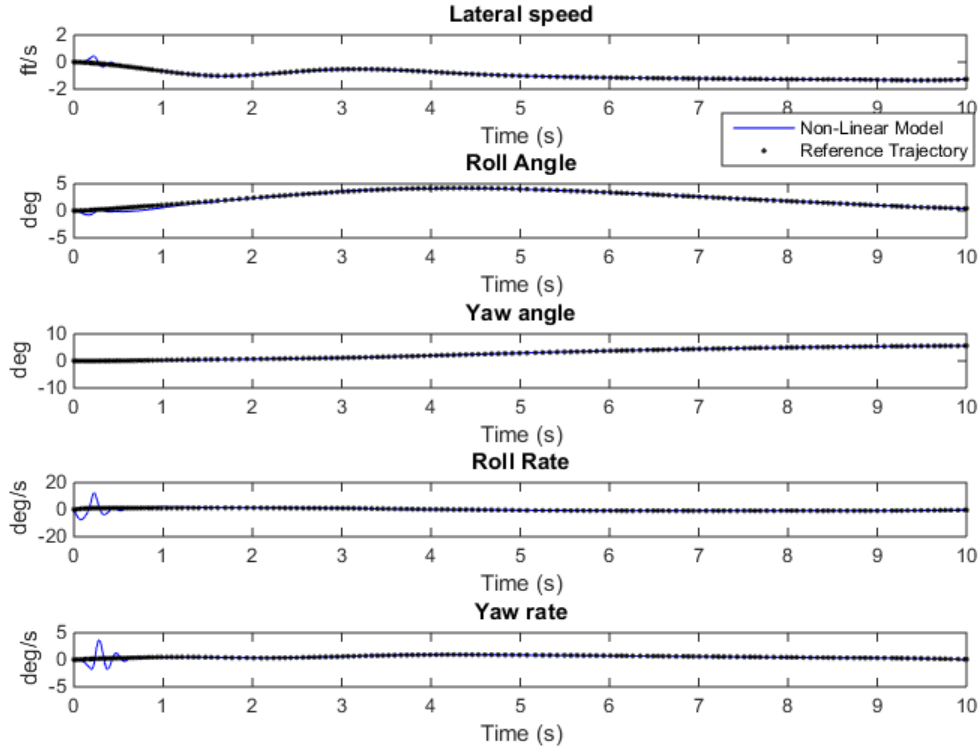
Figure 4.29. Nonlinear Tracking of a heading change in presence of a persistent disturbance – Lateral States

states. These can either be generated by using a linear lateral and longitudinal state space model or by using a time history of the linear states and control inputs to generate an ideal output by using the sensor blended C matrix as referenced in equation 3.53 and, 3.54. These longitudinal and lateral outputs are then used to create output error vectors $e_{y_{long}}$ and $e_{y_{lat}}$ which are used in the adaptive scheme. The simulation is set up and the controller is required to track a $5°$ change in heading and a 50 ft climb simultaneously in a 10 second interval while being acted upon by a persistent sinusoidal disturbance of frequency 1rad/sec. The results obtained are presented below.
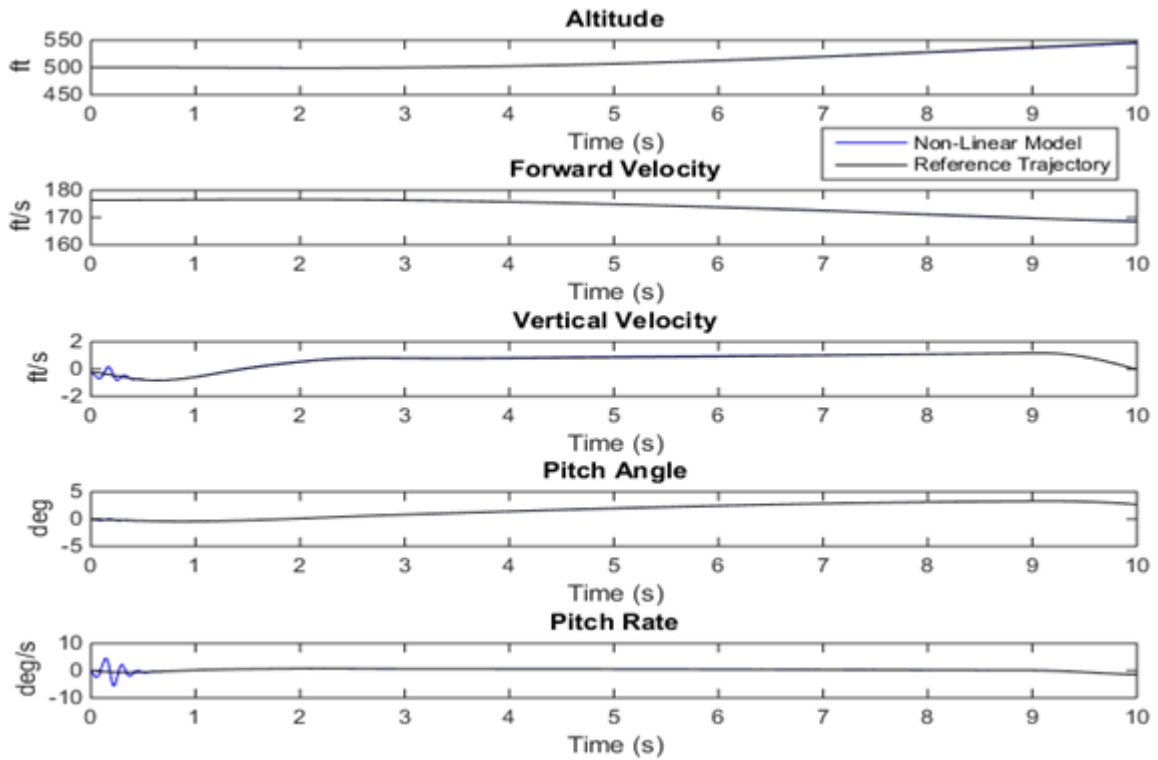
Figure 4.30. Nonlinear Tracking of a heading change in presence of a persistent disturbance – Longitudinal States

The closed-loop simulation results, shown in Figures 4.29-4.31, demonstrate that the adaptive controller is successfully able to mitigate the persistent disturbances while track-ing a reference maneuver in 3-D space. It should be noted that the adaptive system is the only controller in operation, and there are no other inner or outer loop controllers em-ployed for the tracking or stabilization of any states or outputs. The control effort required to achieve these objectives are within the bounds of the physical actuators. Even though the control effort during the beginning of the maneuver is relatively large, likely because of the higher output error, the lateral and the longitudinal states are closely tracked. The adaptive gains for these cases are bounded, but do not stabilize to a certain value, which is not required to ensure the stability of the system.
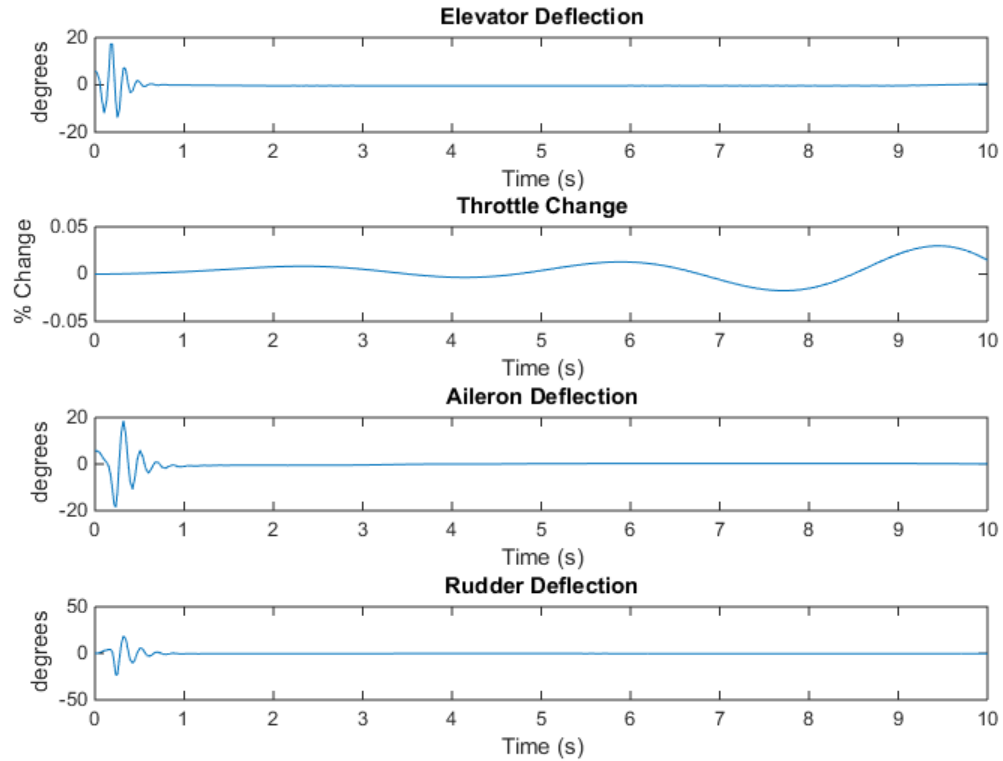
Figure 4.31. Adaptive control inputs required to track a heading and altitude change

The next test scenarios to analyze the performance of the controller will be to track a figure 8 trajectory as described in 4.22. The simulation is set up and the control efforts obtained from the path planner to track a figure 8 trajectory are set up as references. A sinusoidal disturbance with constant frequency of 1 rad/s is fed into the aileron and the elevator simultaneously. The results of the simulation are presented below. An average error analysis was done over the time of the maneuver, the modulus of the error between the reference trajectory and the simulation was noted at each time step and an average for both altitude and yaw was calculated. Over the course of the figure 8 maneuver (about 540
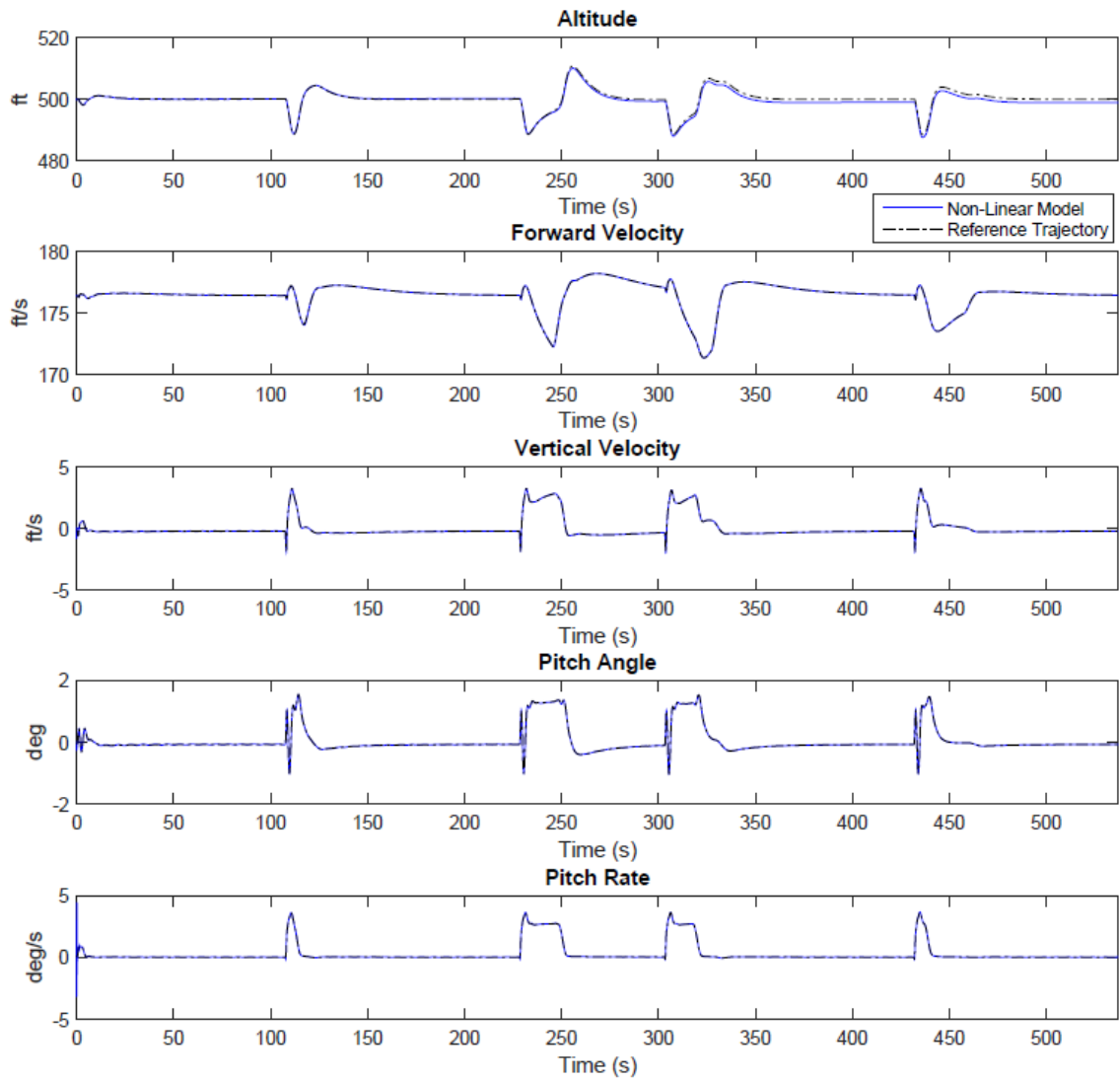
Figure 4.32. Nonlinear Tracking of a Figure 8 pattern: Longitudinal States

seconds) the average error in altitude is 3.4 ft wile the yaw error was calculated to be 1.5 degrees.

The longitudinal states and controls are shown in figure 4.32 and 4.33 respectively. The adaptive scheme is able to account for the persistent disturbances and successfully tracks the reference altitude within a ± 1 ft error. The control effort required to achieve this result lies within the actuator range even thought the initial elevator deflections are large.

Figure 4.35 and 4.34 portray the lateral states and control deflections the direct adaptive scheme follows while tracking a figure 8 loop. There is a very high initial aileron and rudder deflection that can be observed during this maneuver, this can be attributed to the initialization of the UAV at zero yaw angle and the sudden change to a yaw angle change of $350°$. The states are tracked with minimal steady state error or overshoot and the figure 8 loop is tracked, the UAV hits all 4 given waypoints within an error margin of 50t which was set into the algorithm. The tracked x-y coordinates can be seen in figure 4.36. It should also be noted that the adaptive controller is tracking the aircraft states (not north-east-altitude trajectory). The error/divergence of the trajectory in the figure 8 loop can also be attributed to a linear model being used as a reference by a nonlinear system to track aircraft states using the adaptive controller. There is no explicit outer-loop tracking of the north-east position within the adaptive control implementation.
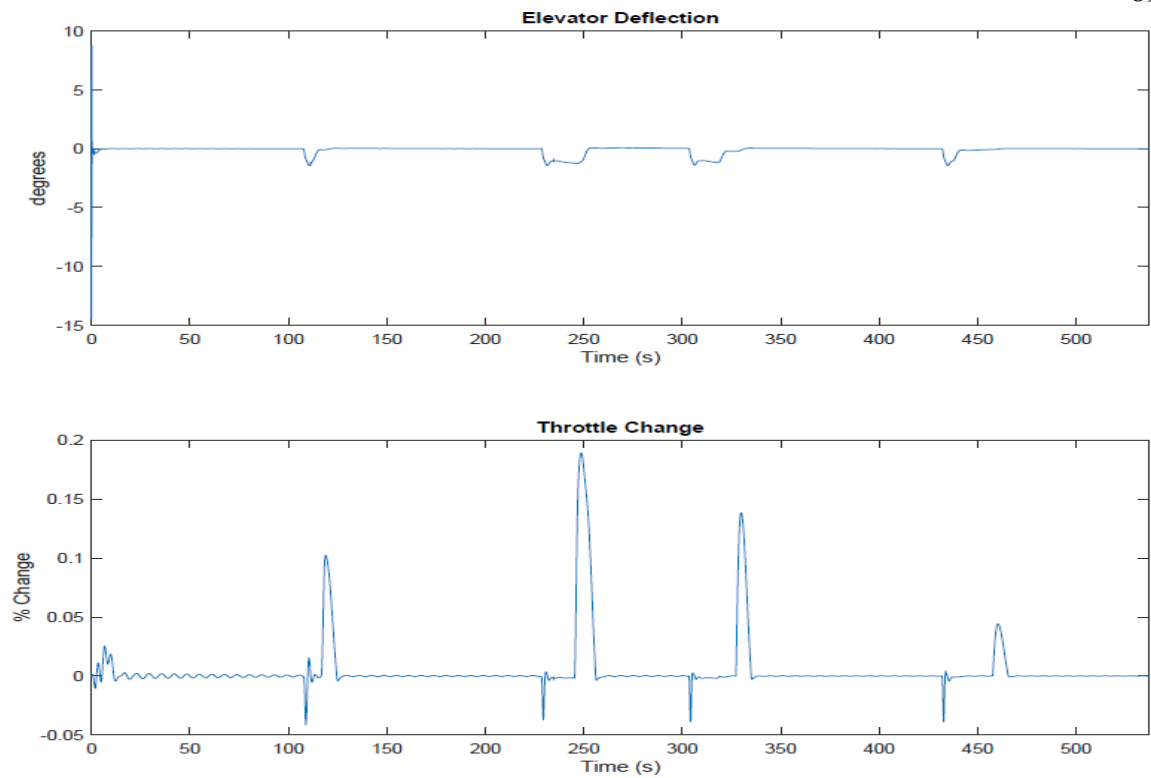
Figure 4.33. Nonlinear Tracking of a Figure 8 pattern: Longitudinal Controls
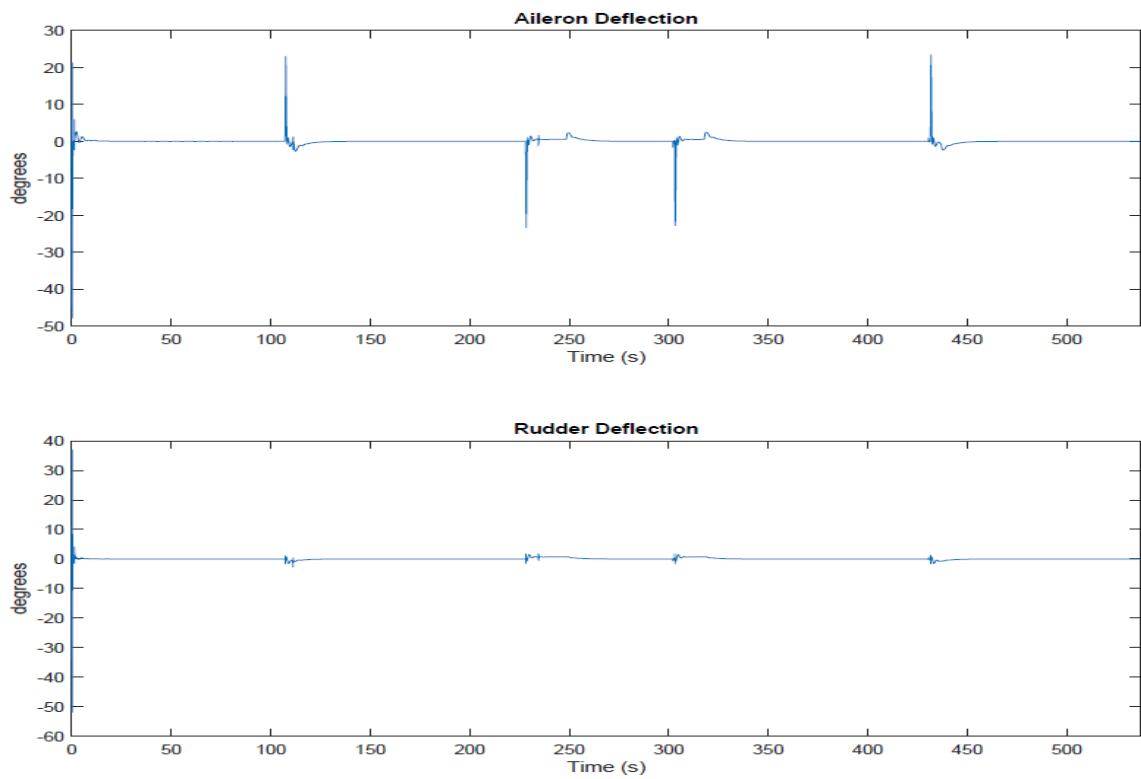

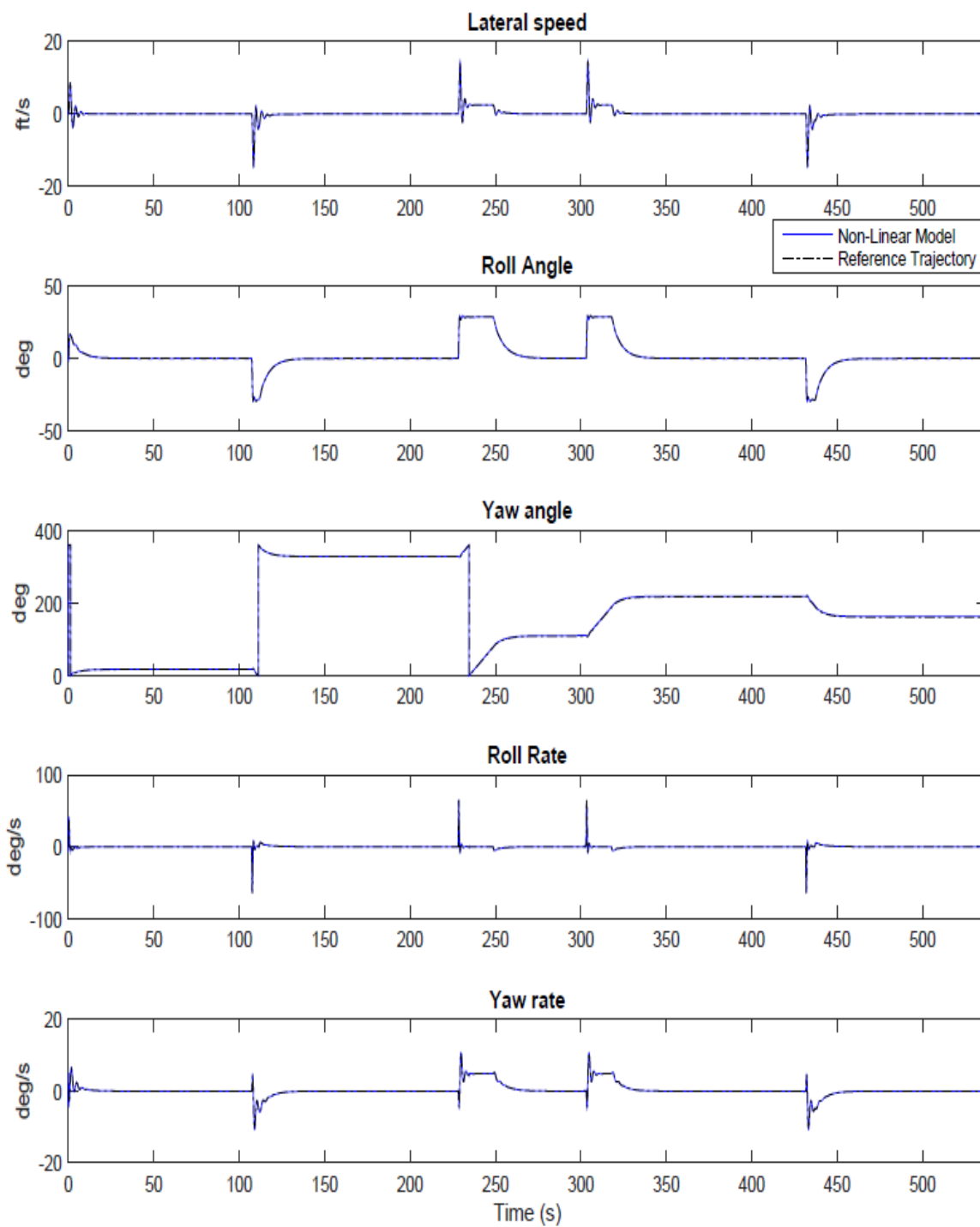Figure 4.34. Nonlinear Tracking of a Figure 8 pattern: Lateral Controls

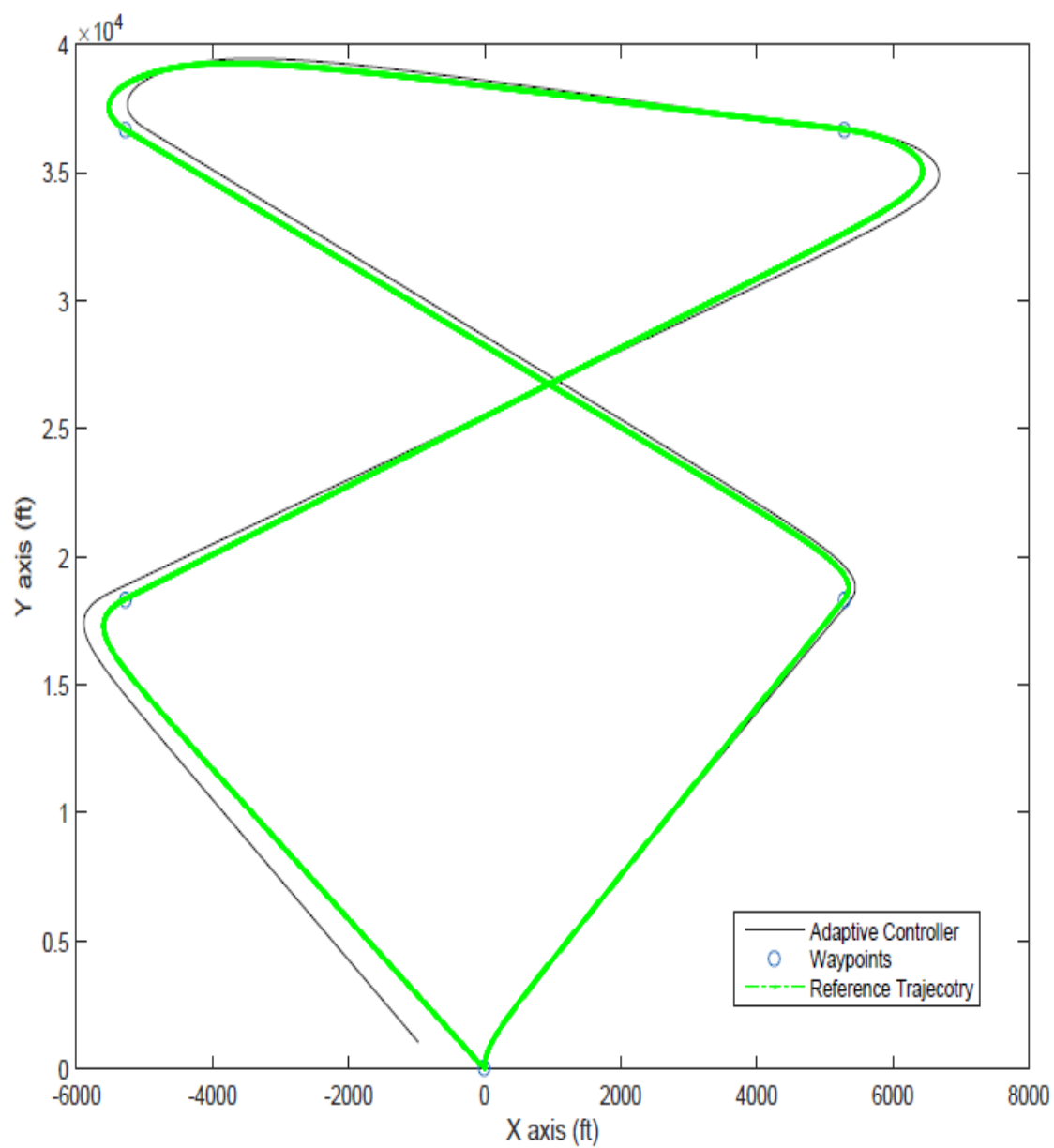Figure 4.35. Nonlinear Tracking of a Figure 8 pattern: Lateral States

Figure 4.36. Nonlinear Tracking of a Figure 8 pattern: Tracked Trajectory vs Reference Trajectory

4.3   Disturbance Accommodation in Direct Adaptive Control Scheme

To further understand this phenomenon of disturbance mitigation while there is a discrepancy in the modeled disturbance and the disturbance being injected into the system the adaptive gains need to be analyzed. Since the Adaptive Regulator gain and the Disturbance Adaptive Gain are coupled together to regulate the output error to zero, the tracking part of the simulation is turned off to isolate the effects of the regulatory behavior of the adaptive scheme. The first case to be studied will be regulating the UAV states with both the regulator and disturbance gains, while there is a persistent disturbance being fed into the system the frequency of which matches the modeling frequency of the disturbance adaptive gain.

 Here, the adaptive system is largely able to mitigate any effects of the persistent disturbances in the states of the UAV, although there is a small steady state error ($\approx 0.05°$) in the yaw angle as seen in figure 4.37. From figure 4.38 it can be observed that the disturbance adaptive gain increases in amplitude over time until it adapts to the disturbance signal being fed into the system (negates it), the regulator gain at that point decays until it goes to zero. This provides an insight towards the working of this adaptive scheme, in the beginning of the simulation when the the disturbance adaptive gain has not yet stabilized, the error is propagated into the output and is mitigated with a combination of both the regulator and the disturbance gain. Further, to investigate the error accommodation in the modeling of disturbances and the persistent disturbance being fed in, the above simulation is repeated with the modeling frequency set to 1rad/s while the input disturbance is 5 rad/s. Figure 4.39 depicts the states of the UAV begin regulated by the direct adaptive controller, com-
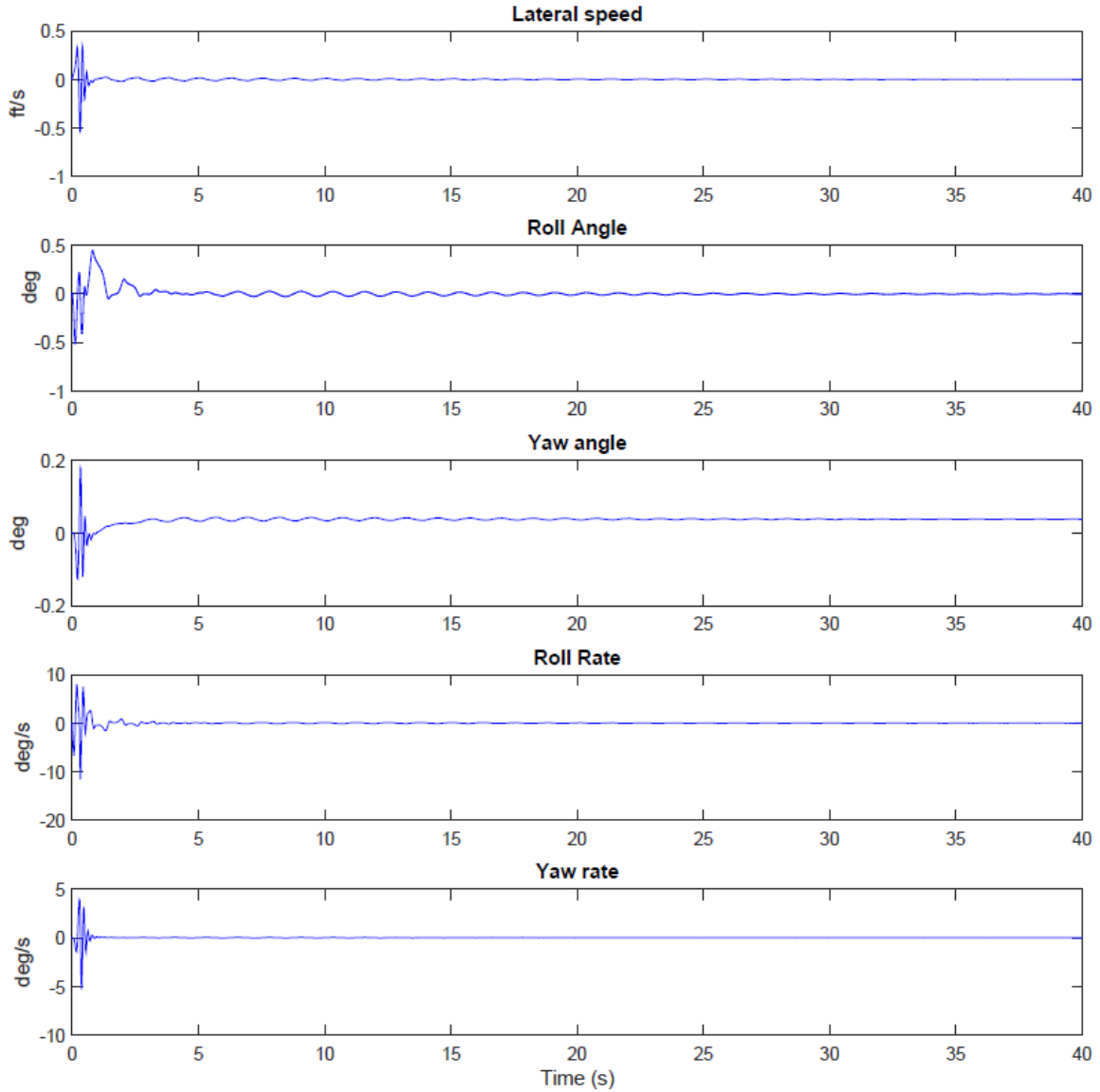
Figure 4.37. UAV States with Disturbance Adaptive Regulation and no Disturbance Freq Modeling Error

paring it to figure 4.37 it can be observed that the controller performance has deteriorated slightly, lateral speed and yaw angles have not stabilized even though the simulation has been run for the same amount of time. The steady state yaw angle has almost doubled ($\approx 0.05°$) and initial amplitude fluctuation of the states has also increased. The Regulator adaptive gain (figure. 4.40) does not reduce to zero like in the previous case implying that
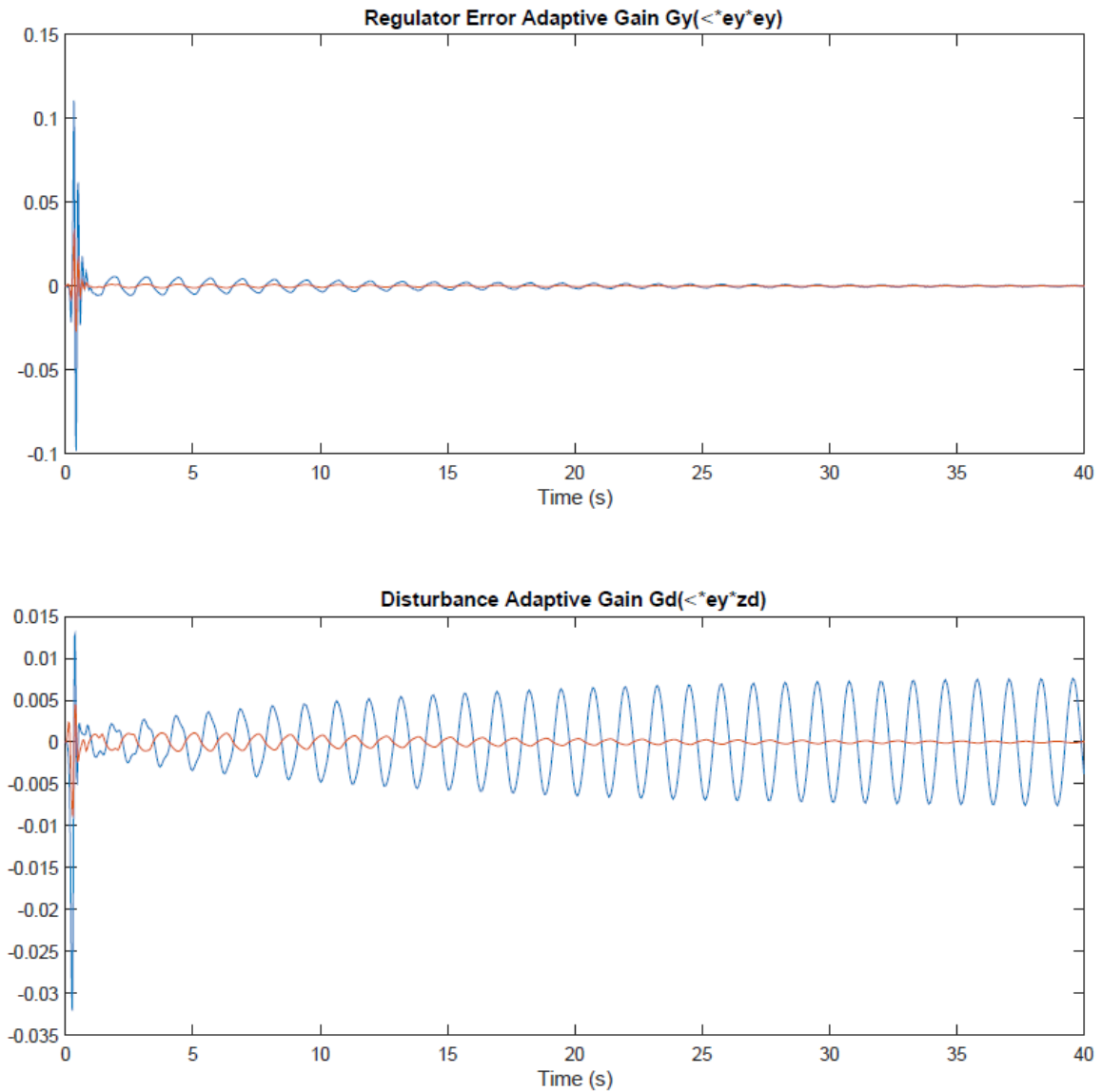
Figure 4.38. Adaptive Gains with Disturbance Adaptive Regulation and no Disturbance Freq Modeling Error

the disturbance gain Gd has not been able to find the right frequency, this can be observed

in the superimposed frequency in the figure. This can be attributed to the 5rad/s frequency

superimposed on the 1rad/s signal that was modeled. Continuing this analysis, the final

logical step will be to analyze the regulating effect of the direct adaptive controller with just

the Adaptive regulating gain and comparing it to the previous case to determine how much
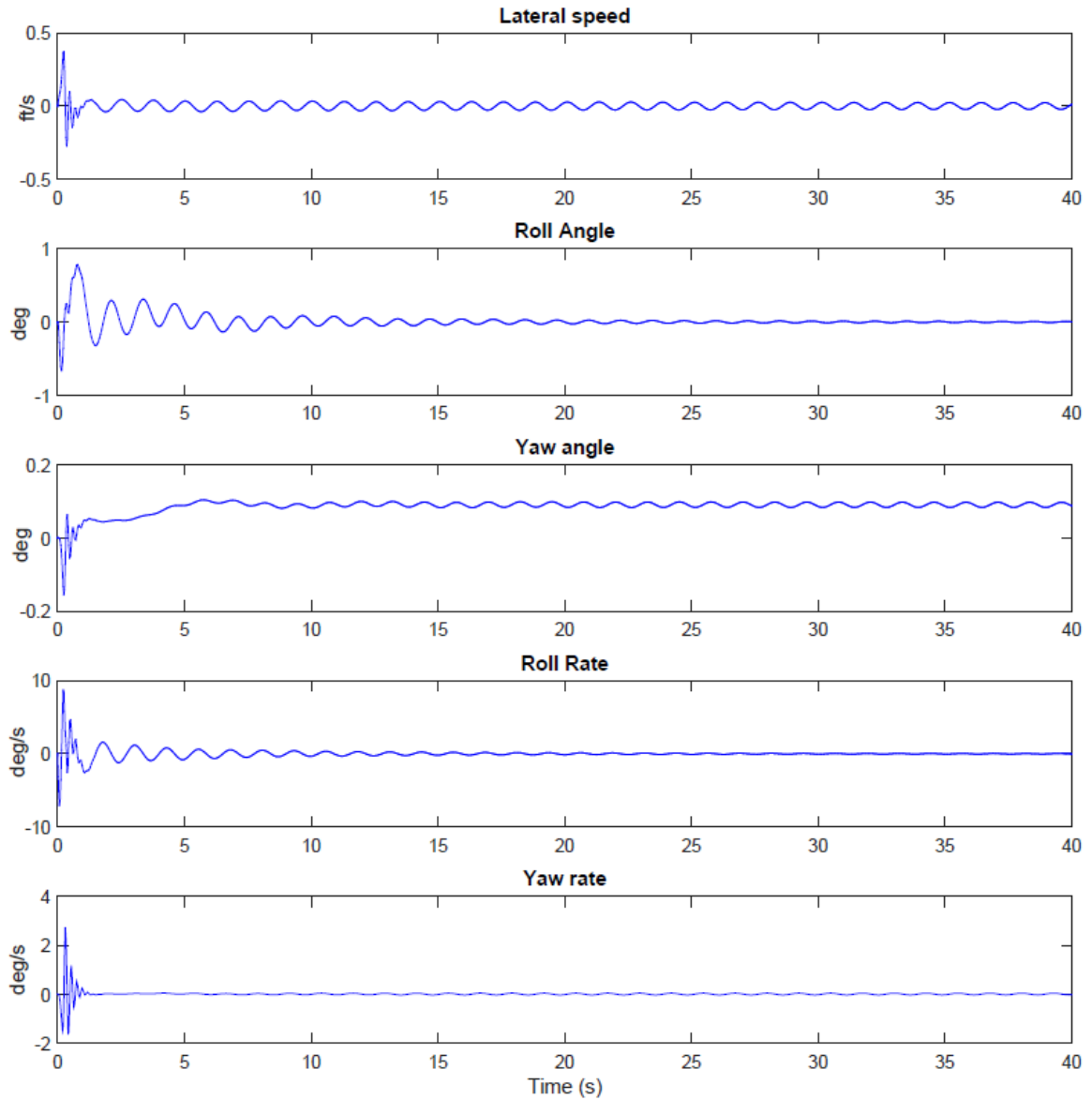
Figure 4.39. UAV States with Disturbance Adaptive Regulation and Disturbance Freq Modeling Error

performance enhancement is achieved by using Disturbance adaptive gain while there is a mismatch between the modeling frequency and the disturbance being fed into the system. Figure 4.41 depicts the UAV states, comparing them to the results obtained in figure 4.39 it can be observed that there is no significant difference between these cases. The same
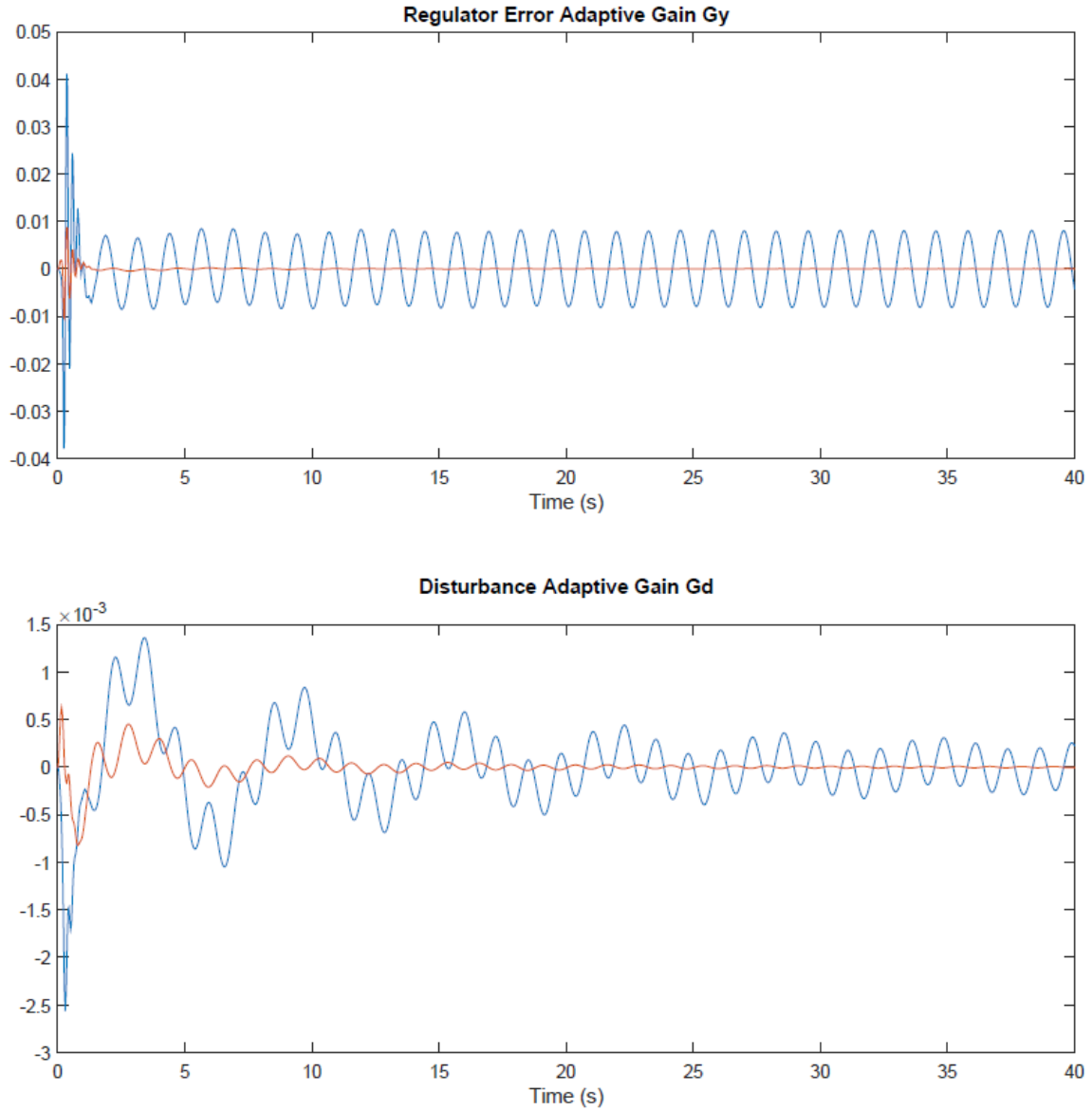
Figure 4.40. Adaptive Gains with Disturbance Adaptive Regulation and Disturbance Freq Modeling Error

can be stated for figure 4.42 where the regulator adaptive gain is similar in both amplitude

and frequency. Therefore, it is safe to conclude that the adaptive disturbance gain does not

contribute much to the regulation of the UAV states while there is an error in the modeling
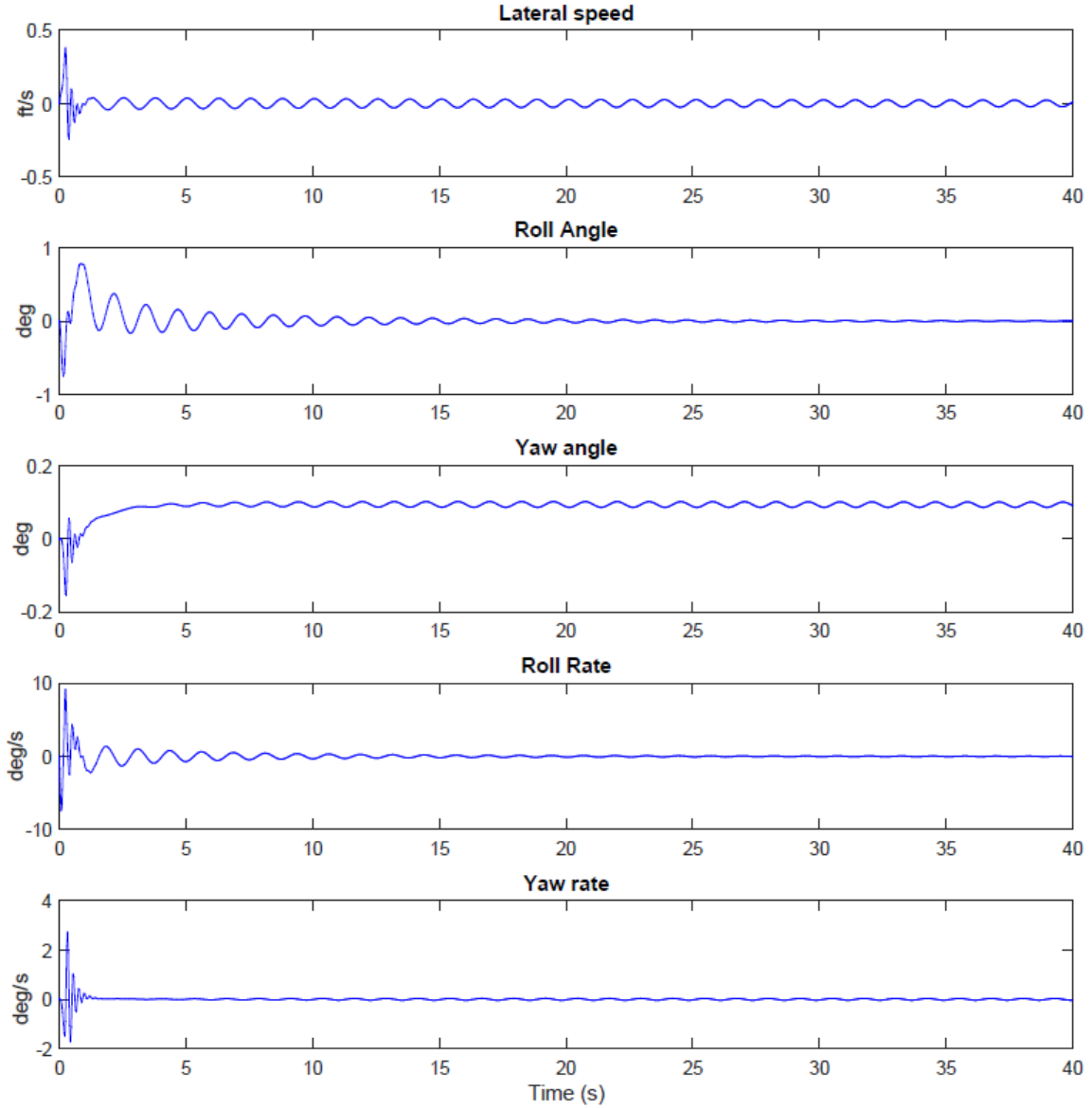
Figure 4.41. UAV States with Disturbance Adaptive Regulation and Disturbance Freq Modeling Error

frequency. This implies that the disturbance error is propagated into the outputs which is then regulated by the regulator part of the adaptive scheme($G_y = \sigma e_y e_y^T$).

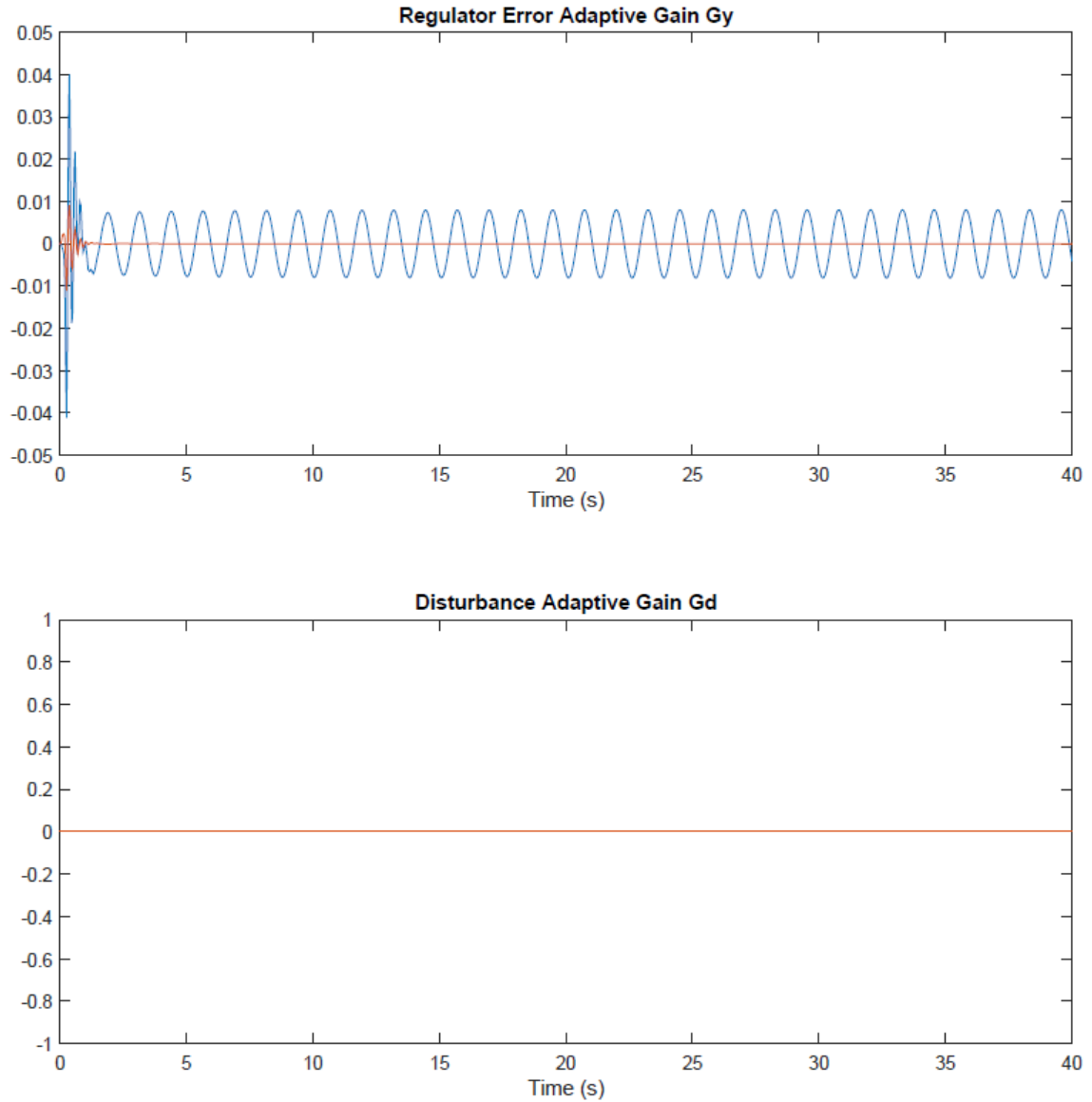Figure 4.42. Adaptive Gains with Disturbance Adaptive Regulation and Disturbance Freq Modeling Error

4.4 Modeling Error Analysis

An important benefit of the adaptive controller is the robustness of the controller; therefore, a modeling error analysis is conducted to evaluate the performance of the controller in the presence of various forms of modeling errors. Several cases are studied to determine

the performance of the adaptive system in the presence of modeling errors. The first and the most basic cases correspond to a percentage error in the A matrix $(A \pm \Delta A)$. The two cases run in this scenario are a $\pm 20\%$ modeling error compared against the baseline linear model. The study of modeling error performance is limited to the lateral system, as the results of the performance of this case can be generalized for to the longitudinal controller. The next set of test cases includes introducing common modeling errors into the system that are associated with the aerodynamic coefficients that appear in the UAV model. These coefficients change certain values within the A matrix, unlike the previous test cases (e.g. a 10% error in the roll damping of the aircraft translates to a change in only one coefficient in the 5x5 lateral A matrix). For the first modeling error case, the eigenvalues of the system vary as a function of the multiple that is added to the system (i.e. the eigenvalues of 1.2A will be scaled by that factor). It is important to check during this modeling error study that the system being controlled still satisfies all the assumptions mentioned in Section 3.3. A robustness limit can be generated based on the amount of error that can be attributed to the system before the transmission zeros (other than the ones that were initially unstable/neutrally stable) become unstable, which in turn defines theoretical limitations on the implementation of the controller.

In the second modeling error scenario, where only a few coefficients of the A matrix differ, there needs to be a check performed on every iteration to verify that all the assumptions are satisfied before the adaptive system can be implemented. It should be noted, however, that these checks are a guarantee of a stable system as per the results derived in Section 3.3 and no further modifications to the controller are required.
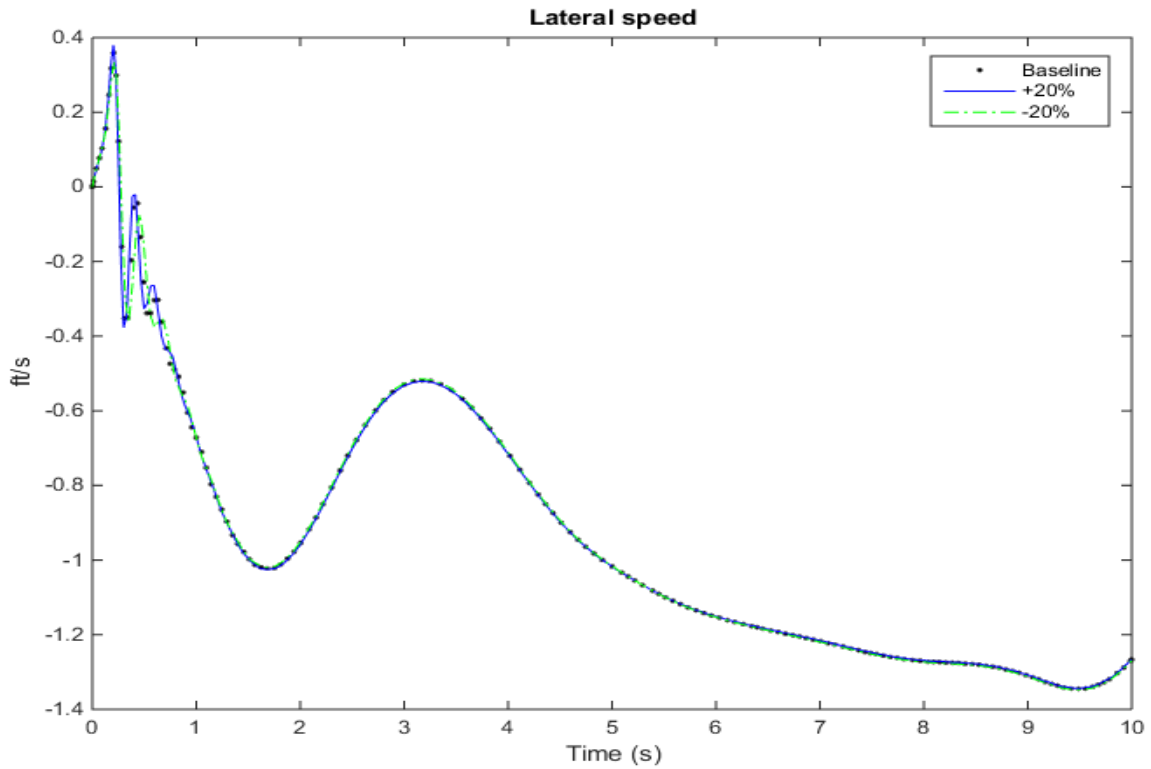
Figure 4.43. Lateral Speed change with Modeling Error

The results in Figures 4.43-4.47 show that the adaptive controller is able to account for ±20 modeling error in the A matrices of the linear lateral UAV model. Retuning of the control gains would help achieve better tracking of the reference states.

To model this uncertainty into the linear lateral dynamic system, two important lateral-directional aerodynamic coefficients are varied and their effects are propagated into the lateral A matrix. The results depicted in Figures 4.51-4.54 show the controller performance while inducing a 20% error into the roll and yaw damping coefficients. The first case introduced a 20% increase in the roll damping while decreasing the yaw damping by 20%, and the second test scenario corresponded to decreasing both roll and yaw damping by 20%. The dynamical effects of changing the lateral-directional damping can be observed
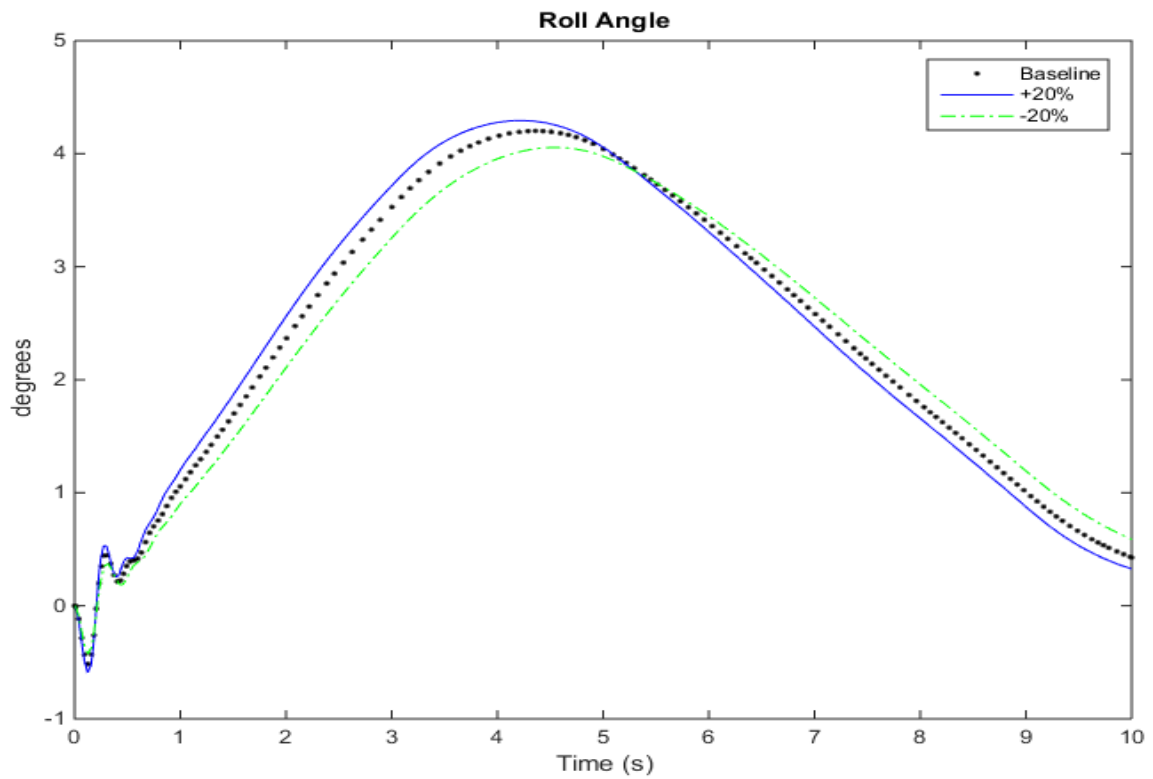
Figure 4.44. Roll Angle change with Modeling Error

in the figures. The deviation in roll angle (Figures 4.51 and 4.53) for a damping increase

corresponds with a lower magnitude rise in the roll angle, whereas the opposite occurs for

the reduction in damping. Similar trends can be observed for the decrease in yaw damping.

The control deflections for these cases do not vary much from the baseline mode, validating

the ability of the controller to fulfill the given objectives.
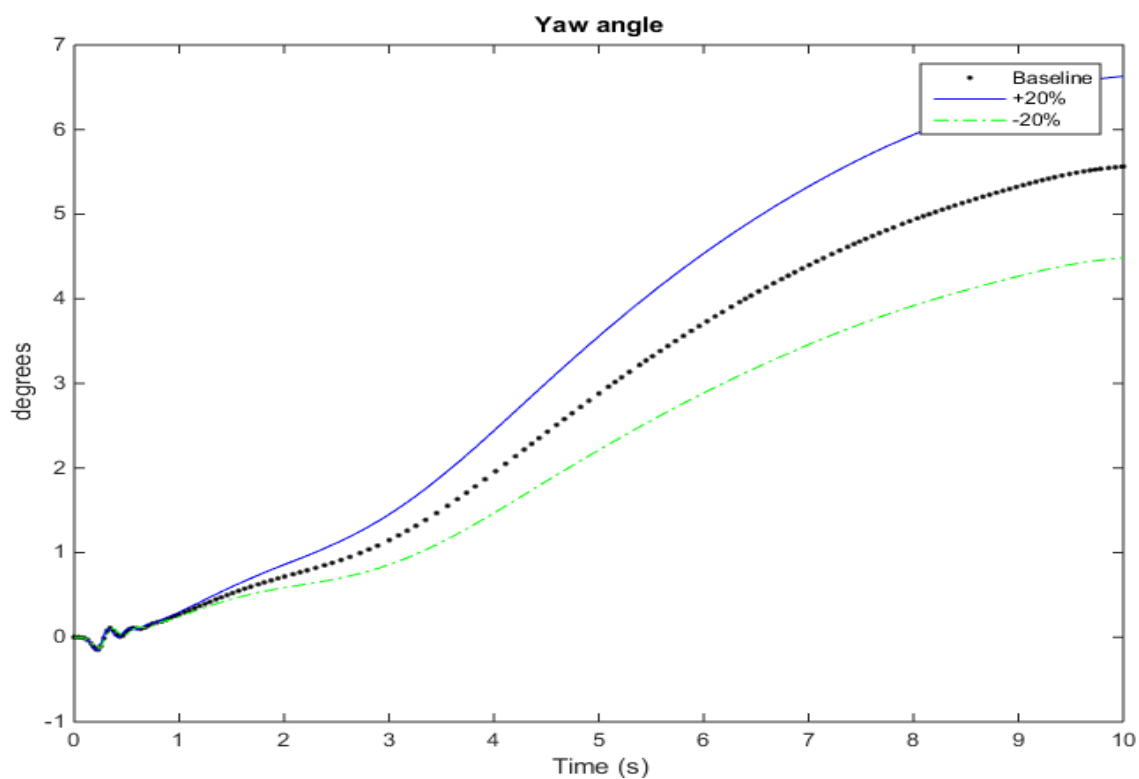
Figure 4.45. Yaw Angle change with Modeling Error
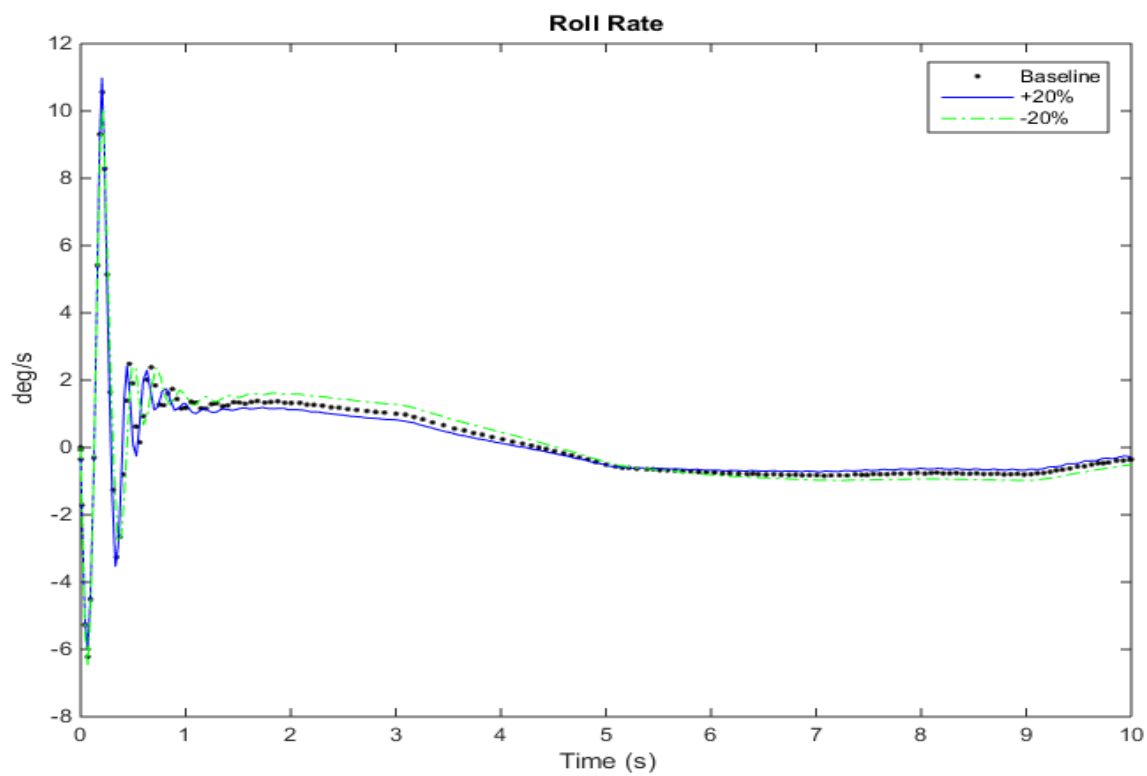
Figure 4.46. Roll Rate change with Modeling Error
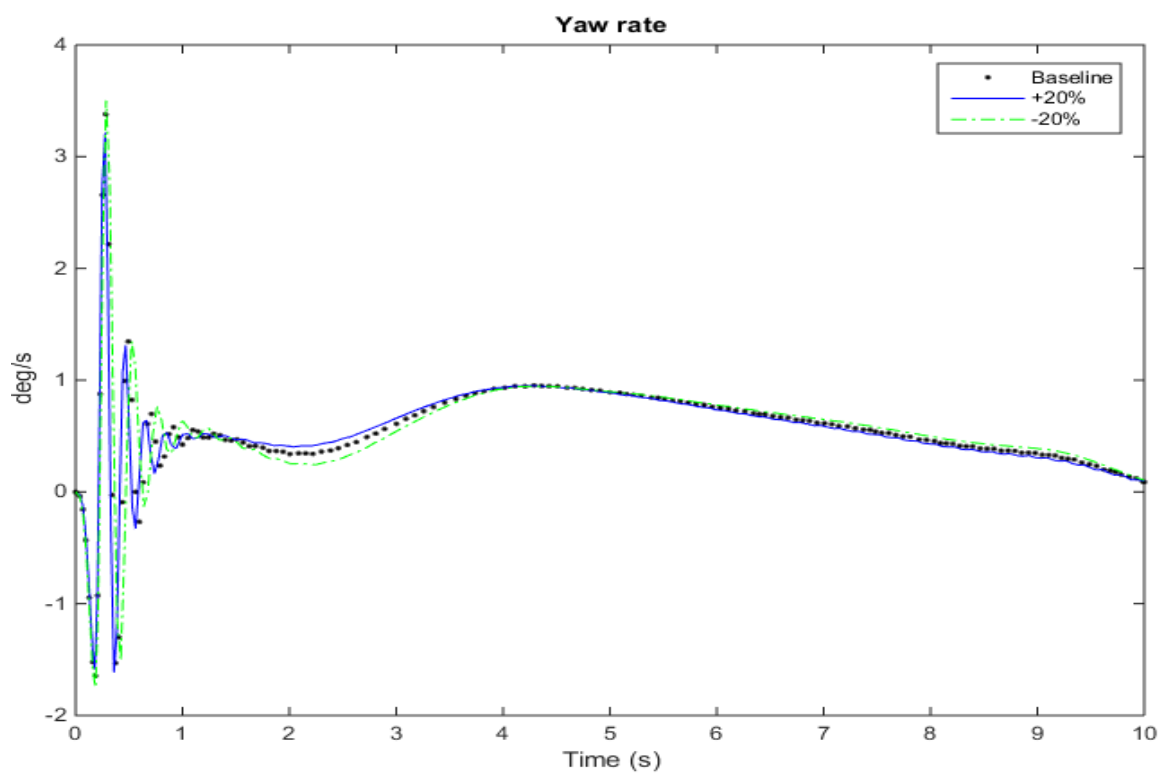
Figure 4.47. Yaw Rate change with Modeling Error
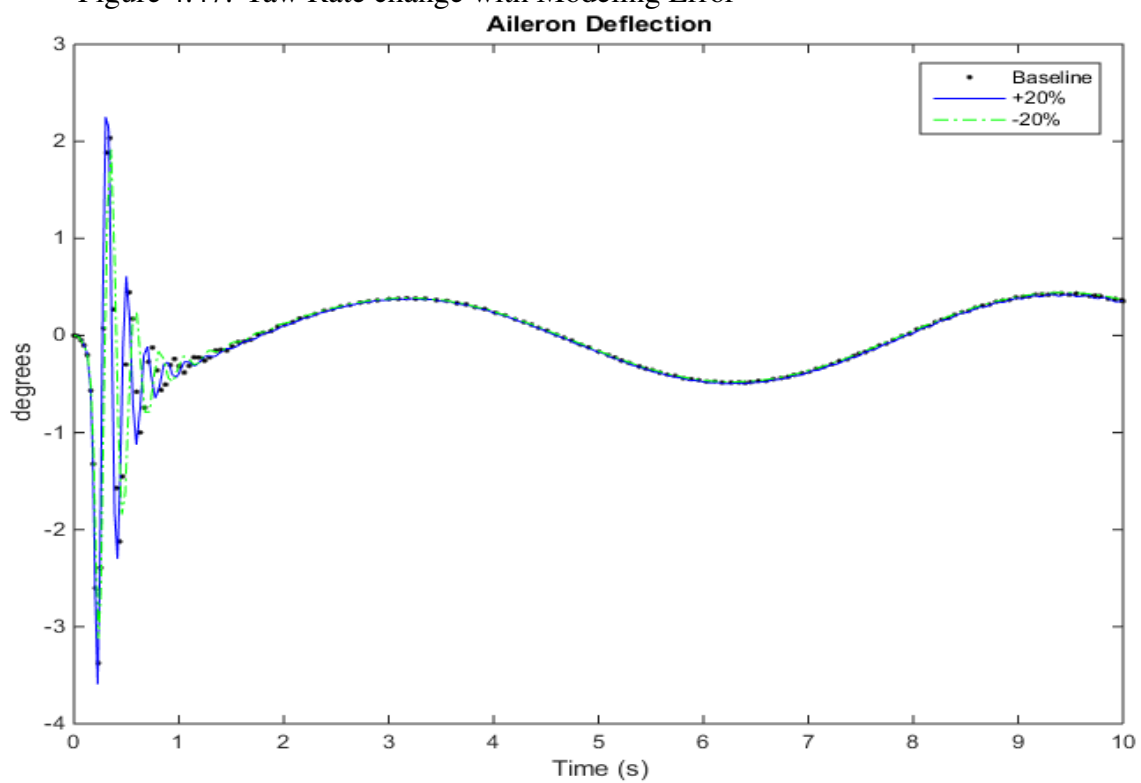
Figure 4.48. Aileron Deflection Change with Modeling Error
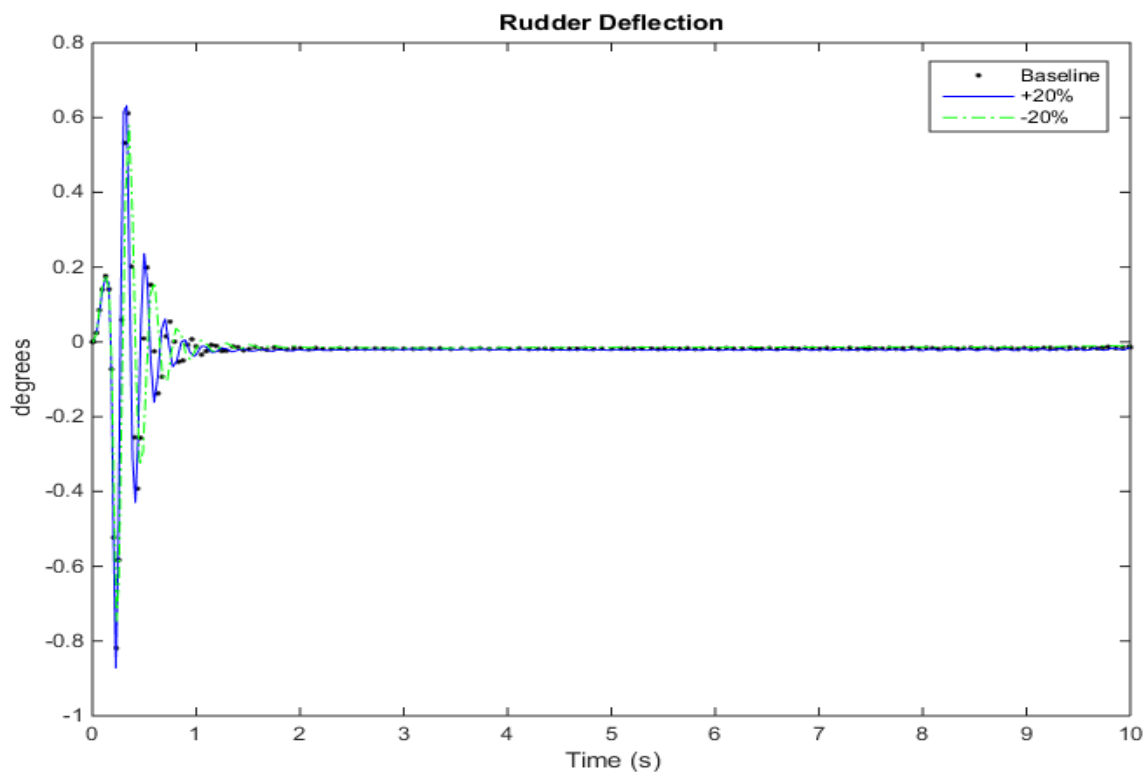
Figure 4.49. Rudder Deflection change with Modeling Error

Figure 4.50. Lateral Speed change with Aerodynamic Modeling Error

Figure 4.51. Roll Angle change with Aerodynamic Modeling Error
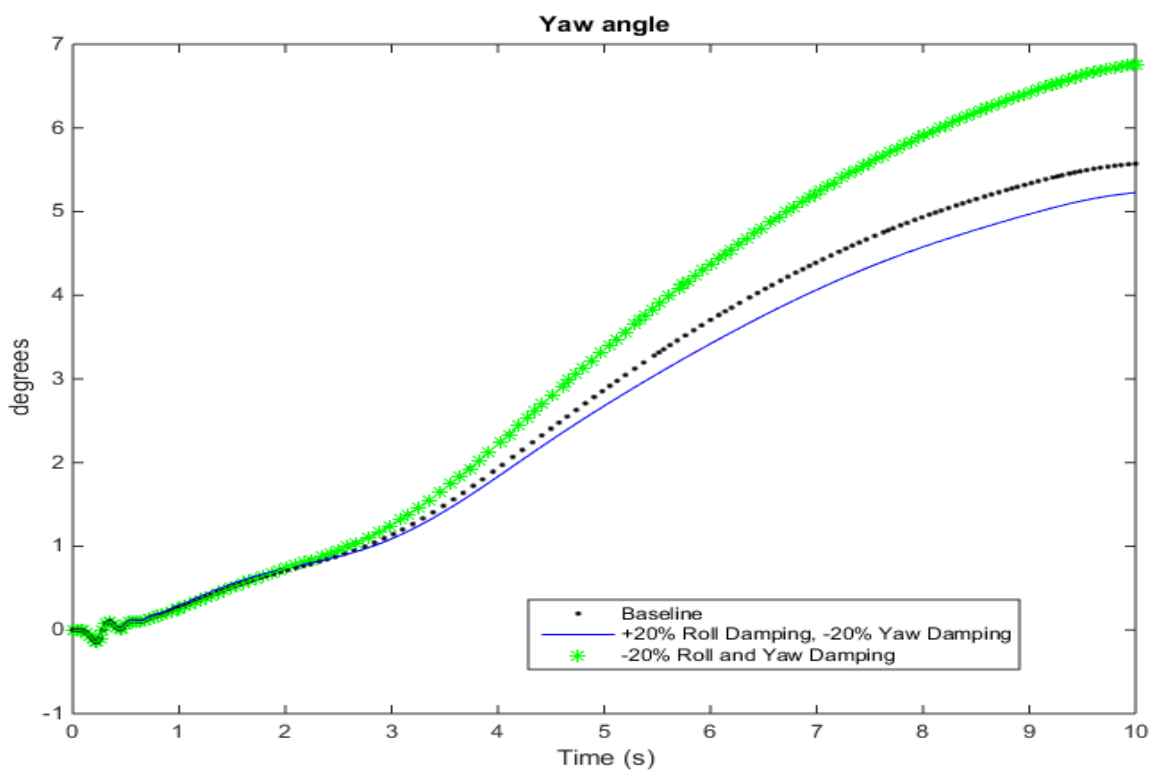
Figure 4.52. Yaw Angle change with Aerodynamic Modeling Error
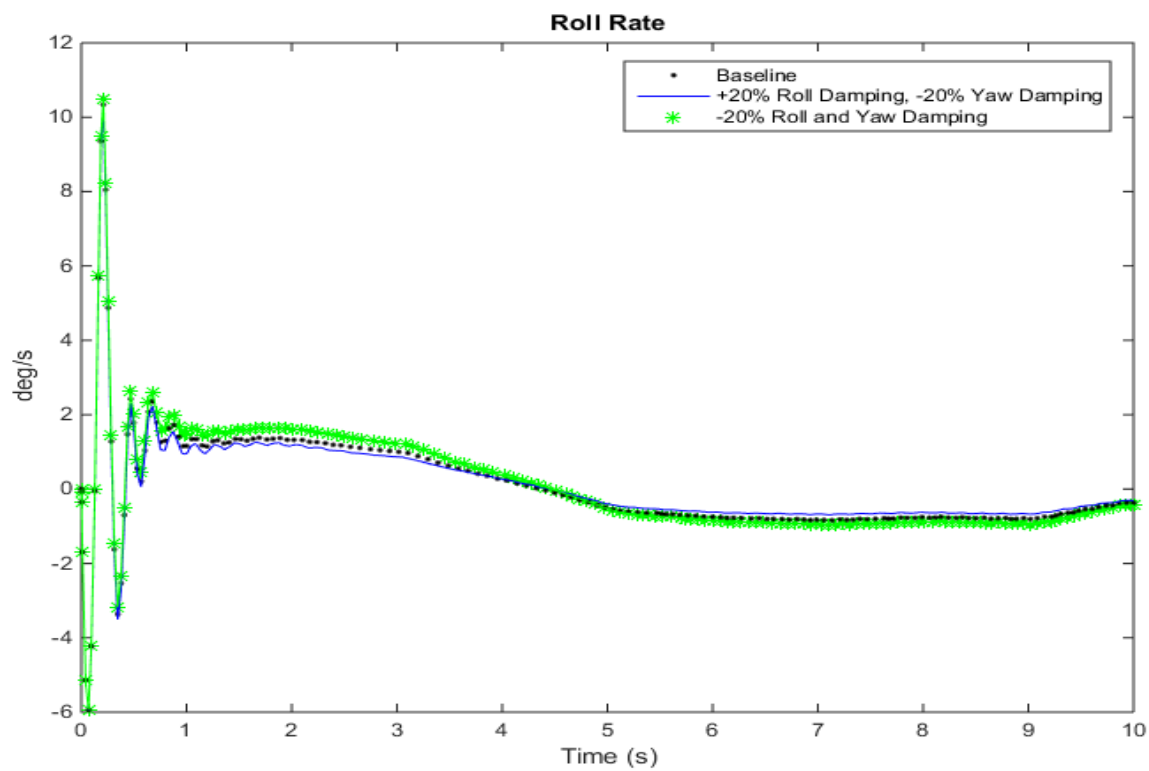
Figure 4.53. Roll Rate change with Aerodynamic Modeling Error
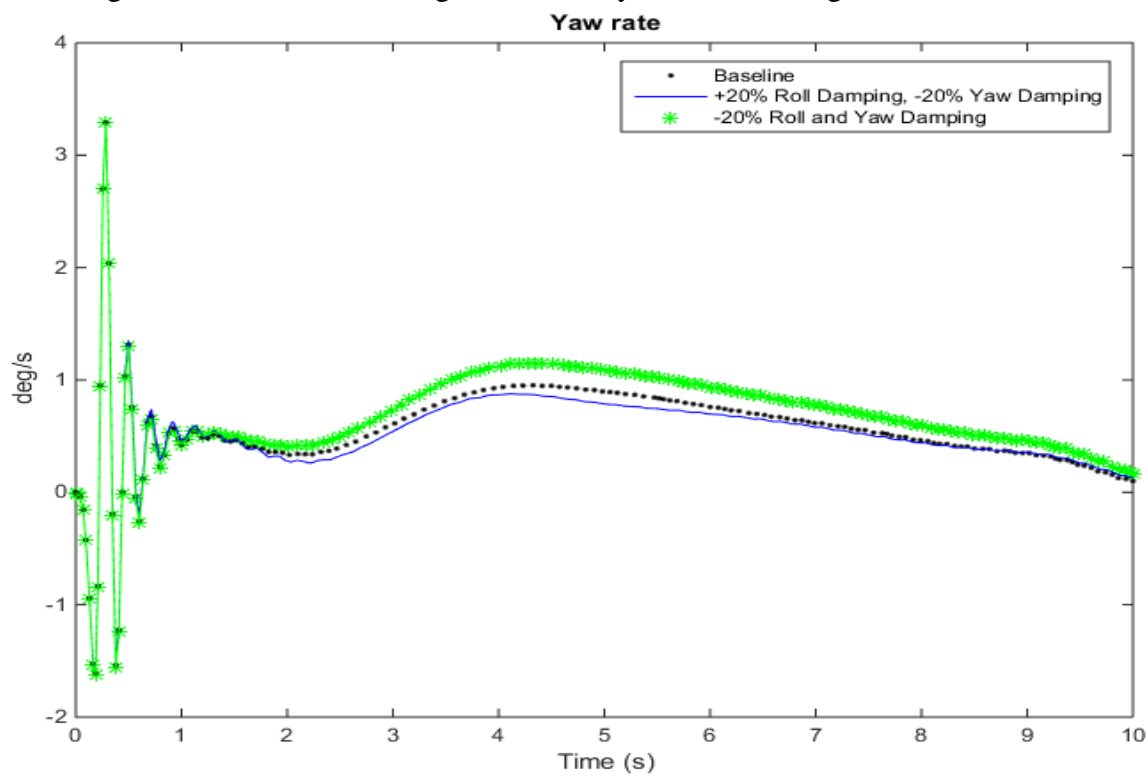
Figure 4.54. Yaw Rate change with Aerodynamic Modeling Error
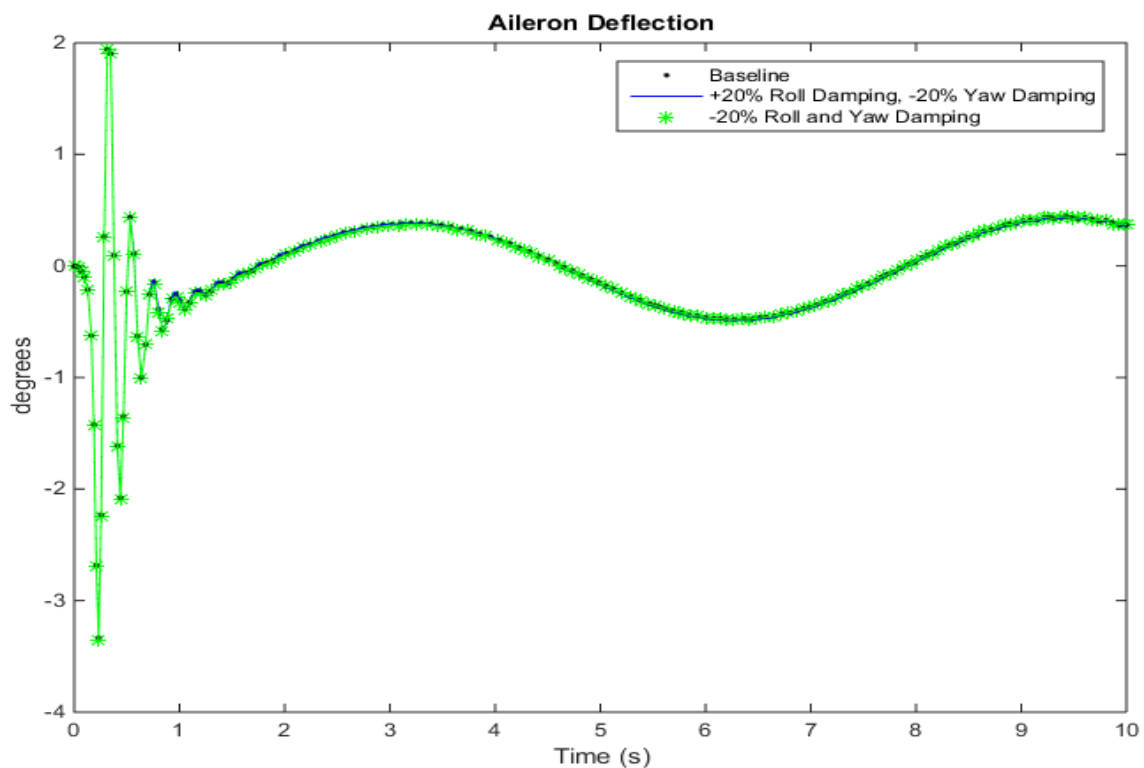
Figure 4.55. Aileron Deflection change with Aerodynamic Modeling Error
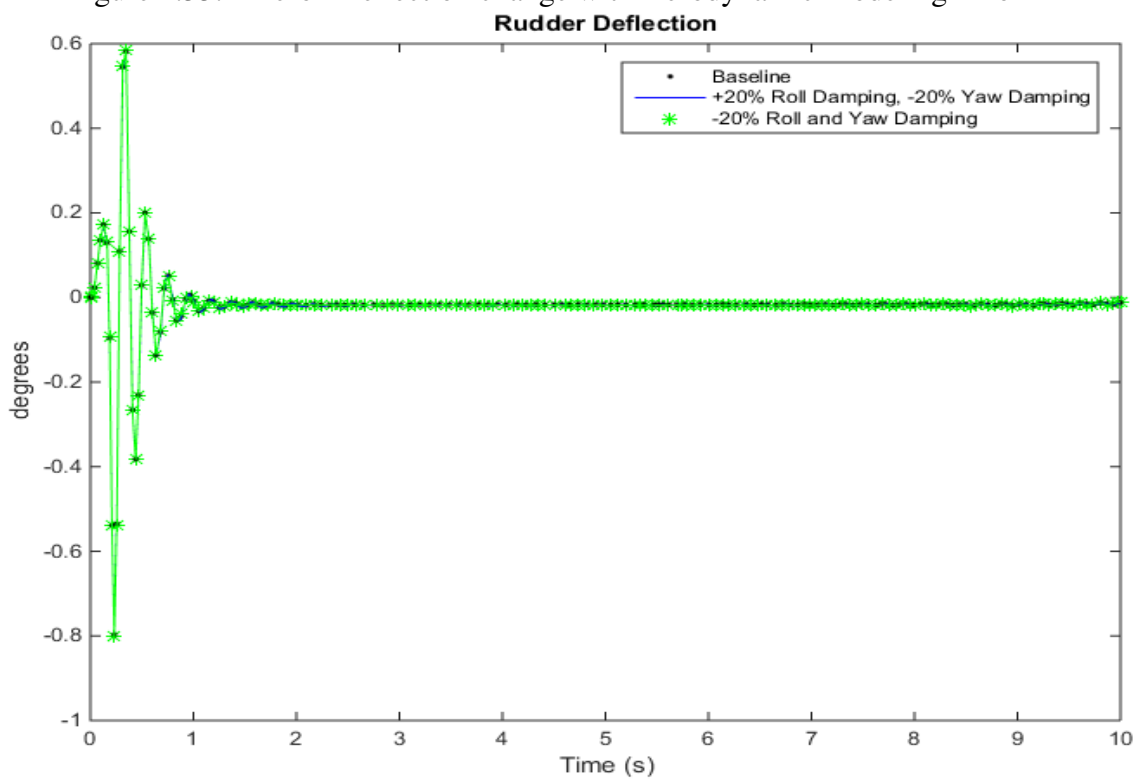
Figure 4.56. Rudder Deflection change with Aerodynamic Modeling Error
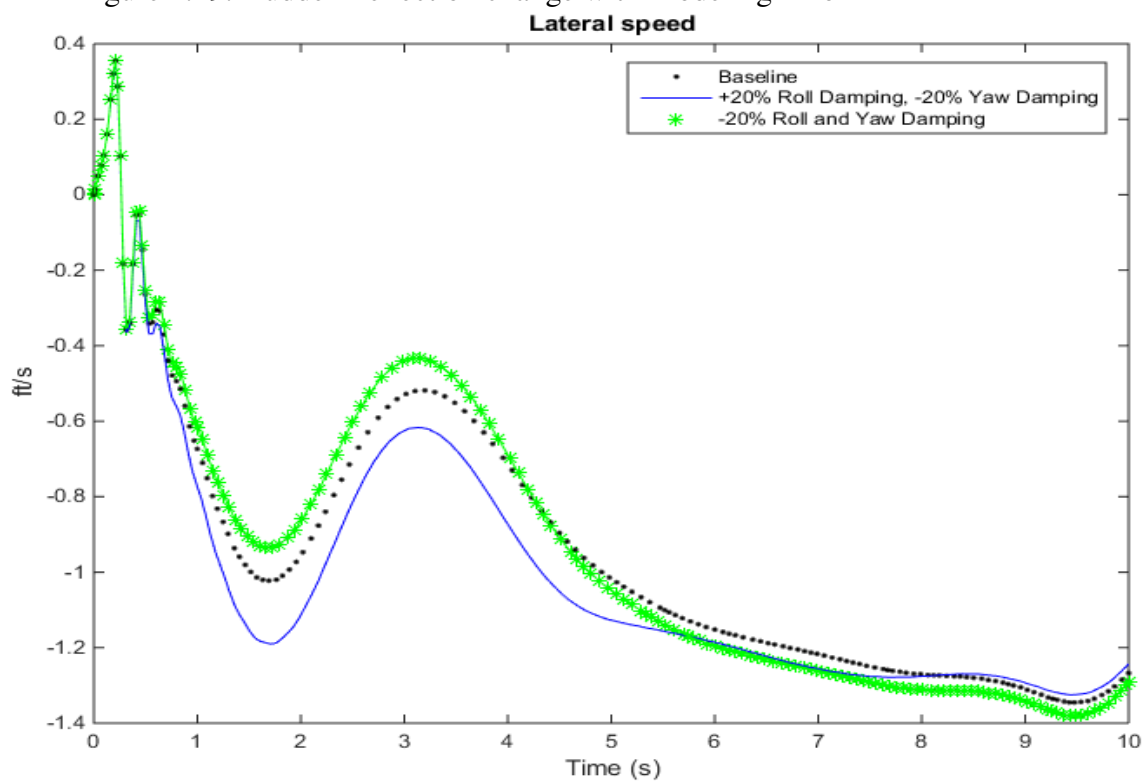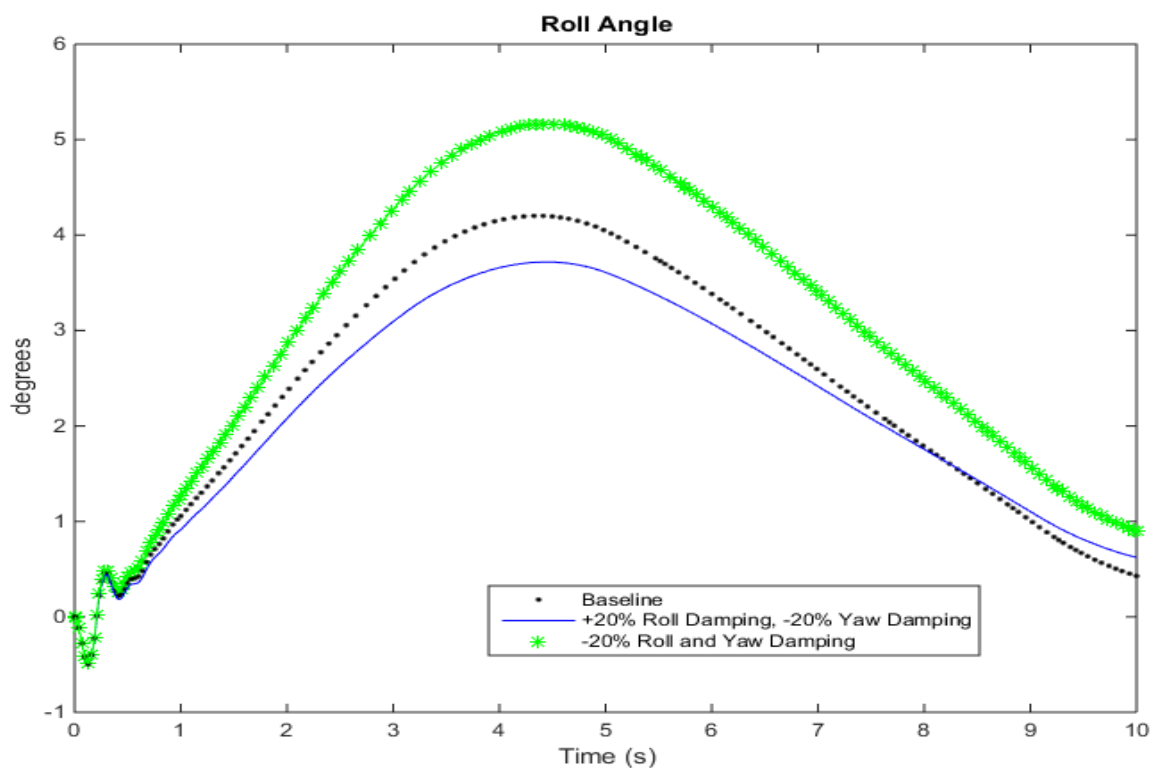
5. Conclusion

This dissertation has developed trajectory tracking control laws to enable a UAV to track a reference trajectory in the presence of disturbances. A disturbance accommodating controller (DAC) was developed to control the lateral and longitudinal UAV dynamics for cases in which the general form of the external disturbance is known and can be modeled as a state-space system. Simulation results were presented in which the DAC was applied to a linear UAV model to regulate the UAV to its trim state while rejecting sinusoidal disturbances. These results were compared to those obtained using a standard LQR controller, showing that the DAC was able to provide superior disturbance rejection than the LQR. The DAC was then successfully applied to track reference trajectories while subjected to persistent disturbances.

A direct adaptive controller was then developed to address cases in which there is significant modeling error and variations in the flight conditions. The adaptive controller was applied to regulate the simulated lateral and longitudinal UAV models to the trim condition in the presence of sinusoidal disturbances. Simulation results were then presented in which the adaptive controller was employed to track a reference lateral and longitudinal trajectories while subjected to the sinusoidal disturbance. The DAC was shown to also be able to track reference trajectories in the presence of disturbances; however, it requires the solution of a set of matching conditions for every disturbance that is modeled. In contrast, the adaptive controller requires the disturbance model and the existence of solutions to the matching conditions, but does not require the explicit solutions of these conditions. In ad-

dition, because the adaptive controller is not directly based on a system model, it is better suited than the DAC and other model-based controllers for implementation when there is significant modeling error, as is frequently the case with UAV models. Sensor blending of non-minimum phase systems was achieved using Bass-Gura method. This guarantees the assumptions needed to prove stability are satisfied. Further, an analysis on the relations between aircraft dynamics and the stability assumptions is carried out in order to analyze the robustness of the adaptive system. The stability criteria is presented in terms of aircraft dynamic coefficients and an example analyzing robustness in C_{nr} damping is provided. An argument is made for the use of adaptive control to augment the handling qualities of a poorly handling UAV.

Linear and Nonlinear simulations results are presented comprising of various scenarios encompassing complex trajectories and disturbance models to demonstrate the performance of the adaptive control scheme. The propagation of errors in the adaptive gains is looked at in depth. It is found that an error in the disturbance model will cause the disturbance error to propagate into the adaptive regulator, which causes the adaptive regulator gain to increase. Simulation results are provided to validate the same. Modeling error and its effects on the performance on adaptive control scheme is analyzed. An error in roll and yaw damping is propagated through the linear system to obtain various cases where the adaptive controller is required to follow an ideal model reference. The results are promising and show that the adaptive controller is able to accommodate for a 20% error in the stability coefficients.

Overall, the results in this paper demonstrate the feasibility of developing a UAV guidance and control system that corresponds to generating a maneuver database from a base-

line linear model, which can be used for vehicle path planning, and then applying a direct adaptive controller to enable the UAV to follow the prescribed trajectory while subject to modeling error and external disturbances.

6. Future Works

The future work for this dissertation will be to focus on expanding the study of the controller performance by inculcating more trajectories and disturbances into the simulations. Importance will also be given to formulating a mathematical relation between modeling error and stability of the adaptive system. The relations between stability of transmission zeros in the normal form and the stability derivatives will also be considered. The future work will consist of the following:

- Formulating a mathematical relationship between modeling error and stability.

- Investigating how the stability of the adaptive system is affected by different stability derivatives.

- Standardizing the results of the modeling error analysis to further analyze the effect modeling error has on the performance of the controller.

- Performing simulation studies of the above modeling error analysis and analyzing the results obtained.

- Expanding the disturbance generators to include various other kinds of disturbances like steps, ramps and a combination of these with sinusoidal disturbances.

- Generate results from disturbances with varying amplitudes.

- Possibly include the NASA-Dryden atmospheric turbulence generator to model real time continuous disturbances and study the results of the controller performance in those conditions.

- Including output (sensor) noise into the simulation.

- Including more trajectories for the UAV to track over a longer time frame to study the performance of the controller over a longer duration, while in presence of disturbances and noisy sensors.

REFERENCES

Adami, Tony M, and J Jim Zhu. "6DOF Flight Control of Fixed-Wing Aircraft by Trajectory Linearization." In *American Control Conference (ACC), 2011*, 1610–1617. IEEE, 2011.

Alonge, F., M. Cirrincione, F. D'Ippolito, M. Pucci, and A. Sferlazza. "Robust Active Disturbance Rejection Control of Induction Motor Systems Based on Additional Sliding-Mode Component." *IEEE Transactions on Industrial Electronics* 64, no. 7 (July 2017): 5608–21. https://doi.org/10.1109/TIE.2017.2677298.

Aponso, Gayanath, and Animesh Chakravarthy. "Controller Design for a Nonlinear Morphing UAV," 2013.

Balas, M. J., and S. A. Frost. "Sensor Blending for Direct Adaptive Control of Non-Minimum Phase Linear Infinite-Dimensional Systems in Hilbert Space." In *2017 American Control Conference (ACC)*, 474–80, 2017. https://doi.org/10.23919/ACC.2017.7962998.

Balas, Mark. "Disturbance Accommodating Control, Private Correspondence," April 2016.

Balas, Mark J., and Susan A. Frost. "Adaptive regulation in the presence of persistent disturbances for linear infinite-dimensional systems in Hilbert space: conditions for almost strict dissipativity." *Control Conference (ECC), 2015 European*. IEEE, 2015.

Balas, Mark, and Robert Fuentes. "A Non-Orthogonal Projection Approach to Characterization of Almost Positive Real Systems with an Application to Adaptive Control." In *American Control Conference, 2004. Proceedings of the 2004*, 2:1911–1916. IEEE, 2004.

Balas, Mark, Suraj Gajendar, and Lawrence Robertson. "Adaptive Tracking Control of Linear Systems with Unknown Delays and Persistent Disturbances (or Who You Callin' Retarded?)." In *AIAA Guidance, Navigation, and Control Conference*. American Institute

of Aeronautics and Astronautics. Accessed October 3, 2018.

https://doi.org/10.2514/6.2009-5855.

Balas, Mark J. "Finite-Dimensional Direct Adaptive Control for Discrete-Time Infinite-Dimensional Linear Systems." *Journal of Mathematical Analysis and Applications* 196, no. 1 (1995): 153–171.

Balas, Mark J, and Susan A Frost. "Adaptive Model Tracking Control for Weakly Minimum Phase Linear Infinite-Dimensional Systems in Hilbert Space Using a Zero Filter." In *AIAA Guidance, Navigation, and Control Conference*, 0621, 2016.

Balas, Mark J, Kaman S Thapa Magar, and Susan A Frost. "Adaptive Disturbance Tracking Theory with State Estimation and State Feedback for Region II Control of Large Wind Turbines." In *American Control Conference (ACC), 2013*, 2220–2226. IEEE, 2013.

Baldelli, Dario H, Dong-Hwan Lee, Ricardo S Sanchez Pena, and Bryan Cannon. "Modeling and Control of an Aeroelastic Morphing Vehicle." *Journal of Guidance, Control, and Dynamics* 31, no. 6 (2008): 1687.

Bar-Kana, Izhak, and Howard Kaufman. "Global Stability and Performance of a Simplified Adaptive Algorithm." *International Journal of Control* 42, no. 6 (1985): 1491–1505.

Behal, A., P. Marzocca, V. M. Rao, and A. Gnann. "Nonlinear Adaptive Control of an Aeroelastic Two-Dimensional Lifting Surface." *Journal of Guidance, Control, and Dynamics* 29, no. 2 (2006): 382–90. https://doi.org/10.2514/1.14011.

Brezoescu, A, Rogelio Lozano, and P Castillo. "Lyapunov-Based Trajectory Tracking Controller for a Fixed-Wing Unmanned Aerial Vehicle in the Presence of Wind." *International Journal of Adaptive Control and Signal Processing* 29, no. 3 (2015): 372–384.

Cabecinhas, David, Rita Cunha, and Carlos Silvestre. "A Nonlinear Quadrotor Trajectory Tracking Controller with Disturbance Rejection." *Control Engineering Practice* 26 (May 1, 2014): 1–10. https://doi.org/10.1016/j.conengprac.2013.12.017.

Calise, Anthony J., Naira Hovakimyan, and Moshe Idan. "Adaptive Output Feedback Control of Nonlinear Systems Using Neural Networks." *Automatica*, Neural Network Feedback Control, 37, no. 8 (August 1, 2001): 1201–11. https://doi.org/10.1016/S0005-1098(01)00070-X.

Choe, Ronald, Olaf Stroosma, Enric Xargay, Herman Damveld, Naira Hovakimyan, J. Mulder, and Herman Damveld. "A Handling Qualities Assessment of a Business Jet Augmented with an L1 Adaptive Controller." In *AIAA Guidance, Navigation, and Control Conference*. American Institute of Aeronautics and Astronautics. Accessed October 3, 2018. https://doi.org/10.2514/6.2011-6610.

Cooper, George E., and Robert P. Harper. "The Use of Pilot Rating in the Evaluation of Aircraft Handling Qualities." Advisory Group for Aerospace Research and Development Neuilly-Sur-Seine (France), April 1969. http://www.dtic.mil/docs/citations/AD0689722.

Crespo, Luis G, Megumi Matsutani, and Anuradha M Annaswamy. "Design of a Model Reference Adaptive Controller for an Unmanned Air Vehicle." In *Proceedings of the AIAA Guidance, Navigation, and Control Conference*, 2010.

De Filippis, Luca, Giorgio Guglieri, and Fulvia B. Quagliotti. "A Novel Approach for Trajectory Tracking of UAVs." *Aircraft Engineering and Aerospace Technology: An International Journal* 86, no. 3 (2014): 198–206.

Dinh, Hong Toan, Dang Khoa Truong, Tran Hiep Nguyen, Xuan Tung Truong, and Cong Dinh Nguyen. "Active Disturbance Rejection Control Design for Integrated Guidance

and Control Missile Based SMC and Extended State Observer." In *2017 International Conference on System Science and Engineering (ICSSE)*, 476–81, 2017. https://doi.org/10.1109/ICSSE.2017.8030920.

Doe, Jane L., and John Q. Public. "The Parameterization of the Rotation Matrix Using Redundant Attitude Coordinates." *Nonlinear Dynamics* 32, no. 3 (2005): 71–92.

Fradkov, Alexander, and Boris Andrievsky. "Combined Adaptive Controller for UAV Guidance." *European Journal of Control* 11, no. 1 (2005): 71–79.

Frost, Susan A, Mark J Balas, and Alan D Wright. "Direct Adaptive Control of a Utility-Scale Wind Turbine for Speed Regulation." *International Journal of Robust and Nonlinear Control* 19, no. 1 (2009): 59–71.

Fuentes, R. J., and M. J. Balas. "Direct Adaptive Disturbance Accommodation." In *Proceedings of the 39th IEEE Conference on Decision and Control (Cat. No.00CH37187)*, 5:4921–25 vol.5, 2000. https://doi.org/10.1109/CDC.2001.914711.

Fuentes, Robert J, and Mark J Balas. "Direct Adaptive Rejection of Persistent Disturbances." *Journal of Mathematical Analysis and Applications* 251, no. 1 (2000): 28–39.

Gandhi, Neha, Akhilesh Jha, Jeffrey Monaco, Thomas Michael Seigler, David Ward, and Daniel J Inman. "Intelligent Control of a Morphing Aircraft." In *Proceedings of the 46th AIAA/ASME/ASCE/AHS/ASC Structures, Structural Dynamics and Materials Conference*, 18–21. AIAA, 2007.

Gavilan, Francisco, Rafael Vazquez, and José Á. Acosta. "Adaptive Control for Aircraft Longitudinal Dynamics with Thrust Saturation." *Journal of Guidance, Control, and Dynamics* 38, no. 4 (2015): 651–61. https://doi.org/10.2514/1.G000028.

Gavilan, Francisco, Rafael Vazquez, and Sergio Esteban. "Trajectory Tracking for Fixed-Wing UAV Using Model Predictive Control and Adaptive Backstepping." *IFAC-PapersOnLine* 48, no. 9 (2015): 132–137.

Gregory, Irene, Enric Xargay, Chengyu Cao, and Naira Hovakimyan. "Flight Test of an L1 Adaptive Controller on the NASA AirSTAR Flight Test Vehicle." In *AIAA Guidance, Navigation, and Control Conference*. American Institute of Aeronautics and Astronautics. Accessed October 3, 2018. https://doi.org/10.2514/6.2010-8015.

Han, Jingqing. "From PID to Active Disturbance Rejection Control." *IEEE Transactions on Industrial Electronics* 56, no. 3 (2009): 900–906.

Ioannou, P. A., and P. V. Kokotovic. "Paper: Instability Analysis and Improvement of Robustness of Adaptive Control." *Automatica* 20, no. 5 (September 1984): 583–594. https://doi.org/10.1016/0005-1098(84)90009-8.

Jeong, S., and D. Chwa. "Coupled Multiple Sliding-Mode Control for Robust Trajectory Tracking of Hovercraft With External Disturbances." *IEEE Transactions on Industrial Electronics* 65, no. 5 (May 2018): 4103–13. https://doi.org/10.1109/TIE.2017.2774772.

Johnson, CD. "Disturbance-Accommodating Control; an Overview." In *American Control Conference, 1986*, 526–536. IEEE, 1986.

Kahn, Aaron D. "Adaptive Control for Small Fixed-Wing Unmanned Air Vehicles." In *AIAA Guidance, Navigation, and Control Conference*, 1–17, 2010.

Kailath, Thomas. *Linear Systems*. Englewood Cliffs, NJ: Prentice-Hall, 1980.

Ko, Jeonghwan, Andrew J. Kurdila, and Thomas W. Strganac. "Nonlinear Control of a Prototypical Wing Section with Torsional Nonlinearity." *Journal of Guidance, Control, and Dynamics* 20, no. 6 (1997): 1181–89. https://doi.org/10.2514/2.4174.

Kreisselmeier, G., and B. Anderson. "Robust Model Reference Adaptive Control." *IEEE Transactions on Automatic Control* 31, no. 2 (February 1986): 127–33. https://doi.org/10.1109/TAC.1986.1104217.

Lavretsky, Eugene, Ross Gadient, and Irene M. Gregory. "Predictor-Based Model Reference Adaptive Control." *Journal of Guidance, Control, and Dynamics* 33, no. 4 (2010): 1195–1201. https://doi.org/10.2514/1.46849.

Liu, Yu, Gang Tao, and Suresh M. Joshi. "Modeling and Model Reference Adaptive Control of Aircraft with Asymmetric Damage." *Journal of Guidance, Control, and Dynamics* 33, no. 5 (2010): 1500–1517. https://doi.org/10.2514/1.47996.

Marina, H. G. de, Y. A. Kapitanyuk, M. Bronz, G. Hattenberger, and M. Cao. "Guidance Algorithm for Smooth Trajectory Tracking of a Fixed Wing UAV Flying in Wind Flows." In *2017 IEEE International Conference on Robotics and Automation (ICRA)*, 5740–45, 2017. https://doi.org/10.1109/ICRA.2017.7989674.

Marina, Hector Garcia de, Yuri A Kapitanyuk, Murat Bronz, Gautier Hattenberger, and Ming Cao. "Guidance Algorithm for Smooth Trajectory Tracking of a Fixed Wing UAV Flying in Wind Flows." In *Robotics and Automation (ICRA), 2017 IEEE International Conference On*, 5740–5745. IEEE, 2017.

Moncayo, Hever, Mario Perhinschi, Brenton Wilburn, Jennifer Wilburn, and Ondrej Karas. "UAV Adaptive Control Laws Using Non-Linear Dynamic Inversion Augmented with an Immunity-Based Mechanism." In *AIAA Guidance, Navigation, and Control Conference*. American Institute of Aeronautics and Astronautics. Accessed October 3, 2018. https://doi.org/10.2514/6.2012-4678.

Morelli, Eugene A. "Flight Test Maneuvers for Efficient Aerodynamic Modeling." *Journal of Aircraft* 49, no. 6 (2012): 1857–1867.

Narendra, Kumpati S, and Lena S Valavani. "Stable Adaptive Controller Design Part I: Direct Control." In *Decision and Control Including the 16th Symposium on Adaptive Processes and A Special Symposium on Fuzzy Set Theory and Applications, 1977 IEEE Conference On*, 16:881–886. IEEE, 1977.

Nelson, Robert C. *Flight Stability and Automatic Control*. New York: McGraw-Hill, 1998.

Nigam, Nikhil, Yingchuan Zhang, Peter C Chen, Gary Wolfe, Thomas Pillsbury, Norman M Wereley, and Peter M Suh. "Adaptive Control and Actuation System Development for Biomimetic Morphing." In *24th AIAA/AHS Adaptive Structures Conference*, 1084, 2016.

Nobleheart, W. G. "Control System Design for Morhing Aircraft." PhD Thesis, Wichita State University, 2008.

Noriega, Alfonso, Mark J Balas, and Richard P Anderson. "Sensor Blending with an Application to Robust Direct Adaptive Control of a Non-Minimum Phase Aircraft." *AIAA SciTech*, 2017.

Patel, Vijay V., Chengyu Cao, Naira Hovakimyan, Kevin A. Wise, and Eugene Lavretsky. "$\mathscr{L}$ 1 Adaptive Controller for Tailless Unstable Aircraft in the Presence of Unknown Actuator Failures." *International Journal of Control* 82, no. 4 (April 1, 2009): 705–20. https://doi.org/10.1080/00207170802225955.

Prabhakar, Nirmit, Andrew Painter, Richard Prazenica, and Mark Balas. "Trajectory-Driven Adaptive Control of Autonomous Unmanned Aerial Vehicles with Disturbance Accommodation." *Journal of Guidance, Control, and Dynamics* 41, no. 9 (2018): 1976–89. https://doi.org/10.2514/1.G003341.

Prabhakar, Nirmit, Richard Prazenica, Snorri Gudmundsson, and Mark Balas. "Transient Dynamic Analysis and Control of a Morphing UAV." In *AIAA Guidance, Navigation, and Control Conference*, 0893, 2016.

Probst, Troy A, Brian David, Kevin Kochersberger, and Osgar J Ohanian III. "Design and Flight Test of a Morphing UAV Flight Control System." In *51st AIAA Aerospace Sciences Meeting Including the New Horizons Forum and Aerospace Exposition*, 1148, 2013.

Ragheb, M. "Wind Turbines in the Urban Environment." *Retrieved July* 12 (2008): 2009.

Rajagopal, Karthikeyan, S. Balakrishnan, James Steck, and Dwayne Kimball. "Robust Adaptive Control of a General Aviation Aircraft." *AIAA Atmospheric Flight Mechanics Conference 2010*, January 1, 2010. https://doi.org/10.2514/6.2010-7942.

Ren, Wei, and Ella Atkins. "Nonlinear Trajectory Tracking for Fixed Wing UAVs via Backstepping and Parameter Adaptation." In *Proceedings of the AIAA Guidance, Navigation, and Control Conference and Exhibit*, 10:6–2005, 2005.

Ren, Wei, and Randy W Beard. "Trajectory Tracking for Unmanned Air Vehicles with Velocity and Heading Rate Constraints." *IEEE Transactions on Control Systems Technology* 12, no. 5 (2004): 706–716.

Rysdyk, Rolf T., and Anthony J. Calise. "Adaptive Model Inversion Flight Control for Tilt-Rotor Aircraft." *Journal of Guidance, Control, and Dynamics* 22, no. 3 (1999): 402–7. https://doi.org/10.2514/2.4411.

Seigler, T. Michael. "Dynamics and Control of Morphing Aircraft." PhD Thesis, Virginia Polytechnic Institute and State University, 2005.

Seigler, Thomas M, David A Neal, Jae-Sung Bae, and Daniel J Inman. "Modeling and Flight Control of Large-Scale Morphing Aircraft." *Journal of Aircraft* 44, no. 4 (2007): 1077–1087.

Seigler, TM, and DA Neal. "Analysis of Transition Stability for Morphing Aircraft." *Journal of Guidance, Control, and Dynamics* 32, no. 6 (2009): 1947–1954.

Shahnazi, R., and M. Akbarzadeh-T. "PI Adaptive Fuzzy Control With Large and Fast Disturbance Rejection for a Class of Uncertain Nonlinear Systems." *IEEE Transactions on Fuzzy Systems* 16, no. 1 (February 2008): 187–97. https://doi.org/10.1109/TFUZZ.2007.903320.

Sharma, Manu, Eugene Lavretsky, and Kevin Wise. "Application and Flight Testing of an Adaptive Autopilot on Precision Guided Munitions." In *AIAA Guidance, Navigation, and Control Conference and Exhibit*. American Institute of Aeronautics and Astronautics. Accessed October 3, 2018. https://doi.org/10.2514/6.2006-6568.

Shi, Rongqi, and Weiyu Wan. "Analysis of Flight Dynamics for Large-Scale Morphing Aircraft." *Aircraft Engineering and Aerospace Technology: An International Journal* 87, no. 1 (2015): 38–44.

Stastny, Thomas, Adyasha Dash, and Roland Siegwart. "Nonlinear Mpc for Fixed-Wing Uav Trajectory Tracking: Implementation and Flight Experiments." In *AIAA Guidance, Navigation, and Control (GNC) Conference*, 2017.

Stengel, Robert F, and LE Ryan. "Stochastic Robustness of Linear Time-Invariant Control Systems." *IEEE Transactions on Automatic Control* 36, no. 1 (1991): 82–87.

Wang, Lu, and Jianbo Su. "Disturbance Rejection Control of a Morphing UAV." In *American Control Conference (ACC), 2013*, 4307–4312. IEEE, 2013.

Wen, John Ting-Yung, and Mark J Balas. "Robust Adaptive Control in Hilbert Space." *Journal of Mathematical Analysis and Applications* 143, no. 1 (1989): 1–26.

Wise, K. A., E. Lavretsky, and N. Hovakimyan. "Adaptive Control of Flight: Theory, Applications, and Open Problems." In *2006 American Control Conference*, 6 pp.-, 2006. https://doi.org/10.1109/ACC.2006.1657677.

Yamasaki, Takeshi, Hirotoshi Sakaida, Keisuke Enomoto, Hiroyuki Takano, and Yoriaki Baba. "Robust Trajectory-Tracking Method for UAV Guidance Using Proportional Navigation." In *Control, Automation and Systems, 2007. ICCAS'07. International Conference On*, 1404–1409. IEEE, 2007.

Yucelen, Tansel, and Anthony J. Calise. "Derivative-Free Model Reference Adaptive Control." *Journal of Guidance, Control, and Dynamics* 34, no. 4 (2011): 933–50. https://doi.org/10.2514/1.53234.

Zheng, Qing, Lili Dong, Dae Hui Lee, and Zhiqiang Gao. "Active Disturbance Rejection Control for MEMS Gyroscopes." In *2008 American Control Conference*, 4425–30, 2008. https://doi.org/10.1109/ACC.2008.4587191.

Zheng, Qing, L. Q. Gaol, and Zhiqiang Gao. "On Stability Analysis of Active Disturbance Rejection Control for Nonlinear Time-Varying Plants with Unknown Dynamics." In *2007 46th IEEE Conference on Decision and Control*, 3501–6, 2007. https://doi.org/10.1109/CDC.2007.4434676.